Automatic Extraction of Water Features at Multiple Scales

Thesis submitted to the Andhra University, Visakhapatnam
in partial fulfilment of the requirement for the award of
Master of Technology in Remote Sensing and GIS

Submitted By
Manohar Kumar. C. V. S. S.

Under the Supervision of

Dr. Poonam Seth Tiwari
Scientist/Engineer 'SE'
Photogrammetry & Remote Sensing Department
Indian Institute of Remote Sensing
Dehradun

Dr. Hina Pande
Scientist/Engineer 'SE'
Photogrammetry & Remote Sensing Department
Indian Institute of Remote Sensing
Dehradun

Indian Institute of Remote Sensing,
Indian Space Research Organization,
Department of Space, Govt. of India
Dehradun – 248001
Uttarakhand, India
June, 2015

Acknowledgements

First I would like to thank my parents who always motivated and supported me in all good and hard times of my life. Then I would like to express my sincere gratitude and great regards to my supervisor Dr. Poonam Seth Tiwari, Scientist/Engineer – 'SE', IIRS, Dehradun and co-supervisor Dr. Hina Pande Scientist/Engineer – 'SE', IIRS, Dehradun. who has given tremendous support for this entire research. Without the help of these supervisors the research would have been incomplete.

I wish to express my sincere gratitude and humble thanks to Ms. Shefali Agarwal, course director and Head PRSD whose advice has been most commendable in the formulation of the topic of this research and also helped in the completion of this research.

I am also grateful to Dr. S.K. Srivastav, (Group Head RS & Geoinformatics), Prof. P.L.N.Raju (PPEG Director), Dr. S.P.S.Kuswaha (Dean Academics), Dr. S.K.Saha (former Dean Academics)**,** Dr. A. Senthil Kumar (Director IIRS), and Dr. Y.V.N. Krishna Murthy Scientific Secretary, ISRO for their valuable advices and support during my research work.

I thank Ms. Rajasweta Datta for her help, support and company during the field work. I thank Azhar (driver) for coordination and help in field work.

I thank CMA people who has continuously updated my PC with a great patience, especially Mr. Rahul Chauhan, Mr. Awadhesh Deyondi, Mr. Hemant Bisht, Mr. Surendra Kotiyal, Mr. Rajesh Dabral, Mr. Azam Ali, and Ms. Jyoti Madhwal from the past two years.

I thank to some special people who make this campus beautiful, without them something is missing in IIRS are my friends Rigved, Varun, Akshat, Rohit, Mayank, Sureshbabu, Richa, Ridhika, Jenia, Amol, Sukant, Dr. Kuldeep, Rajkumar, Vineet, Harjeet, and Raunak.

Thank you wardens Mr. Ajanta and Mr. Arpit Choksey, and care-taker, Prashant Ji, Jitender Ji and Vishakha people for making my stay at IIRS comfortable.

I express my gratitude towards all the seniors and juniors and all the people staying at IIRS.

I thank to Andhra University for affording me this opportunity to carry out this research work.

It is my essence to thank wholeheartedly to all my well-wishers and my critics who has motivated, and encouraged to achieve this research work. I am also grateful to all those who have been associated with this research directly or indirectly.

(Manohar Kumar. C. V. S. S.)

Disclaimer

This work has been carried out in partial fulfilment of Masters in Technology program in Remote Sensing and Geographic Information System at Indian Institute of Remote Sensing, Dehradun, India. The author is solely responsible for the contents of the thesis.

అమ్మనాన్నకు అంకితం.....

Dedicated to My Mom and Dad.....

Water – The Elixir of Life.

"What you are is what you have been, and what you will be is what you do now."

The Buddha

Certificate

This is to certify that ***Mr. Manohar Kumar. C. V. S. S.*** has carried out the dissertation entitled ***"Automatic Extraction of Water Features at Multiple Scales"*** in partial fulfilment of the requirements for the award of ***Master of Technology in Remote Sensing and GIS***. This work has been carried out under the supervision of **Dr. Poonam Seth Tiwari,** Scientist/Engineer 'SE', and **Dr. Hina Pande** Scientist/Engineer 'SE', Photogrammetry and Remote Sensing Department, Indian Institute of Remote Sensing, ISRO, Dehradun, Uttarakhand, India.

……...
Dr. Poonam Seth Tiwari
Project Supervisor
Photogrammetry and Remote Sensing Department
IIRS, Dehradun

……..……
Dr. Hina Pande
Project Supervisor
Photogrammetry and Remote Sensing Department
IIRS, Dehradun

……...
Dr. Satya P.S. Kushwaha
Dean Academics
IIRS, Dehradun

……..……
Ms.ShefaliAggarwal
Head, PRSD
IIRS, Dehradun

Declaration

I, ***Manohar Kumar. C. V. S. S.***, hereby declare that this dissertation entitled "**Automatic Extraction of Water Features at Multiple Scales"** submitted to Andhra University, Visakhapatnam in partial fulfilment of the requirements for the award of ***Master of Technology in Remote Sensing and GIS***, is my own work and that to the best of my knowledge and belief. It is a record of original research carried out by me under the guidance and supervision of **Dr. Poonam Seth Tiwari,** Scientist/Engineer 'SE', PRSD, and **Dr. Hina Pande** Scientist/Engineer 'SE', PRSD, Indian Institute of Remote Sensing, Dehradun. It contains no material previously published or written by another person nor material which to a substantial extent has been accepted for the award of any other degree or diploma of the university or other institute of higher learning, except where due acknowledgment has been made in the text.

Place: Dehradun Mr. Manohar Kumar. C. V. S. S.

Date: June 2015

Abstract

Water is a natural resource and changes dynamically over large geographical area, it is available in an abundant amount on the earth surface. At present 0.767% of total availability of water on the earth surface is useful for mankind. Due to dynamic change in the water spread information, continuous monitoring and proper planning is required for the utilizing of water resources efficiently. For continuous monitoring huge amount of time and labour is required. In present trend, developments in the application domain of geospatial technologies, Satellite Remote Sensing and Geographical information Systems (GIS) offers immense scope in the active collection of data and management on a temporal basis.

In the geospatial domain, several methods or mechanisms are developed on the basis of a particular available datasets which is dependent on the sensor at a fixed or standard scales. For overcoming these difficulties a new methodology has been proposed for extracting and classifying the water features at a variable scales

A set of knowledge based rules set was proposed for delineating and classifying water features at multiple scales for Uttarakhand state, India. Top of Atmosphere (TOA) reflectance calculated from the Landsat 8 data and Digital Elevation Model (DEM) were taken as the inputs for this study. At first, the threshold conditions were applied on Surface wetness Index (SWI) for separating the snow or ice from images. Next the rules were defined for Normalized Difference Vegetation Index (NDVI), Normalized Difference Water Index (NDWI), Modified Normalized Difference Water Index (MNDWI), and Normalized Difference Pond Index (NDPI) for separating the water features in an image. The shadows (caused due to elevated terrain) which is misinterpreted as water features in an image, has been removed from the slope map derived from the DEM. Binary water mask was generated by combining slope map with the ruleset. This mask was overlaid on the input image to extract the spectral signatures of the water features refined by it. Finally the rules are generated based on the spectral values of the water feature collected from each band, for classification of the water features in to different classes like, clear water, deep water, shallow water, snow/ice cover and wetland. The overall accuracy attained in this analysis is 91.67% for the Landsat 8 OLI. The prepared mask was overlaid on LISS – III and LISS – IV, to extract the water features. The extracted water features that were classified based on the spectral properties had the overall accuracy of 84.17% and 87.50% respectively. Apart from major water feature extraction thin network for river and canals were extracted separately using canny edge detection. The study demonstrates extraction of the water features from multiple resolution data and to classify it into relevant classes.

Keywords: Multispectral indices, DEM, and edge detection.

Table of Contents

List of Figures

List of Tables

1. Background and Introduction

1.1 Background

"Bharat" is geographical term and it is also official name of the country "India" (Goverment of India, 2007). There several natural geographical features in that water plays pivotal role in the geographical context. Water is abundant resource in the form of rivers, lakes, ponds, ice and snow. India has several cultures and traditions that vary from place to place. In a similar way, the topographical and geological variations are also observed with in the 329 M ha of geographical area (Prakashvel & Scholar, 2003). Because of this variation, India has been experiencing the extreme hot and cold conditions in places like Alwar, Rajasthan (50 ^{0}C) and Dars, Ladakh (-50 ^{0}C) respectively (IMD, 2010) . Besides temperature, the rainfall of the country also varies drastically from one place to another, like Western Rajasthan observes 100mm whereas Cherrapunji observes 11000mm (Indian Water Resources Society, 1994). Due to unpredictable nature and irregularity in the arrival of monsoon season there are unbearable circumstances like overflowing of lakes and ponds, excess flow of rivers and drowning of agricultural fields and built up area is being observed. During this one part of the country is reeling under floods while the other parts are experiencing drought scenarios. This occurs because of mismanagement and un-planned distribution of the resources (Bindraban, Van Keulen, & Warner, 2006). Imbalance between availability and demand, water sources gets exploited in a very high rate. Exhaustion and lack of abundance in the availability of underground water, there is an inter-state and intra-state competition, and national and international conflicts increases due frequent water related problems. There are several other problems which include expansion desert areas, increase in salinization pattern and water logging due to over-irrigation system. The requirement of fresh water for urban and industrial use are generally recognized as the fundamental issues in water resource planning and administration. These issues influences the people whose applications are focused on integrated water administration (Warner, Bindraban, & Van Keulen, 2006). It requests essential data about the quantity, quality and distribution of available water resources. As of late, driving powers and personalities have contended the criticalness of information technology with public participation in the better appraisal, planning and administration of water resource (Troell, Bruch, Cassar, & Schang, 2005).

Many scientists and engineers throughout the world has estimated the quantity, quality and area occupied by the water features by using the different techniques and mechanisms (S. Kumar, Shirke, & Pawar, 2008). For Water resource management in river basins there is a requirement of integration between researchers and stakeholders is explained in (Jongman & Padovani, 2006). Bhagat estimated the total volume of water in man-made as well as natural water bodies by using the satellite data and GIS techniques (Bhagat Vijay, 2008) and water pollution has discussed in the (S. Kumar et al., 2008) (Pawar, Pawar, Kumar, & Supekar, 2008). Estimations include the area occupied and spread of water storage and blow-out of rivers tracking and high tide conditions of ocean water in coastal zones. These algorithms are useful in anticipating the early flood warning system (Mioca et al., 2008). Remote sensing mechanisms have been utilized to evaluate water availability and productivity with flood and drought effects on agriculture (Van Dam et al., 2006)(Patel, Mohammed, & Rakhesh, 2006).Remote Sensing is required for monitoring water resources due to its flexibility in

covering large area in a small interval of time and also it requires very negligible ground data and surveying.

Water is natural dynamic feature and it has abundant amount on the earth surface in that very less present (0.767% of total availability of water on the earth surface) of water is useful for human kind ("How much water is there on Earth, from the USGS Water Science School," 1983), due to mismanaging and doesn't not have proper plan for utilising water resources effectively. Due to these reasons, low income community are mostly effected by the lack of access to a water-based productivity framework.(Warner et al., 2006). The major user of the available fresh water is agriculture field. On the analysis of irrigation pattern, the framework is required to be transformed and modernised to better performance, and for reaching out the low income group (Pavlov, Roerink, Hellegers, & Popovych, 2006). Agricultural water stability and the volume of irrigated water in comparison to the financial yield and expenses are considered as irrigation performance indicators or pointers. The estimate of available water that can be utilized in irrigation security during circumstances of crop failure in droughts is of a major concern for managment purpose. (Bhagat & Sonawane, 2011). To meet these needs automated methods are required, several knowledge based methods are explained different scientist or engineers. (Subramaniam, Suresh Babu, & Roy, 2011) developed a knowledge based algorithm using hierarchical decision tree approach has been developed for automated spread mapping using the Resourcesat – 1 AWiFS dats for maintaining the water information system. An Automated Water Extraction Index (AWEI), improving classification accuracy in areas that include shadow and dark surfaces that other classification methods often fail to classify correctly and they tested the accuracy and robustness of the new method using Landsat 5 TM images of several water bodies in (Feyisa, Meilby, Fensholt, & Proud, 2014). Extraction of water bodies automatically using whole – R method is explaind in (Nawaz, Srinivasulu, & Rao, 2013). (Feyisa et al., 2014; Jiang et al., 2014; Nawaz et al., 2013; Subramaniam & Saxena, 2011; Subramaniam et al., 2011) in this also extraction of water features has done in automation for maintaining the geospatial database of dynamically varying water features. These mechanisms are totally work for the single dataset at fixed scales.

Wetland ecosystem play a pivotal role among all the ecosystem present on earth's surface. Most of the fossil fuel using in the present period have been preserved in the swampy environment of past geological era. In addition to this, there are other significant sources, sinks and transformers of chemical/biological and a genetic information base with the richest bio-multiplicity. They can be portrayed as the "kidneys of scene" for the capacity they perform in hydrologic and chemical cycle and as the downstream recipients of waste from both natural and human sources. They have been found to clean polluted waters, prevent floods, and protect shoreline. It does, not only provide foods, resources and water source for human beings, but also recharges ground water source for mitigating drought and natural disaster avoidance. Apart from above, they play major role in the landscape by providing habitat for a wide variety of flora and fauna.

Wetlands have been characterized contrastingly by distinctive individuals for diverse purposes relying upon the object and the need. They are defined as biophysical flat lands or

slopes with perennial water tables at or near the surface (Ramsar Convention, 2013). To say in simpler form "wetlands are lands with soils that are periodically flooded". In the present context it is defined as "All submerged or water saturated lands, natural or manmade. inland or coastal, permanent or temporary, static or dynamic, vegetated or non—vegetated, which necessarily have, a land—water interface are defined as wetlands" and this follows the definition of Ramsar Convention (Cowardin et al., 2013; EPA, 2011; Ramsar Convention, 2013). The extraction of wetland features using remote sensing has so far been carried out using visual/ hybrid digital analysis techniques, which is time consuming (De Roeck et al., 2008a; Gilmore et al., 2008; Islam et al., 2008a; S. Zhang, Zhang, & Zhang, 2000a). To monitor the wetland and their features at National/ State level, there is a need for the development of automated technique for the extraction of wetland features. A knowledge based algorithm has been developed using hierarchical decision tree approach for automated extraction of wetland features such as surface water spread, wet area, turbidity and wet vegetation including aquatic for pre and post monsoon period (Subramaniam & Saxena, 2011).

In the universe, every object or material have its own physical and chemical properties which are alike, to measure these properties there are several measuring methods, for measuring the physical properties of the material there are two types: 1. In-situ measurements and 2. Remote sensing measurements. In-situ measurements are based on the physical contact with the target.

1.1 Principles of space borne earth observation

Remote Sensing have several definitions defined by several authors in their books and papers.

Lillesand and Kiefer has defined remote sensing is "the science and art of obtaining information about an object, area, or phenomenon through the analysis of data acquired by a device that is not in contact with the object, area, or phenomenon under investigation"(Lillesand & Kiefer, New York : Wiley & Sons, c1994).

Remote Sensing according to F.F. Sabins is "the science of acquiring, processing and interpreting images that record the interaction between electromagnetic energy and matter"(Sabins, 2007).

"The term Remote Sensing means the sensing of the Earth's surface from space by making use of the properties of electromagnetic waves emitted, reflected or diffracted by the sensed objects, for the purpose of improving natural resources management, land use and the protection of the environment" this definition is extracted from the United Nations in their annex 'Principles Relating to Remote Sensing of the Earth from Space'.

Remote Sensing has broadly defined by Charles Elachi by "the acquisition of information about an object without being in physical contact with it"(Elachi, New York : Wiley, c1987).

By observing all the definitions, remote sensing can be defined as acquiring the properties of an object by collecting and processing the electromagnetic energy radiated from that object.

1.1.1 Electromagnetic Radiation

Electromagnetic radiation is an energy that is yielded by the oscillating the electric and magnetic fields perpendicularly or movement of electrons (electrically charged particles)

travelling or passing through the medium (vacuum or matter). The passing of perpendicularly oscillating electric and magnetic fields are combined, then the entire wave also passes perpendicular to both the electric and magnetic fields at a speed of light thus the energy. Radiation of electrons releases photons (photons contains the light energy) it also travels at a speed of light in the quantized harmonic waves ("Electromagnetic Radiation," 2015).

Electromagnetic wave have some characteristics amplitude, frequency and wavelength. It have general properties like travels at a speed of light, travels through vacuum. Amplitude is maximum height or extent of the wave or oscillation or vibration measuring from the middle or centre or equilibrium position. Frequency of the wave is defined as the number of cycles per second and it units are sec^{-1} or Hertz (Hz). Wavelength is termed as the distance between two successive crests or troughs or distance of one complete cycle of wave or oscillation

Generally, wavelength increases means frequency decreases and vice versa. When an energy of the electromagnetic spectrum as released, wavelength decreases. The electromagnetic energy is gathered into categories based on their wavelength or frequency into the electromagnetic spectrum. The categories of electromagnetic radiation in electromagnetic spectrum are long waves, radio waves, microwaves, infra-red, visible, ultraviolet, x-rays, gamma rays.

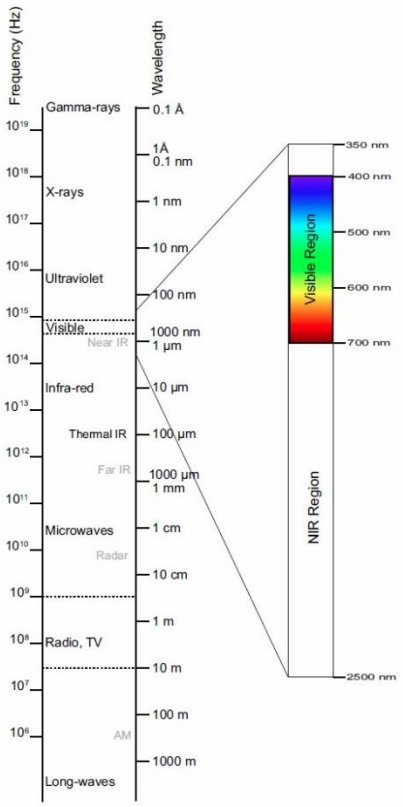

Figure 1-1: Electromagnetic Spectrum
(Source: ("Electromagnetic Radiation," 2015))

In the nature, when an object interacts or strikes with the electromagnetic energy the electromagnetic energy is radiated, transmitted and absorbed. Collecting the radiated energy

from an object and processing the energy for acquiring the properties of the material or object of interest. The radiation of energy from every material is different from the other material, from this the material or object can be distinguished. Recalling the definition of Sabins, "Remote Sensing is the science of acquiring, processing and interpreting images that record the interaction between electromagnetic energy and matter".

Remote sensing is defined as measuring the properties of an object or features on earth's surface by using the images acquired from the satellite. Satellites can collect data (acquire images) in different types based on which kind of sensor (optical, microwave, etc.) used. Optical sensors can collect data in panchromatic, multispectral, and hyperspectral. The modern era of satellite remote sensing has started, when the world scientific community received a set of synoptic, high resolution datasets by the Landsat multi-spectral scanner system (MSS) for the first time in 1972 (Schowengerdt, 2007). From that time, several countries Canada, India, Israel, Japan, etc. developed different types of coarser resolution to high resolution multispectral sensors. India developed OCM, AWiFS, LISS-III, LISS-IV, France developed SPOT system, etc.

1.2 Motivation and Problem Statement

Remote sensing data are used for estimations of water bodies by many researchers and planners in different fields, viz. hydrology, oceanography, ecology, etc. Remote areas by their geographical inaccessibility or location in hostile/foreign territory present numerous challenges in their mapping despite advances in the field of remote sensing. The primary challenge still remains in achieving reasonable accuracy standards in locational and feature extraction domains. The plethora of open domain RS and GIS resources present us with a credible feasibility of obtaining information to generate mapping products. The remote sensing technology today gives us an opportunity to remotely obtain data of inaccessible areas. The definition of inaccessible areas can be many; it could be inaccessible because of its typical geographic layout or it happens to be in hostile areas within or outside the country. The detailed planning, visualization and analysis required for operating in such areas for developmental, peaceful or corrective engagements necessitate an approach primarily dependent upon remote means of obtaining information.

However, most of the manmade water reservoirs are located in hilly zones. Fresh water and topographic shadows appears similar in optical–infrared remote sensing data and cause confusion in the detection and delineation of water bodies in hilly zones (Small, 2004). Automated delineation of shadows remains a challenging task (Bhagat & Sonawane, 2011) and visual interpretation with manual editing has been widely suggested for the correction of topographic shadowing effects. The water features are extracted by the different scientists and engineers by different methods, statistical methods(Wang, Pan, & Zheng, 2008; Z. Zhang, Prinet, & Ma, 2003), spectral and spatial separation methods (Luo, Sheng, Shen, & Li, 2010; Nawaz et al., 2013; Nguyen Dinh Duong, 2012), spectral indices methods (Bhagat & Sonawane, 2011; Feyisa et al., 2014; Haibo, Zongmin, Hongling, & Yu, 2011; Lacaux, Tourre, Vignolles, Ndione, & Lafaye, 2007; McFeeters, SK, 1996; Subramaniam & Saxena, 2011; Subramaniam et al., 2011; Xu, 2006).

Water resources planning and management requires data collection, analysis and monitoring of critical parameters like spatio-temporal water spread information and expected volumes. Temporal fluctuations in water resources can be studied through frequent spatial inventory of surface water bodies. Application of geospatial information technologies, namely Satellite Remote Sensing and Geographical information Systems (GIS), offer immense scope for replacing/supplementing the traditional monitoring methods (Subramaniam et al., 2011). A knowledge based algorithm using hierarchical decision tree approach has been developed for automated extraction of wetland features such as surface water spread, wet area, turbidity and wet vegetation including aquatic for pre and post monsoon period and this approach yields satisfactory results for the state Chhattisgarh, India (Subramaniam & Saxena, 2011) . (Feyisa et al., 2014) developed an Automated Water Extraction Index (AWEI), improving classification accuracy in areas that include shadow and dark surfaces that other classification methods often fail to classify correctly and they tested the accuracy and robustness of the new method using Landsat 5 TM images of several water bodies in Denmark, Switzerland, Ethiopia, South Africa and New Zealand. AWEI classifier was relatively more accurate in classifying edge pixels compared to the Modified Normalized Difference Water Index (MNDWI) and Maximum Likelihood (ML) classification methods. Besides, the optimal threshold of AWEI was shown to be less variable with images of different locations and times compared to that of MNDWI (Feyisa et al., 2014). (Nawaz et al., 2013)., proposed Whole-R method, that extracts water bodies with perfect edges and also filters out false water bodies and a high precise water body extraction is achieved with improved accuracy and this system needs no manual intervention throughout the extraction process (Nawaz et al., 2013). Hao Jaing proposed an automated method for extracting rivers and lakes (AMERL) for extracting mixed water pixels by considering not only their spectral characteristics, but also their topological connections. In this method, a series of processes have been introduced to filter out noise caused by shadows, roads and small segments by considering both their spatial and spectral characteristics and threshold optimization procedure is also simplified (Jiang et al., 2014). These automated approaches are totally dependent upon the sensor units and also with the fixed scales. In this research, extraction of water features at multiple scales using the multi resolution data.

1.3 Research Objectives

The principle destination of this research is to develop a customize package for extracting the water features at variable scales using multi-resolution satellite images through the automation process. To achieve this main objective, following sub-objective are to be achieved.

1.1.2 Sub-objectives

The sub objective are

1. To estimate a range of optimum threshold values for feature of interest to be used as input for automation of the process.
2. To develop an automated approach for the classification of water feature at variable scale.

1.1.3 Research Questions

To attain to achieve the listed objectives the subsequent queries need to be answered

1. How to decide the threshold factor for satellite derived parameters for water features? *(S.ob-1)*
2. Which rules and parameters are appropriate for classifying the extracted image? *(S.ob-2)*
3. How can accuracy be assessed for the extracted and classified features?

1.4 Innovation Aimed at

The expected novelty from this study is to extract the water features at multiple scales i.e. global scale to local scale (using different resolution images are captured by the different sensors) with less computation cost.

1.5 Structure of Thesis

This record has been comprises in respective chapters as given below,

Chapter – 1 : Introduction it covers the background of the study and the definitions of remote sensing and wetlands areas, availability of remote sensing and geographical information mechanisms used for classified mapping of various water features. The chapter delineates the motivation and problem statement, the objective of the research, sub-objectives, research questions, and innovation aimed.

Chapter – 2 : Literature Review and Theoretical Concepts. This chapter covers the review of some of the relevant research taken up in this field in the recent past and few important theoretical concepts which have been utilized in this research.

Chapter – 3 : Study Area and Materials. As the banner of this chapter encapsulates, it describes study area of the research, datasets, software and hardware employed in this research.

Chapter – 4 : Methodology. This chapter deals with the details of researched methodology adopted for meeting the objectives of this research.

Chapter – 5 : Results and Discussion. This chapter has the detailed results obtained from the study and discussion on the inference obtained.

Chapter – 6 : Conclusion and Recommendations. This chapter delineates the conclusion of the research in brief and few recommendations.

2. Literature Review and Theoretical Concepts

2.1 Literature Review

Image processing is an emerging concept since past few decades that involves image enhancing and image analysis. Image enhancing means improving properties of images like contrast, sharpness, texture, etc. Image analysis comprises edge detection, segmentation, classification, feature extraction, etc. Feature extraction relates to extorting the features of interest from an image, features may be point features, line features or polygon features. Several algorithms have been developed for wresting the features of interest in an image. This study comprises extracting the water features from the multi-source satellite images at variable scales.

The review of literature has been divided into different categories depend upon the statistical parameters, spectral and spatial information, spectral indices and other relevant literature.

2.1.1 Statistical Parameters

Extraction of water bodies from different sources (ERS SAR and LANDSAT-7 ETM+) of satellite images is done using the calculation of entropy image from the subtraction image for optical and directly for SAR sensor (Z. Zhang et al., 2003).

Multi-texture model (Directional Variance Model and Grain Table Analysis) is used for the extraction of water features through high resolution panchromatic images. Directional Variance Model is first applied to identify inland water features and Grain Table Analysis is then used for removing the noise from features which having same variance characteristics(Wang et al., 2008).

2.1.2 Spectral and Spatial Information

Extracting water information is done by "Whole-Local" mechanism. Which is an iterative approach of coupled spectral (based on water index calculated through Spectral Angle Method) and spatial remote sensing information(Luo et al., 2010). Nawaz extended this by replacing the spatial information by R colour component called red band of multispectral image then the mechanism have been named has "Whole-R" method (Nawaz et al., 2013).

The different spectral signature patterns of water for green, red, NIR, and SWIR bands has been collected from LANDSAT 5 TM and SPOT 5 satellite images and thus classified. Through this 1:100,000 and 1:50,000 water classified maps are generated from LANDSAT 5 TM and SPOT 5 images respectively(Nguyen Dinh Duong, 2012).

2.1.3 Spectral Indices

Mc Feeters in 1996 developed normalized difference water index (NDWI) using the normalized difference of green and NIR bands to delineate the open or surface water features. It is extended by Hanqiu in 2005, where NIR band is replaced MIR band then it is called the modified normalized difference water index (MNDWI) (Xu, 2006).

Haibo explained the extraction of water bodies by different methods i.e. unsupervised classification (based on the spectrally distributed features of the ground objects), supervised classification (classifying with the prior knowledge), single band threshold (threshold to near

infrared or mid infrared bands) and water index (NDWI, MNDWI and derived new index NWI) (Haibo et al., 2011).

(Subramaniam & Saxena, 2011) developed an automated algorithm for the extraction of wetland areas and wetland vegetation. This is achieved by the calculation of threshold levels for the NDWI, MNDWI, NDPI and NDTI of low resolution data LISS III.

Use of high-spatial resolution satellite images for making a map of correct distribution of pond regions (small water regions) through two new indices: NDPI and NDTI (Lacaux et al., 2007).

Lei analysed the dynamic thresholds for the water indices NDWI, MNDWI and NDPI of different multispectral sensors of LANDAST ETM+, SPOT-5, ASTER and MODIS (Ji, Zhang, & Wylie, 2009).

Mapping of surface water from LANDSAT 5 TM using Automated Water Extraction Index (AWEI) with an accuracy per pixel and sub-pixel and it is compared with the MNDWI and Maximum Likelihood (Feyisa et al., 2014).

Delineation of water from hilly areas have been carried out by using NDVI, surface wetness index (SWI) from the Tasselled Cap Coefficients and generated slope map from the SOI toposheets(Bhagat & Sonawane, 2011).

Developing an automated water information system from ResourceSat – 1 AWiFS sensor, which provides data in green, red, NIR, and SWIR bands. This can be done by using hierarchical multilevel logic algorithm that depends on the NDWI, MNDWI, brightness and different combination factors (Subramaniam et al., 2011).

2.1.4 Relevant Literature

Tasselled cap transformation based on the Landsat 8 at top of atmosphere reflectance is a useful tool for compressing spectral data into a few bands associated with physical scene characteristics with minimal information loss. TCT was originally evolved from the Landsat multi-spectral scanner launched in 1972 and is widely adapted to modern sensors (Crist & Cicone, 1984; Kauth & Thomas, 1976; Yarbrough, Easson, & Kuszmaul, 2005). Ali Baig (Baig, Zhang, Shuai, & Tong, 2014) in this newly developed standardized mechanism was used to transform the principal component analysis (PCA)-based rotated axes through Procrustes rotation (PR) conformation according to the Landsat thematic mapper (TM)-based tasselled cap space. OLI data were transformed into TM (Crist & Cicone, 1984) TCT space directly and considered as a dummy target. Then, PCA was applied on the original scene. Finally, PR was applied to get the transformation results in the best conformation to the target image. New coefficients were analysed in detail to confirm Landsat 8-based TCT as a continuity of the original tasselled cap idea. The resulted transformation coefficients successfully differentiated soil from vegetation, vegetation from water and bare soil features from water features (Baig et al., 2014; Crist & Cicone, 1984; DATA, 1984; Kauth & Thomas, 1976; Yarbrough et al., 2005).

2.1.4.1 Wetland

Although wetlands are often wet, a wetland might not be wet year-round. In fact, some of the most important wetlands are only seasonally wet. Wetlands are the link between the land and

the water. They are transition zones where the flow of water, the cycling of nutrients, and the energy of the sun meet to produce a unique ecosystem characterized by hydrology, soils, and vegetation—making these areas very important features of a watershed. Using a watershed-based approach to wetland protection ensures that the whole system, including land, air, and water resources, is protected (US EPA, 2015). (Adhikari & Babu, 2008) explains the floral diversity of Ban-ganga wetland originates near Bishenpur and flows in Idrishpur-Chakheri forest block of Haridwar district in Uttarakhand. (Islam et al., 2008b) developed a comprehensive methodology for mapping natural and human-made wetlands using fine resolution Landsat enhanced thematic mapper plus (ETM +), space shuttle radar topographic mission digital elevation model (SRTM DEM) data and secondary data. A semi-automated approaches were investigated; this involved the: enhancement of images through ratios to highlight wetlands from non-wetlands, display of enhanced images in red, green, blue (RGB) false colour composites (FCCs) to highlight wetland boundaries, digitizing the enhanced and displayed images to delineate wetlands from non-wetlands and classification of the delineated wetland areas into various wetland classes (Islam et al., 2008b). (S. Zhang, Zhang, & Zhang, 2000b) proposed a wetland classification model for a Sanjiang Plain, the geographic analysis and the model establishment are described in the (S. Zhang et al., 2000b). (De Roeck et al., 2008b) it provides the ecologically relevant information on characteristics of temporary and permanent isolated open water wetlands, obtained by standard techniques and relatively cheap imagery. The number, surface area, nearest distance, and dynamics of isolated temporary and permanent wetlands were determined for the Western Cape, South Africa (De Roeck et al., 2008b).

2.1.4.2 Edge detection

The detection of edges in an image has been an important problem in image processing for more than 50 years. In a gray level image, an edge may be defined as a sharp change in intensity. Edge detection is the process which detects the presence and locations of these intensity transitions. The edge representation of an image drastically reduces the amount of data to be processed, yet it retains important information about the shapes of objects in the scene (Basu, 2002). Over the years, many methods have been proposed for detecting edges in images.

(Zhu, 2011) used multi-structure elements morphology and image fusion for the edge detection. Edges are detected using four different orientations SE (structure element) where direction angles of all the structure elements are 00, 450, 900, 1350 and final edge result is got by image fusion using entropy weighted method(Ang, Ang, Xiaolin, & Yan-kui, 2011; N. Kaur, 2012). The eight different edge detection results are obtained by using morphology gradient algorithm and final edge results are obtained by using synthetic weighted method described in (NagaRaju, NagaMani, rakesh Prasad, & Sunitha, 2011).

(Priyadarshini & Sahoo, 2010) is based upon simple arithmetic and logic operations, consisting of three procedures: image binarization, image contraction and image subtraction. It uses of a threshold that is computed automatically during the edge detection process and its simple to compute the threshold value.

A new approach based on cellular automata has proposed by (T. Kumar & Sahoo, 2010). The algorithm will correspond to edge detection for grayscale images. The proposed conception of cellular automata for k grey levels of digital images is on the basis of bi-dimensional cellular automata.

Gradient and standard deviation of pixels value, which both forms a two set of edges which are considered as inputs for fuzzy system and then based on fuzzy logic, final decision is made by fuzzy system about whether each pixel is edge or non-edge according to 5 fuzzy rules and fuzzy membership functions (Institute of Electrical and Electronics Engineers et al., 2009; E. M. Kaur, 2011; Vikram, Upashyaya, Roshan, & Govardhan, 2010).

Ant colony optimization (ACO) based edge detection approach is an optimization algorithm based on real ants' behavior and inspired by the natural behaviour of ant species. In real life, ants deposit pheromone on the ground in order to mark the path they used that should be followed by other members of the colony. The proposed algorithm establishes a pheromone matrix, which represents the edge information at each pixel position of the image. For this number of ants are dispatched to move on the image driven by the local variation of the image's intensity values (J. Zhang, He, Zheng, & Zhou, 2010). This is combined with gradient and relative difference of statistical means to image edge detection is proposed in (Tian, Yu, & Xie, 2008). The values of gradient and the relative difference of statistical means are extracted for the ants' searching.

Sobel edge detection operator and soft-threshold wavelet de-noising for edge detection are combined in the and proposed an improved method in (Gao, Zhang, Yang, & Liu, 2010). This method used on images which include White Gaussian noises. The widely used operators such as Sobel, Prewitt, Roberts and Laplacain are sensitive to noises and their anti-noise performances are poor. Firstly soft-threshold wavelet used to remove noise, then Sobel edge detection used for edge detection on the image(N. Kaur, 2012). The Sobel and Prewitt detectors (Pratt, 2001; Rosenfeld & Kak, 1982), used local gradient operators which only detected edges having certain orientations and performed poorly when the edges were blurred and noisy. It should be mentioned here that one can combine such directional operators to approximate the performance of a rotationally invariant operator. Since then, more sophisticated operators have been developed to provide some degree of immunity to noise, to be non-directional, and to detect a more accurate location of the edge (SINGH, 2014). The majority of these are linear operators that are derivatives of some sort of smoothing filter. Shen and Castan (Shen & Castan, 1993) used a symmetrical exponential filter in edge detection. However, since it was originally proposed by Marr and Hildreth in 1980 (Marr & Hildreth, 1980). (Nadernejad, Sharifzadeh, & Hassanpour, 2008; Ziou, Tabbone, & others, 1998) Sobel operator technique, Roberts Cross Edge Detector, Prewitt technique, Laplacian technique and Edge Maximization Technique (EMT), Marr Hildrith and Canny operators the results and accuracy attained are represented in (K. Kaur & Malhotra, 2013; Oskoei & Hu, 2010; Rashmi, Kumar, & Saxena, 2013).

A nonparametric and unsupervised method of automatic threshold selection for image segmentation is presented in (Otsu, 1975). An optimal threshold is selected by the discriminant criterion, namely, so as to maximize the separability of the resultant classes in

grey levels. The procedure is very simple, utilizing only the zeroth- and the first-order cumulative moments of the grey-level histogram. It is straightforward to extend the method to multi-threshold problems. This method has been devised using the concept of genetic algorithm in spatial domain in (J.K & Ghosh, 2013). The key of edge detection is the choice of threshold; which determines the results of edge detection. GA has been used to determine an optimal threshold over the image. The threshold value detected in Otsu method is further applied to the canny by (Yu & Jiaxing-Xueyuan, 2009).

Internal self-diagnosis and external evaluation of the obtained results are of major importance for the relevance of any automatic system for practical applications. Obviously, this statement is also true for automatic image analysis in photogrammetry and remote sensing. In the present generation only automatic systems reached a state in which a systematic evaluation of the results seems to be meaningful. (Wiedemann, Heipke, Mayer, & Jamet, 1998) deals with the external evaluation of automatic road extraction algorithms by comparison to manually plotted linear road axes used as reference data. The comparison is performed in two steps: matching of the extracted primitives to the reference network; and calculation of quality measures. Each step depends on the other: The less tolerant is matching, the less exhaustive the extraction is considered to be, but the more accurate it looks. Therefore, matching is an important part of the evaluation process. The quality measures proposed for the automatically extracted road data comprise completeness, correctness, quality, redundancy, plani-metric RMS differences, and gap statistics. They aim at evaluating exhaustivity as well as assessing geometrical accuracy. The evaluation methodology is presented and discussed in detail (Wiedemann et al., 1998).

2.1.4.3 Extraction of water features by non-automation

The normalized difference water index (NDWI) has been successfully used to delineate surface water features and was based on the fact that water absorbs energy at near-infrared (NIR) and shortwave-infrared (SWIR) wavelengths. But, NDWIs calculated from different band combinations such as visible, near infrared, or shortwave-infrared (SWIR) can generate different results, and thresholds applying on NDWI vary depending on the proportions of sub pixel water or non-water components. Lei found that NDWI calculated from green and SWIR, where SWIR is the shorter wavelength region (1.2 to 1.8 mm), has the most stable threshold for delineate water features (Ji et al., 2009). (Z. Zhang et al., 2003) proposed an original entropy-based method for water body extraction from multi-source satellite images and this method is remarkably simple and relies only on the assumption that water body in the image is a smooth area. (Wang et al., 2008) proposed a model to extract inland water that includes wide river, lake and reservoir from high-resolution panchromatic images. Firstly directional variance is used to find river regions, and then grain table was adopted to avoid noise including objects that have similar directional variance characteristic as water surfaces. Jiancheng Luo proposed a step-by-step iterative transformation mechanism to extract water information from LANDSAT images, which uses spatial scale transformation mechanism of “whole-local” based on water index fitted from spectral library using spectral angle method first, and then fuses the hierarchical knowledge of water extraction and achieves the gradually approach of the water body’s optimal margin iteratively by combining the segmentation and classification at whole and local scales respectively and yields better accuracy and efficiency

to extract water features (Luo et al., 2010). Vijay S. Bhagat and Kishor R. Sonawane developed a methodology using Surface Wetness Index (SWI), Normalised Difference Vegetation Index (NDVI) and a slope map for the detection and delineation of water bodies in hilly zones form the Landsat Enhanced Thematic Mapper Plus (ETM^{+}) dataset (Bhagat & Sonawane, 2011). Nguyen Dinh Duong proposed algorithm has been developed based on three processes feature extraction, supervised and unsupervised classification and data fusion and successfully extracted water bodies from Spot 5 and Landsat 5 TM images (Nguyen Dinh Duong, 2012).

2.1.4.4 Extraction of water features by automation

Water is natural dynamic feature on the Earth surface and Wetlands play significant role in maintaining the ecological balance of both biotic and abiotic life in the present environment. Water resources planning and management requires data collection, analysis and monitoring of critical parameters like spatio-temporal water spread information and expected volumes. Temporal fluctuations in water resources can be studied through frequent spatial inventory of surface water bodies. Application of geospatial information technologies, namely Satellite Remote Sensing and Geographical information Systems (GIS), offer immense scope for replacing/supplementing the traditional monitoring methods (Subramaniam et al., 2011). Automated Water Extraction Index (AWEI), improving classification accuracy in areas that include shadow and dark surfaces that other classification methods often fail to classify correctly and they tested the accuracy and robustness of the new method using Landsat 5 TM images of several water bodies in Denmark, Switzerland, Ethiopia, South Africa and New Zealand. AWEI classifier was relatively more accurate in classifying edge pixels compared to the Modified Normalized Difference Water Index (MNDWI) and Maximum Likelihood (ML) classification methods. Besides, the optimal threshold of AWEI was shown to be less variable with images of different locations and times compared to that of MNDWI (Feyisa et al., 2014). (Nawaz et al., 2013)., proposed Whole-R method, that extracts water bodies with perfect edges and also filters out false water bodies and a high precise water body extraction is achieved with improved accuracy and this system needs no manual intervention throughout the extraction process (Nawaz et al., 2013). Hao Jaing proposed an automated method for extracting rivers and lakes (AMERL) for extracting mixed water pixels by considering not only their spectral characteristics, but also their topological connections. In this method, a series of processes have been introduced to filter out noise caused by shadows, roads and small segments by considering both their spatial and spectral characteristics and threshold optimization procedure is also simplified (Jiang et al., 2014). A knowledge based algorithm using hierarchical decision tree approach has been developed for automated extraction of wetland features such as surface water spread, wet area, turbidity and wet vegetation including aquatic for pre and post monsoon period and this approach yields satisfactory results for the state Chhattisgarh, India (Subramaniam et al., 2011).

2.2 Theoretical Concepts

In this division various theoretical concepts required for this study have been discussed briefly.

2.2.1 Spectral Signatures

To distinguish the objects or features from satellite images is difficult because of low spatial resolution, in that situation to differentiate the objects by spectral measurements. The spectral measurements are calculated in terms of spectral signatures. Spectral signature of a material or object or feature is defined in "the solar-reflective region by its reflectance as a function of wavelength, measured at an appropriate spectral resolution" (Schowengerdt, 2007). The main purpose of multispectral remote sensing is distinguish the objects on the basis of their spectral signatures.

When light is intercepted with an object or material then the light is reflected, refracted, transmitted and absorbed. The amount of light is reflected from an object is vary with the wave length of the electromagnetic spectrum. For example, the amount of reflected light from water, vegetation and soil, is shown in the figure. The graph between reflectance and wavelength is called the spectral characteristics of an object or material.

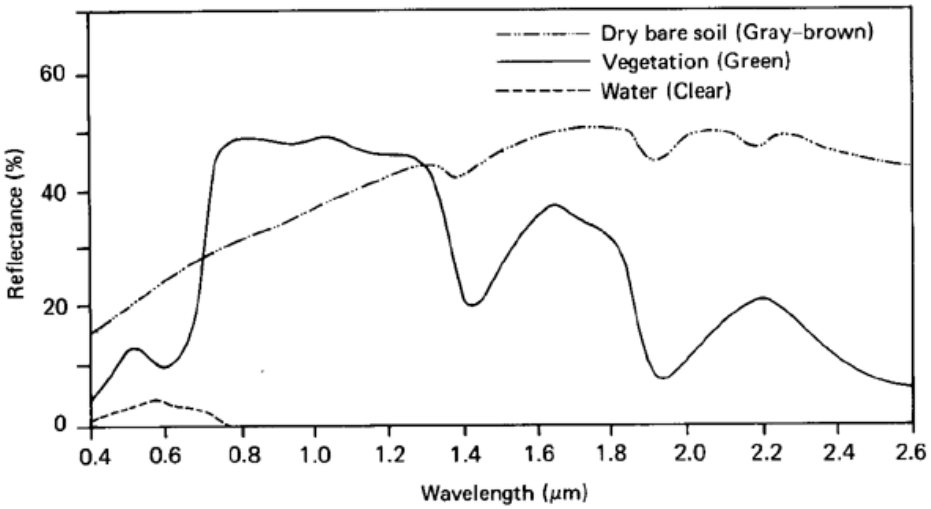

Figure 2–1 : Spectral characteristics of Water (clear), Vegetation (green) and dry bare soil (grey-brown)
(Source: ("The Mathematics of Satellite Images," 2015)).

2.2.1.1 Spectral Signature of water feature

Water immerses a wide spread of electromagnetic radiation due to electronic transition takes place in ultraviolet region, intramolecular vibrational transition in infrared region, far-infrared and microwaves has been absorbing the rotational transitions and intermolecular vibration in the water molecule. So, the water has low reflectance in visible region, and there is no reflectance or zero reflectance in near and short wave infra-red regions. The visible portion of electromagnetic spectrum contains blue band (400nm -500nm), green band (500nm-600nm) and red band (600nm-700nm) in this region water shows different percentage of reflectance value in the different bands. The water has very low reflectance in contrast to the other land features of the earth surface, the water absorbs higher wavelengths of light.

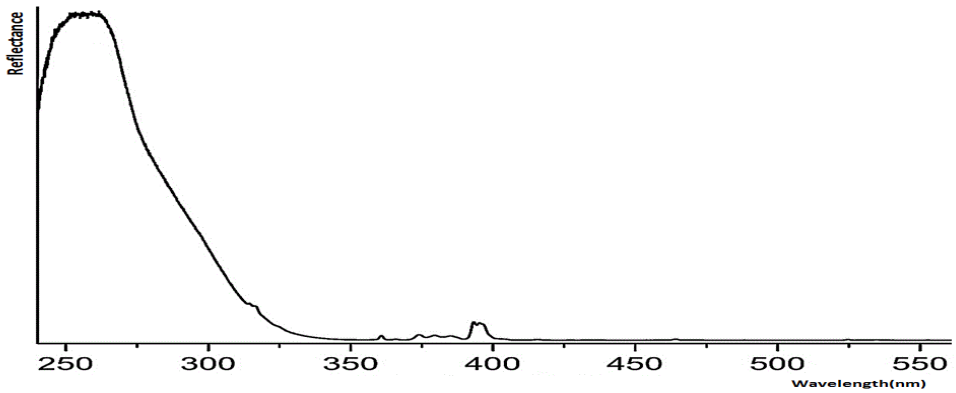

Figure 2–2 : Spectral characteristics of water

The water curve is characterised by a high absorption at near infrared wavelengths range and beyond. Because of this absorption property, water bodies as well as features containing water can easily be detected, located and delineated with remote sensing data. Longer wavelength visible and near infrared radiation is absorbed more by water than shorter visible wavelengths. Thus water typically looks blue or blue-green due to stronger reflectance at these shorter wavelengths, and darker if viewed at red or near infrared wavelengths. If there is suspended sediment present in the upper layers of the water body, then this will allow better reflectivity and a brighter appearance of the water. The apparent colour of the water will show a slight shift to longer wavelengths. Suspended sediment (S) can be easily confused with shallow (but clear) water, since these two phenomena appear very similar. Chlorophyll in algae absorbs more of the blue wavelengths and reflects the green, making the water appear greener in colour when algae is present. The topography of the water surface (rough, smooth, floating materials, etc.) can also lead to complications for water-related interpretation due to potential problems of specular reflection and other influences on colour and brightness ("Introduction to Remote Sensing," 2015).

2.2.2 Multispectral Ratios

The ratio of digital number (DN) of any two bands, pixel by pixel, in a set of multispectral bands of a sensor or in other bands the ratio of DN's of spectral band m to DN's of spectral band n, pixel by pixel, (Schowengerdt, 2007)

$$R_{m,n}(x,y) = \frac{DN_m(x,y)}{DN_n(x,y)} \qquad (2.1)$$

Where,

$R_{m,n}$ is the spectral ratio of band m and band n

DN_m and $DN_n$is the digital number of band m and band n

Generally, DN is the linear function of earth's surface reflectance. The multispectral ratio calculated from the digital numbers where it contains the topographic and atmospheric errors. To remove those errors, earth's surface reflectance is calculated, dependent upon the bias, gain and offset value of the sensor. Then the equation (1) rewritten in terms of reflectance as shown (Schowengerdt, 2007)

$$R_{m,n}(x,y) = \frac{\rho_m(x,y)}{\rho_n(x,y)} \quad (2.2)$$

Where,
ρ_m and ρ_n is the reflectance of band m and band n

When compared simple ratio the modulation ration is much useful, because the gain factor which is common in the both the bands are removed in modulation ration (Schowengerdt, 2007).

$$M_{m,n}(x,y) = \frac{\rho_m(x,y) - \rho_n(x,y)}{\rho_m(x,y) + \rho_n(x,y)} \quad (2.3)$$

Where,
$M_{m,n}$ is the modulation ratio of band m and band n

2.2.3 Spectral Indices

Remote sensing images have been used since quite a while for portraying and recognizing the land cover-land use classes exhibit in an area. Each class focused around its surface properties and structure reflects a particular measure of light incident on it, this special spectral property can be used to identify the same class that is introduced in the remote sensed image. This is carried out by classifying the reflectance properties of distinctive classes introduce on the land surface and afterward leading examinations to discover resemblances between known properties and obscure classes. Accordingly known classes can be used to allocate a class classifications to create class-cover maps of an area. In any case, the measure of solar radiance and the atmospheric conditions differs with time, such a basic system for characterization of classes utilizing reflectance properties alone is unrealistic in a rehashed way. For directing fleeting studies, for example, water mapping, vegetation mapping, change location, and so on the impacts because of atmosphere and time of image procurement need to be diminished. This issue can be illuminated to some degree by consolidating information from two or more spectral groups to structure the broadly used spectral indices.

Spectral indices are generally computed by rationing, differencing, summing, linearly combining, etc. data from two or more spectral bands. They are dimensionless and radiometric measures that are expected to minimize the solar irradiance and also it improves the spectral signature. The use of spectral indices can normalise the effects of differential illumination of features and also helps in the extraction of features of interest in an area. The different multispectral indices are used for the different applications, in that some of indices are used in this research are explained below.

2.2.3.1 NDVI

The concept of normalized difference spectral index was proposed by Kriegler in 1969 (**paper**). The famous Normalized Difference Vegetation Index (NDVI) is first described by Rouse in 1973 (Rouse, Haas, Schell, & Deering, 1974), this was used for monitoring the vegetation in large area. The reflectance of vegetation in the red and infrared bands is high due to the chlorophyll content in leafs and leaf structure. Besides the water reflectance in red and infrared is very low because of absorption capacity of water for the higher wavelengths of light. From this observation, the high reflectance is considered as vegetation and low

reflectance is clear water. The NDVI is the ratio of difference between near infrared and red channels to the summation of these channels.

$$Normalized\ Difference\ Vegetation\ Index\ (NDVI) = \frac{\rho_{NIR}-\rho_{red}}{\rho_{NIR}+\rho_{red}} \quad (2.4)$$

The NDVI value ranges from the -1 to +1, values close to "+1" are treated as dense vegetation and "+1" is clear water features, as the turbidity level increases in the water the value of index shifts towards positive side.

2.2.3.2 NDWI

The Normalized Difference Water Index (NDWI) was first proposed by McFeeters in 1996 (McFeeters, SK, 1996). The water shows the high percentage of reflectance in green band contrast to the near infra-red (NIR), and short wave infra-red (SWIR) bands, these band combinations are used for the partition of water feature from other land features of the earth surface by using the appropriate threshold factor for the NDWI (Subramaniam et al., 2011). The NDWI varies from -1 to +1. The NDWI is the ratio of difference between green band and the NIR band to the sum of these bands.

$$Normalized\ Difference\ Water\ Index\ (NDWI) = \frac{\rho_{Green}-\rho_{NIR}}{\rho_{Green}+\rho_{NIR}} \quad (2.5)$$

2.2.3.3 MNDWI

The Modified Normalized Difference Water Index (MNDWI) is the ratio of difference between the reflectance values of green band and middle infrared bands to the sum of same bands. MNDWI mostly used in the where built-up area and water is almost mixed, the value of MNDWI is ranges from the -1 to +1. This MNDWI has introduced by the HANQIU XU in 2006 (Xu, 2006) on making the assumption of were values of built-up area are occurred in the negative range. The mathematical equation is as shown

$$Modified\ Normalized\ Difference\ Water\ Index\ (MNDWI) = \frac{\rho_{Green}-\rho_{MIR}}{\rho_{Green}+\rho_{MIR}} \quad (2.6)$$

Where in NDWI, MNDWI, and NDVI ρ_{Green} represents the reflectance of green band (band number is different for different sensors), ρ_{NIR} represents the reflectance of NIR band (band number in different sensor), ρ_{Red} represents the reflectance of red band and ρ_{MIR} is the reflectance of MIR band (band number in different sensor).

2.2.3.4 NDPI

The Normalized Difference Pond Index (NDPI) has first used by the Lacaux in 2006 for the detection of small ponds from the high resolution images. It is also used for the distinguish vegetation present inside ponds to that of environs. The NDPI is the ratio of difference between Digital Numbers (DNs) of MIR and green bands to the summation of these bands DNs (Lacaux et al., 2007). The relation mathematically represented as

$$Normalized\ Difference\ Pond\ Index\ (NDPI) = \frac{\rho_{MIR}-\rho_{Green}}{\rho_{MIR}+\rho_{Green}} \quad (2.7)$$

2.2.3.5 NDT

The Normalized Difference Turbidity Index (NDTI) has first used by the Lacaux in 2006. This is the ratio of difference between DNs of red and green bands to their summation (Lacaux et al., 2007). The mathematical relation is represented as

$$Normalized\ Difference\ Turbidity\ Index\ (NDPI) = \frac{DNs_{Red}-DNs_{Green}}{DNs_{Red}+DNs_{Green}} \quad (2.8)$$

2.2.3.6 SWI

The Surface Wetness Index (SWI) used by (Bhagat & Sonawane, 2011) for delineation of water bodies in hilly zones using Landsat ETM+, as modified for our research to delineate the snow/ice from Landsat 8 OLI using the wetness coefficients generated by (Baig et al., 2014). The modified formula used in this research as represented below

$$Surface\ Wetness\ Index\ (SWI) = \big((\rho_{Blue} * 0.1511) + (\rho_{Green} * 0.1973) + (\rho_{Red} * 0.3283) + (\rho_{NIR\ Red} * 0.3407) + (\rho_{SWIR1} * -0.7117) + (\rho_{SWIR2} * -0.4559)\big) \quad (2.9)$$

2.2.4 Images pre-processing

The satellite images which are provided to the users are directly not suitable for the processing, because it has atmospheric noise (clouds, fog, etc.), tilt in sun angle, and topography noise (radiance variation due to undulations in topography, etc.). Pre-processing of the images have to be done to remove or correct these noises. Several steps are involved in image pre-processing, in first step, images which are provided to user are simply Digital Numbers (DNs) which doesn't have any units and it is totally dependent on the sensor gain and offset values. Sensor calibration information is required to measure the radiance at sensor called sensor calibration. Second step, measuring radiance at earth surface from radiance at sensor requires information about atmospheric conditions at the time and location when the image is captured by the sensor. With the help of atmospheric models (contains information about the atmosphere) radiance at earth surface have been measured. In final step, topography noise correction due to the variation in the slope and aspect. This entire process is known as radiometric calibration (Schowengerdt, 2007).

Atmospheric correction required information about atmospheric conditions at that time and position capture of image by the satellite sensor. Now a days, a number of atmospheric correcting methods or techniques are of three sorts, models based on radiative transfer like, FLAASH, SMAC, 6S, MODTRAN, ATCOR, ACORN, ATREM, etc., relative correction models depends on image characteristics like, DOS, Flat Field Correction, PIF, QUAC, etc., and regression models like general linear regression, wavelet regression, Fourier regression, etc., are there to reduce the atmospheric effects from satellite images.

Radiative transfer models needs information other than satellite data like atmospheric information at the time of capture and it also considers variation in topography. Relative correction models doesn't requires the atmospheric data, to correct atmospheric correction, atmospheric parameters has been collected from the satellite image itself. Regression models also as relative correction and it doesn't require any ancillary data, in this model calculation of regression lines for the number of spectrally deviated surface materials.

2.2.5 Canny Edge detection

The Canny edge detection algorithm is known to many as the optimal edge detector. It was formulated with three main objectives:

1. Optimal detection with no spurious responses
2. Good localization with minimal distance between detected and true edge position
3. Single response to eliminate multiple responses to a single edge.

The first requirement aims to reduce the response to noise. This can be effected by optimal smoothing; Canny was the first to demonstrate that Gaussian filtering is optimal for edge detection (within his criteria). The second criterion aims for accuracy: edges are to be detected, in the right place. This can be achieved by a process of non-maximum suppression (which is equivalent to peak detection). Non-maximum suppression retains only those points at the top of a ridge of edge data, while suppressing all others. This results in thinning: the output of non-maximum suppression is thin lines of edge points, in the right place. The third constraint concerns location of a single edge point in response to a change in brightness (Canny, 1986). This is because more than one edge can be devoted to be present, consistent with the output obtained by earlier edge operators (Zhou, Ye, Xia, & Wang, 2011).

2.2.6 GIS Terminology used

2.2.6.1 Scale

The world can never be studied, modelled, or represented in all of its full detail and complexity. Scale is important in part because of its consequences for the extent to which geographic information is generalized.

Generalization refers to the amount of detail included in information; it is essentially an issue of simplification, but also includes aspects of selection and enhancement of features of particular interest. As one studies or represents smaller pieces of the earth, one tends strongly to deal with more detailed or finer grained aspects of geographic features. Studied most extensively by cartographers, generalization is in fact relevant to all three meanings of scale, and to all three domains of spatial, temporal, and thematic scale.

Cartographic scale is becoming 'visualization' scale. How is scale, spatial and temporal, communicated in dynamic, multidimensional, and multimodal representations, including visualization in virtual environments? Progress continues on the problem of automated generalization, programming intelligent machines to make generalization changes in geographic data as scale changes. The ability to perform multi-scale and hierarchical analysis will be developed further(D. R. Montello, 2015.).

Scale generally defined as the ratio of a distance on the map to the corresponding distance on the ground or in other terms the relationship of the distance on the map/data to the actual distance on the ground or mathematically scale is represented as

$$Scale = \frac{Distance\ on\ the\ map}{Distance\ on\ the\ ground} \qquad (2.10)$$

2.2.7 Relation between Scale and Resolution

In 1987, Waldo Tobler, a famous cartographer given the relation between resolution and scale as “The rule is: divide the denominator of the map scale by 1,000 to get the detectable size in meters. The resolution is one half of this amount”(Tobler, 1987). Tobler given relation note “Of course the cartographer fudges. He makes things which are too small to detect much larger on the map because of their importance. But this cannot be done for everything so that most features less than resolution size get left off the map. This is why the spatial resolution is so critical” (Tobler, 1987) (Tobler, 1988) (ArcGIS, 2010).

Similarly, if you need to find out the mapping scale from a known imagery resolution you can do so using the formula below:

Map Scale = Raster resolution (in meters) * 2 * 1000 (2.16)

Table 2-1 : Resolution and scale

Scale	Detectable Size (m)	Raster Resolution (m)
1:1,000	1	0.5
1:5,000	5	2.5
1:10,000	10	5
1:50,000	50	25
1:100,000	100	50
1:250,000	250	125
1:500,000	500	250
1:1,000,000	1,000	500

(Source: (ArcGIS, 2010))

2.2.8 Cartosat – DEM

Indian Space Research Organization (ISRO) prepared a National DEM for entire India by using the Cartosat – 1 stereo payload (launched in May 2005 through) is known as Cartosat – 1 Digital Elevation Model in short Carto-DEM. The Cartosat – 1 can acquire stereo image data through a pair of Panchromatic cameras having an along track stereoscopic capability using its near-nadir viewing and forward viewing telescopes with a base-to-height ratio of about 0.63. The spatial resolution of cartosat – 1 in a horizontal plane is 2.5m and swath about 27km.

The methodology adopted to produce the Carto-DEM involved stereo-strip triangulation of 500km strip stereo pairs using high precise ground control points, interactive cloud masking, and automatic dense conjugate pair generation using matching approach. Seamless homogeneous DEM is produced by TIN modelling of irregular DEM, interpolation for regular DEM generation and automatic strip to strip mosaicking. These automatically generated DEM tiles are further evaluated for quality and tile editing to remove anomalies. Carto-DEM products are extremely useful in contour generation; drainage network analysis; quantitative analysis of run-off and soil erosion; volume-area calculations; design of hydraulic structures; design of new road, rail and pipeline alignments; watershed planning; urban utility planning; landslide zonation; river configuration studies and flood proofing; and fly through visualization; etc, (NRSC, 2013)**.**

3. Study area and materials

This chapter gives detailed information about the study area required for this research, datasets, Instruments and finally the computer system with the useful image processing and GIS software's. This chapter has two sections one is study area and another one is the materials required for this research.

3.1 Study Area

Uttarakhand has formed on 09th November 2000 separated from the Uttara Pradesh and it is the 27th state in the Republic of India and also in 10th in the Himalayan region. Uttarakhand is located between 28^0 43' – 31^0 27' North latitudes and 77^0 34' – 81^0 02' East longitudes. The total geographical area of the state is 53,483 sq. km., of which is approximately 89% is mountains and 19% of the geographical area is under permanent snow cover, glaciers and steep slopes. The state as two National and two international boundaries the national boundaries are river Tons separates the state from the Himachal Pradesh in the northwest, and foot-hills of the grater Himalayas in the south are bounded to the Uttara Pradesh. It has two international boundaries, the river Kali separates Nepal in the east and the greater Himalaya is the northern boundary of the state with China (Tibet) (Pal, 2015).

Uttarakhand predominantly a hilly area, due to this it has varied hydrological setups can be divided broadly into two distinct hydrogeological regimes, the Gangetic alluvial plain and the Himalayan mountain belt. The former is covered with a vast expanse of alluvium and unconsolidated sedimentary material of varying size fractions (ranging from boulder to clay) and is a promising zone for ground water development. The latter zone, being predominantly hilly, offers much less potential for large scale development of ground water. Ground water in the hilly region occurs mostly in fissures/fractures and emerges as springs (Pal, 2015). The springs are amenable to small scale development of ground water resources in the State.

Major River Basins and Sub Basins

The main drainage system of Uttarakhand have been grouped into following six catchments:

Yamuna Catchment - The Yamuna river originates from the base of Bandarpunch peak. It has carved a deep V- shaped gorge. The Yamuna cuts across the Nag Tibba range and Mussoorie range near a place called Yamuna bridge (Pal, 2015). The rivers Tons, Pabar and Aglar are its important tributaries. It passes through the Doon valley on its Western boundary.

Bhagirathi Catchment – This is one of the two rivers which join to form the river Ganga. It originates from the snout of the Gangotri glacier at Gaumukh which is at the base of Chaukhamba peak. The Bhagirathi river has cut a deep gorge across the granitic rocks of the higher Himalayas of Garhwal. Its main tributaries are the river Janhavi and the Bhilangana (Pal, 2015).

Alaknanada Catchment - This river joins the river Bhagirathi at Devprayag to form the river Ganga. It originates from the eastern slopes of Chaukhamba – from the Bhagirathi kharak and Satopanth glaciers. The river flows along the Badrinath temple. Its main tributaries are the Khiraonganga, Pindar Dhauliganga, Birahi, Nandakini, Mandakini etc. It has formed a broad valley at Srinagar (Garhwal) (Pal, 2015).

Mandakini Catchment - It comes out from the Mandakini glacier near Kedarnath. It cuts through a gorge of glacial debris. The river has formed road terraces at Augustmuni and Tilwara. At Tilwara it is joined by the river Lastar Gad(Pal, 2015). The river Mandakini joins the river Alaknanda at Rudraprayag.

Pindar Catchment- The river Pindar originates from the Pindari Glacier which is located between Nanda Devi and Nanda kot peaks. Sundardhunga river joins the Pindar near Dhakuri. The Pindar joins the river Alaknanda near Karanprayag (Pal, 2015).

Kali Catchment – The river Kali forms the boundary between Kumaon and Nepal. The Towns of Champawat and Pithoragarh are situated on the back of the Kali river. Its important tributaries are Darma and Saryu rivers (Pal, 2015).

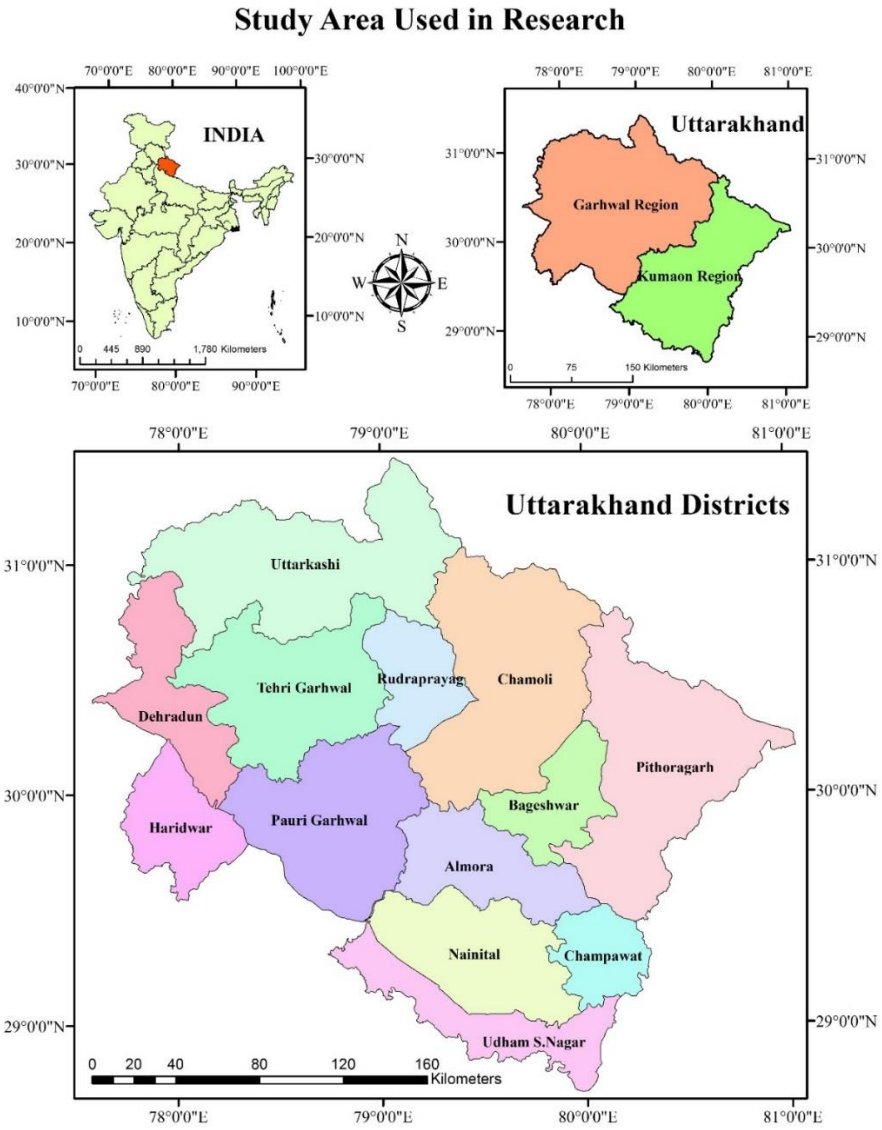

Figure 3-1 : Field Based Study Area of the Project

3.2 Materials

This section explains the details of the used datasets, requirements of software to process the datasets and used instruments in the field for validation purposes.

3.2.1 Datasets

The study area has utilized the Landsat 8 payload Operational Land Imager (OLI) datasets and Resourcesat-2 payloads Linear Imaging Self Scanning sensor (LISS-III) and a high resolution multi-spectral sensor LISS-IV. The required details for this research about the sensors has given below Table 3-1 acquired from (Landsat Team, 2012; Resourcesat-2 Project Team, ISRO, 2011).

Table 3-1: Details of Sensors

Datasets	Spatial Resolution (m)	Radiometric Resolution (bits)	Bands	Wavelengths (µm)
Landsat 8 OLI	30	16	Band – 2 Blue Band – 3 Green Band – 4 Red Band – 5 NIR Band – 6 SWIR Band – 7 SWIR	0.450 – 0.515 0.525 – 0.600 0.630 – 0.680 0.845 – 0.885 1.560 – 1.660 2.100 – 2.300
LISS – III	23.5	10	Band – 2 Green Band – 3 Red Band – 4 NIR Band – 5 MIR	0.52 – 0.59 0.62 – 0.68 0.77 – 0.86 1.55 – 1.70
LISS – IV	5.8	10	Band – 2 Green Band – 3 Red Band – 4 NIR	0.52 – 0.59 0.62 – 0.68 0.77 – 0.86

To cover entire Uttarakhand for the Landsat 8 OLI sensor requires five datasets the details of the used datasets are given below Table with less cloud cover and the scenes are belongs to the same season.

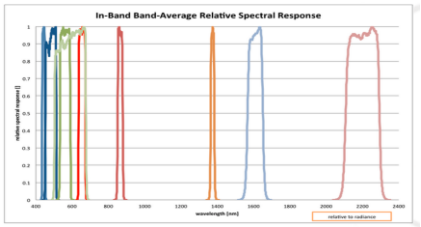

Figure 3-2 : Spectral Response of Landsat 8
(Source :(J. A. Barsi, Markham, & Pedelty, 2011; J. Barsi, Lee, Kvaran, Markham, & Pedelty, 2014))

Table 3-2 : Used Landsat 8 OLI sensor datasets

S.No.	landsat Scene ID	Path	Row	Year	Julian Day	Day	Month	Year
1	LC81440392013343LGN00	144	39	2013	343	9	Dec	2013
2	LC81450392013334LGN00	145	39	2013	334	30	Nov	2013
3	LC81450402013334LGN00	145	40	2013	334	30	Nov	2013
4	LC81460382013325LGN00	146	38	2013	325	20	Nov	2013
5	LC81460392013341LGN00	146	39	2013	341	7	Dec	2013

For the LISS – III and LISS – IV selected datasets are used. The information about these datasets used in this research is given below Table.

Table 3-3 : Used LISS –III datasets of Resourcesat – 2

S.No.	Product ID	Path	Row	Orbit No	Day	Month	Year
1	143642811	96	49	13513	26	Nov	2013
2	143642821	96	50	13513	26	Nov	2013
3	143642841	97	50	13584	1	Dec	2013
4	143642851	98	49	13996	30	Dec	2013
5	143642861	98	50	13996	30	Dec	2013
6	143642871	98	51	13996	30	Dec	2013
7	143642881	99	50	13726	11	Dec	2013

Table 3-4 : Used LISS – IV datasets of Resourcesat – 2

S.No.	Product ID	Path	Row	Scene	Orbit	Day	Month	Year
1	143642891	96	49	B	13172	2	Nov	2013
2	1436428131	97	50	B	13584	1	Nov	2013
3	1436428141	97	50	A	15289	31	Mar	2014
4	1436428151	97	50	D	13584	1	Dec	2013
5	1436428161	97	50	C	15289	31	Mar	2014
6	1436428171	98	50	A	13996	30	Dec	2013
7	1436428191	98	50	D	13655	6	Dec	2013
8	1436428201	98	51	B	13655	6	Dec	2013
9	1436428211	98	51	A	13996	30	Dec	2013
10	1436428221	97	51	B	14948	7	Mar	2014
11	1436428231	96	50	B	12490	15	Sep	2013
12	1436428251	96	50	C	13513	26	Nov	2013
13	1436428261	97	49	A	12561	20	Sep	2013
14	1436428281	97	49	D	13584	1	Dec	2013
15	1436428301	98	49	C	13996	30	Dec	2013
16	1436428321	98	49	D	16383	16	Jun	2014
17	1436428331	99	50	A	13385	17	Nov	2013

3.2.2 Computer System and Software

The computer system is suitable for remote sensing and geographical information system software listed below in table

Table 3-5 : List of software

Software/Tool	Purpose
ERDAS 2014	To process the images and also for visualization
ESRI ArcGIS 10.2	To prepare maps and also used for visualization
Envi 5.1	For pre-processing images
eCognition Developer 8	To develop the rules for river and canal network
PyCharm	IDE used for the developing python tool

3.2.3 Hardware Instruments

The hardware instruments used in field to collect data are listed below in table

Table 3-6 : Information about Instruments

Instruments	Purpose
Leica Zeno 5 GPS Handheld	To collect the GPS points for validation
SVC HR 1024	To collect spectra for classifying the water features

3.2.3.1 SVC HR 1024

Spectra Vista Corp (SVC) has developed a HR 1024 instrument. Which is a high performance single beam field spectroradiometer. It collects the spectral signatures over a range from visible to short wave infra-red (SWIR) wavelength. It has features low noise indium gallium arsenide (InGaAs) photodiode arrays for the SWIR spectrum, higher resolution throughout, a robust compact light weight housing and wireless communication to laptop or PDA computers("FSF: SVC HR-1024 Field Spectroradiometer," 2015).The specification of the instrument as mention below table.

Table 3-7 : Specification of SVC HR 1024

Specifications	
Spectral Range	350-2500 nm
Sampling Interval	1.5 nm, 350-1000 nm 3.8 nm, 1000-1890 nm 9.5 nm, 1890-2500 nm
Spectral Resolution (FWHM)	3.5 nm @ 700 nm 9.5 nm @ 1500nm 6.5 nm @ 2100 nm
Scanning Time	Automatic with programmable options or manual control. Typical multi-scan acquisition time <10 seconds
Fore Optic Lenses	Field of View 4°, 7°, 14°
Digitisation	16 bit

3.2.3.2 Leica Zeno 5 GPS Handheld

Leica Zeno 5 GPS handheld receiver is used for finding the GPS positions, it has a better accuracy compared to the other handheld GPS. It is an ergonomic device with full phone functionality.It has ahigh-speed processor, delivering uncompromised performance, fully integrated into the Leica Zeno GIS series ("Leica Zeno 5 - GPS Handheld - Leica Geosystems - India," 2015.). The specification of the instrument as mention below table.

Table 3-8 : Specification of Leica Zeno 5 GPS Handheld

Specifications	
Processor	Industrial TI AM3715 Sitara microprocessor (ARM Cortex A8) @ 800 MHz
Integrated GPS	1. SirfStarIV GPS with SiRFInstantFix and A-GPS support (48 channel) and active jammer removal 2. GPS Real-Time Accuracy: 2 – 5 m / SBAS (WAAS, EGNOS, MSAS, GAGAN)*: 1 – 3 m
Integrated communication modules	1. On-board IEEE 802.11a/b/g/n (CCX V4 Certified) radio: i. Security: 802.1X, WPA / WPA2-Enterprise ii. Authentication: FAST-MSCHAPv2; LEAP; PEAPv0-MSCHAPv2; PEAPv1-GTC; TLS iii. Encryption: 64/128 WEP, AES-CCMP, TKIP 2. Bluetooth® v2.0 + EDR radio 3. UMTS 3.8G HSPA+ radio i. Five Band UMTS: 800/850, AWS, 1900, 2100 MHz ii. Quad-Band GSM: 850, 900, 1800, 1900 MHz 4. CDMA EVDO Rev A radio i. Dual Band: 800/1900 MHz 5. Integrated 5 band Antenna, supports both voice and data
Operating System	Microsoft Windows® Embedded Handheld 6.5.3
Optional GNSS Sensors	Leica Zeno GG02 plus SmartAntenna
Optional Software	1. Leica Zeno Field 2. Leica Zeno Connect

Note: * WAAS available in North America only, EGNOS available in Europe only; GAGAN available in Indian Subcontinent only; MSAS available in Japan only

3.2.4 Field Data

The field survey was carried out for collecting the ground truth points through the Leica Zeno 5 GPS Handheld. These points are used for the validating the results, and also the visual interpretation which type of water is present. The field spectra which is collected by the spectro-radiometer is used for the classification of the water features. The field spectra collected is a continuous with a 1nm resolution over a range of 350nm to 2500nm. This raw spectra is not suitable for classification, so resample the spectral features according to the

wavelength of the data. The resampled spectral library is used for the classification of different water features.

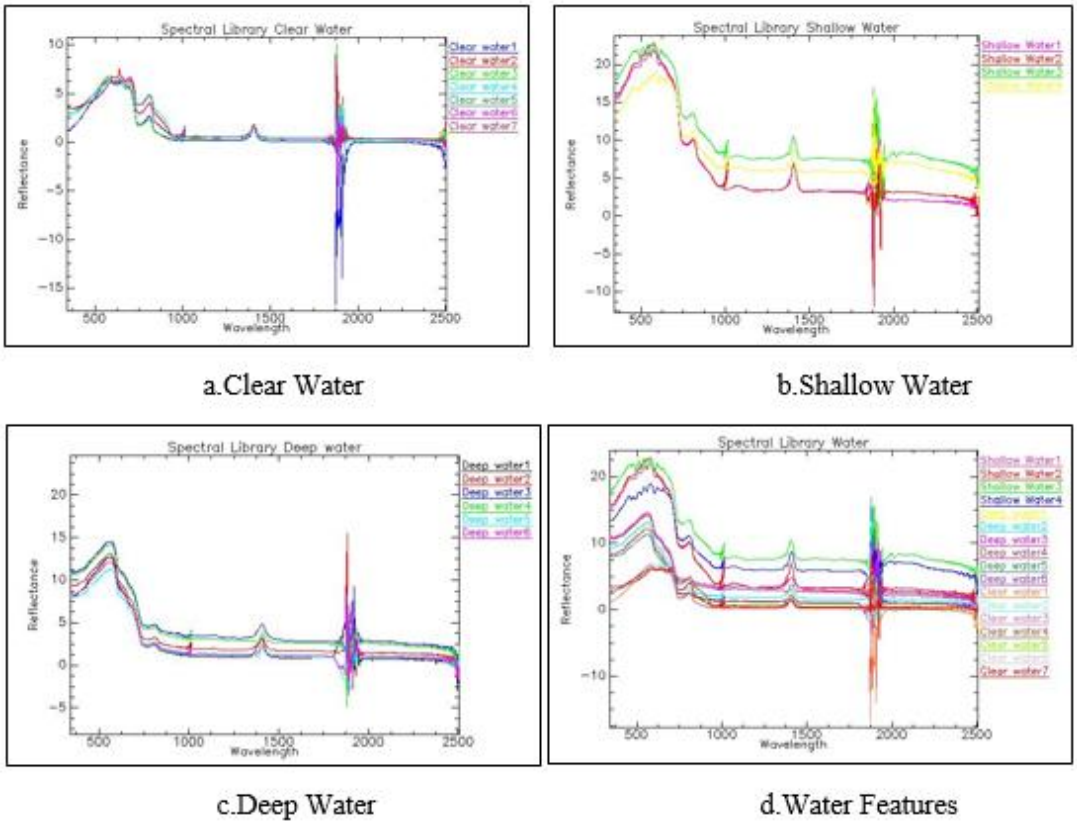

Figure 3-3 : Spectral Libraries of water features

Figure 3-4 : Field photos

4. Methodology

This chapter introduces the research process for performing the extraction of water feature at variable scales using the multi-resolution data.

The sequence of approach has been divided into the four different phases

Phase – 1 Images pre-processing

Phase – 2 Extraction of water features at variables scales

Phase – 3 Extracting and classifying the water feature at higher resolution images

The first phase explains the image pre-processing that comprises image to image registration and conversion of digital number or raw data to the surface reflectance called calibration. Second phase describes extraction of water features on small scales by combining of slope information with spectral information. The final phase illuminates with the classification of water classes on the high resolution images to prepare large scale maps.

4.1 Experimental Approach

This section gives an outline or summary of the research mechanism embraced for this study. The flowchart of the investigated approach followed for this is demonstrated in figure 4.1. The elaborated clarification of the adopted methodology succeeded for extraction the water features at variable scales using the multi-resolution is clarified in the accompanying sections of this chapter.

The major objective of the research is to estimate a range of optimum threshold values for extracting water features from different multispectral sensors of low and coarser resolution. To do this, first of all the available images from the different multi-resolution sensors LISS – IV, LISS – III, Landsat – 8, AWiFS, and OCM were pre-processed using image to image registration and radiometric calibration. After finding the optimized threshold values from the normalized values of the different sensors, and then combined with the slope map generated from the cartoDEM. In this combination the steep to precipitous slope are subtracted to extract water features from the low resolution raster data. The extracted water feature raster data is to mask over lay on the high resolution datasets for extracting the water from the high resolution data. Extracted water features are classified using the spectral signatures to prepare the large scale maps.

Keeping in view the complexity of the problem, the methodology was divided three parts they are image pre-processing, extraction of water feature at variable scales and extracting and classifying the water feature at higher resolution images. The broad methodology of the entire workflow is as shown in figure 4.1.

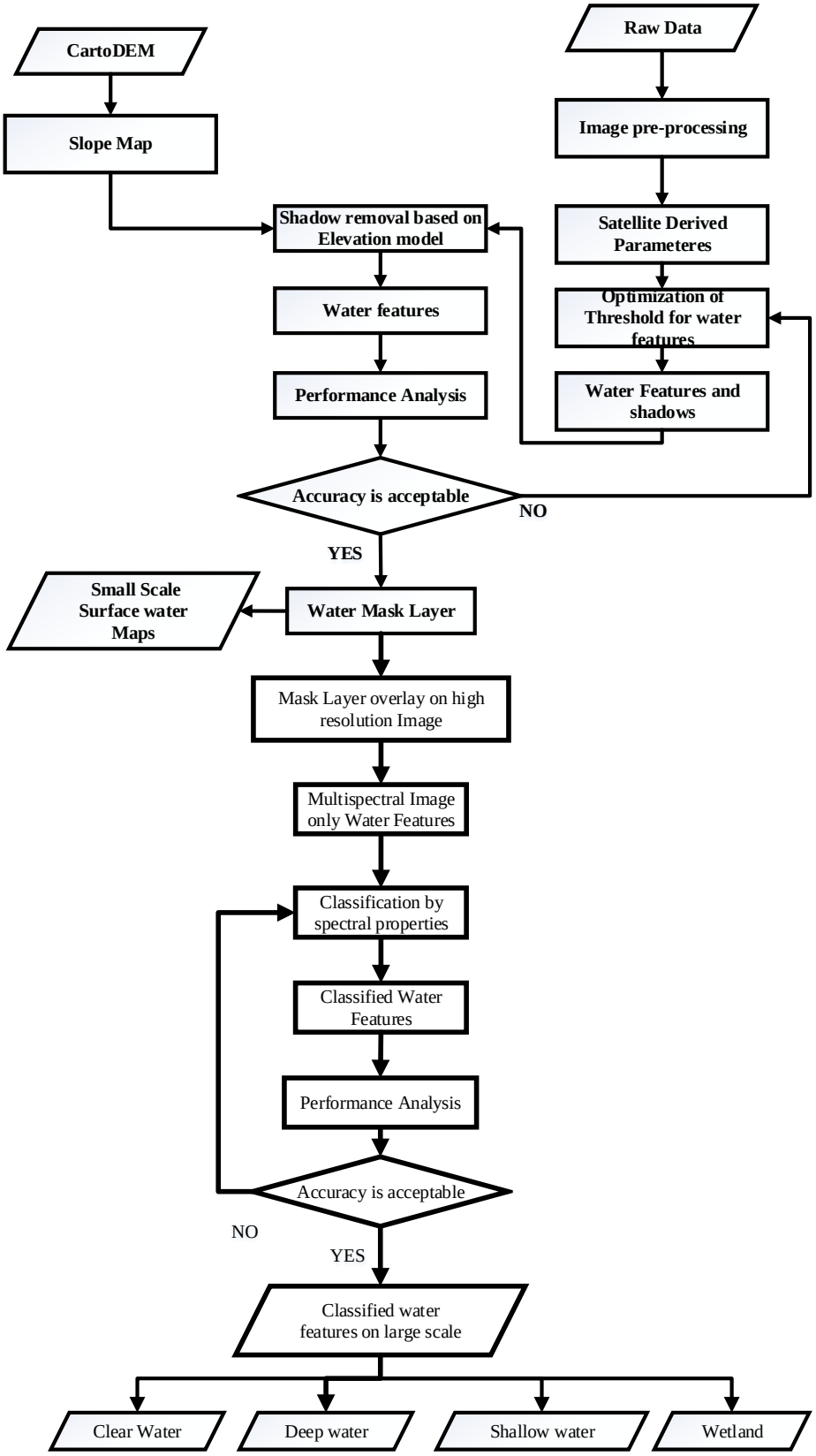

Figure 4-1 : Extraction of water features at variable scales.

4.2 Image pre-processing

The satellite sensors records the data as radiance and stores in the form DNs. To further process of data, these DNs are converted back to radiance and reflectance. The process of transformation from the DN to radiance and then reflectance is called radiometric calibration.

4.2.1 Radiometric Calibration

The radiometric calibration is the process of conversion from DNs to Radiance and reflectance. The procedure for calculating the radiance and reflectance is different for different sensors.

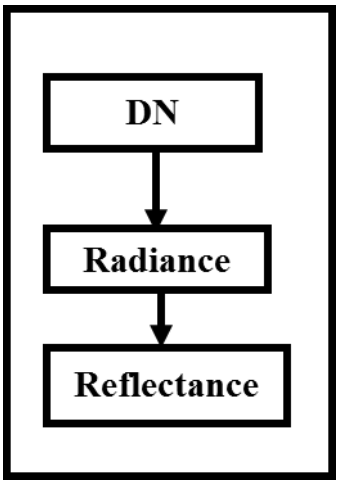

Figure 4-2 : Conversion of DN to Reflectance is Radiometric Calibration

4.2.1.1 Landsat-8

USGS EROS center provides the standard landsat 8 data comprise of quantized and aligned scaled Digital Numbers (DN) speaking to multispectral image information procured by both the Operational Land Imager (OLI) and Thermal Infrared Sensor (TIRS). The data products are conveyed in 16-bit unsigned integer format and can be rescaled to the Top Of Atmosphere (TOA) reflectance and/or radiance by applying radiometric rescaling coefficients (metadata file (MTL file)) in the mathematical relation of radiance eq(1) and reflectance eq(2) ("Using the USGS Landsat 8 Product," 2015).

4.2.1.1.1 Radiance

The OLI and TIRS bands are transformed for the DN to TOA spectral radiance using radiance rescaling factors by the following mathematical relation

$$L_\lambda = M_L Q_{cal} + A_L \ldots\ldots\ldots\ldots\ldots\ldots\ldots\ldots (3.1)$$

Where

L_λ is TOA spectral radiance (Watts/(m2 * srad* μm))

M_L is Bandspecific multiplicative rescaling factor (value of RADIANCE_MULT_BAND_x, where x is the band number in metada file)

A_L = Bandspecific additive rescaling factor (value of RADIANCE_ADD_BAND_x, where x is the band number in metada file)

Q_{cal} = Quantized and calibrated standard product pixel values (DN)

4.2.1.1.2 Reflectance

OLI bands are directly transformed from DN to TOA reflectance using the reflectance rescaling factors by the following computation.

$$\rho'_\lambda = M_\rho Q_{cal} + A_\rho \, A_L \ldots\ldots\ldots\ldots \quad (3.2)$$

Where

ρλ' = TOA planetary reflectance, without correction for solar angle.

M_ρ= Bandspecific multiplicative rescaling factor (value of REFLECTANCE_MULT_BAND_x, where x is the band number in metada file)

A_ρ = Bandspecific additive rescaling factor (value of REFLECTANCE_ADD_BAND_x, where x is the band number in metada file)

Q_{cal} = Quantized and calibrated standard product pixel values (DN)

TOA reflectance with a correction for the sun angle is then:

$$\rho_\lambda = \frac{\rho'_\lambda}{\cos(\theta_{sz})} = \frac{\rho'_\lambda}{\sin(\theta_{sz})} \ldots\ldots\ldots\ldots\ldots (3.3)$$

Where

ρλ = TOA planetary reflectance

θ_{SE} = Local sun elevation angle (scene center sun elevation angle) in degrees (SUN_ELEVATION).

θ_{SZ} = Local solar zenith angle; $\theta_{SZ} = 90° - \theta_{SE}$

4.2.1.2 Resourcesat sensors

The standard ortho metadata of Resourcesat-2 products provided by the NRSC Center consist of quantized and calibrated scaled Digital Numbers (DN) representing multispectral image data acquired by the Advanced Wide Field Sensor (AWiFS), Linear Imaging Self Scanning sensor (LISS-III) and a high resolution multi-spectral sensor (LISS-IV). The products are delivered in 10-bit unsigned integer format and can be rescaled to the Top Of Atmosphere (TOA) reflectance and/or radiance using radiometric rescaling coefficients provided in the product metadata file (MTL file).

4.2.1.2.1 Radiance

The standard ortho metadata of Resourcesat-2 products in 10-bits, this data products can be transformed from DN to radiance by using radiance rescaling factors (provided in the metadata file) applied in the following mathematical equation

$$L_\lambda \; or \; L_{rad} \; = \frac{DN_{10}}{1023}(L_{max} - L_{min}) + L_{min} \ldots\ldots\ldots (3.4)$$

Where

DN_{10} = 10-bit pixel value

Lmin = Minimum radiance value provided in scene metadata for each band

Lmax = Maximum radiance value provided in scene metadata for each band

L_λ or L_{rad}= TOA spectral radiance

4.2.1.2.2 Reflectance

The reflectance is calculated by using the radiance, Earth-sun distance, solar irradiance and Sun elevation. Sun elevation details is available in metadata file. The reflectance is calculated by the using the relation

$$\rho_\lambda = \frac{\pi L_\lambda d^2}{ESUN_\lambda * sin\theta} \text{.....(3.5)}$$

Where:

L_λ= Radiance in units of W/(m^2 * sr * µm)

d= Earth-sun distance, in astronomical units.

$ESUN_\lambda$= Solar irradiance in units of W/(m^2 * µm) in table-1

θ= Sun elevation in degrees

Table 4-1 : Solar irradiance values for different sensors

ESUN Units = W/(m^2 * µm) from ISRO			
Bands	LISS – IV	LISS – III	AWiFS
Band 2	1853.6	1849.5	1854.7
Band 3	1581.6	1553	1556.4
Band 4	1114.3	1092	1082.4
Band 5	-----	239.52	239.84

4.3 Extraction of Water Features

To delineate the water feature from radiometrically corrected multispectral images (LISS-III, Landsat-8, AWiFS, OCM) can be done, by finding the optimized threshold factors for multispectral indices (like NDVI, NDWI, MNDWI, NDPI, and NDTI) by adopting the slicing method. From this the water feature are extracted with shadows, to separate the shadows from this features by using the slope map which is generated from Cartosat-1 Digital Elevation Model (CartoDEM). The methodology adopted for extracting the water features is

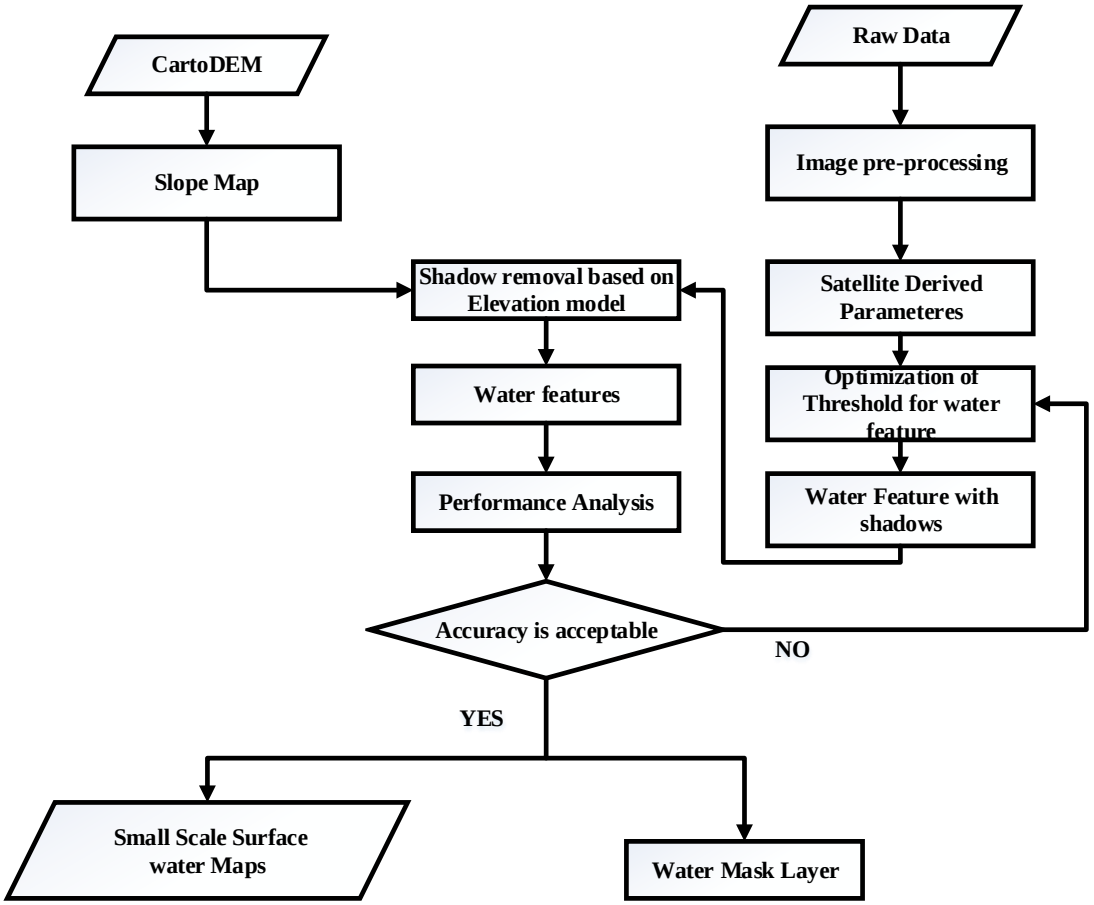

Figure 4-3 : Methodology for extraction of water features

4.3.1 Satellite derived parameters

There are a number of satellite derived parameters used for the different purposes among them NDWI, MNDWI, NDPI, SWI, and NDVI are used. These parameters are calculated independently for each sensor based on their band designations.

4.3.1.1 Calculating spectral indices

After pre-processing of initial raw datasets, Spectral indices are normally computed or figured by proportioning, differencing, summing, linearly combining, and so on, data from two or more spectral bands.

4.3.1.1.1 SWI

The SWI is used in this methodology is to separate the snow/ice in the hilly region. The threshold used for this delineation is 0.14. This threshold is used for the clean separation of snow from the hilly zone of this study area.

4.3.1.1.2 NDWI

The NDWI is utilized to depict open water features and upgrade their vicinity in remotely-sensed digital imagery. It is functions on the earth surface reflectance of green band and near infrared band to highlight water feature from the other features of earth surface.

To delineate water feature from the other surface feature of earth surface could be possible by choosing the appropriate threshold factor by the density slicing. When choosing threshold factor zero (0), for delineating the water from the other features of earth surface. From this ratio, where NDWI greater than zero (NDWI > 0) are treating as water features and NDWI less than or equal to zero (NDWI ≤ 0) are considered as other than water features. Here, some of urban or manmade features are also classified as water for the selected threshold factor, because of those features green band reflectance is less than the NIR band.

4.3.1.1.3 MNDWI

To overcome these drawbacks the NDWI is superseded by replacing the NIR band by the middle infra-red (MIR) or SWIR band then it is called as Modified Normalized Difference Water Index (MNDWI). In MNDWI, by physically setting the zero as a threshold factor could acquire more accurate result than the NDWI. However, seasonal vegetation cover over the water surface cannot identified, because, vegetation cover over the water is predominant, the reflectance of the vegetation cover in the infra-red (IR) region was very high.

4.3.1.1.4 NDPI

To conquer the snags of NDWI and MNDWI by transforming the MNDWI can get the Normalized Difference Pond Index (NDPI). The same threshold is used for the extraction of water feature, here seasonal vegetation cover on the water has been removed, because of the green band has taken off from the middle infrared band, where the reflectance of vegetation is high in the middle infrared band.

4.3.2 Slope generation

Slope is a measurement of how steep the ground surface is. The steeper the ground surface the greater the slope. Slope is measured by calculating the tangent of the surface. The tangent is calculated by dividing the vertical change in elevation by the horizontal distance. Slope is normally expressed in planning as a percent slope which is the tangent (slope) multiplied by 100. Another form of expressing slope is in degrees. To calculate degrees one takes the Arc Tangent of the slope,

$$\text{Degrees Slope} = \text{Arctangent (Height / Base)}. \quad \ldots\ldots\ldots\ldots\ldots\ldots\ldots\ldots\ldots\ldots (3.6)$$

Reliable estimation of slope is very demanding because it is important for terrain analysis to understand the natural process in the disciplines of topography, geology, soils, hydro-geology, infrastructure planning, hazard management both at surface and subsurface. In view of this, slope will plays an important role while doing decentralized planning at grassroots level under the mission on Space based Information Support for Decentralized Planning (SIS-DP) (S. Muralikrishnan, Shashivardhan Reddy, B.Narender, & Abhijit Pillai, 2011) (NRSC, 2013).

The Slope calculates the maximum rate of change in value from that cell to its neighbors. Basically, the maximum change in elevation over the distance between the cell and its eight neighbors identifies the steepest downhill descent from the cell.

The rates of change (delta) of the surface in the horizontal (dz/dx) and vertical (dz/dy) directions from the center cell determine the slope("ArcGIS Help 10.1 - Slope function," 2015.). The basic algorithm used to calculate the slope is:

$$Slope\ in\ radians = \tan^{-1}\left(\sqrt{\left(\frac{dz}{dx}\right)^2 + \left(\frac{dz}{dy}\right)^2}\right) \quad (3.7)$$

Slope is commonly measured in units of degrees, which uses the algorithm:

$$Slope\ in\ radians = \tan^{-1}\left(\sqrt{\left(\frac{dz}{dx}\right)^2 + \left(\frac{dz}{dy}\right)^2}\right) * 57.29578 \quad (3.8)$$

The values of the center cell and its eight neighbors determine the horizontal and vertical deltas. The neighbors are identified as letters from a to i, with e representing the cell for which the aspect is being calculated.

a	b	c
d	e	f
g	h	i

Figure 4.3 : Face Scanning Window

The rate of change in the x direction for cell e is calculated with the following algorithm:

$$\left(\frac{dz}{dx}\right) = \frac{((c+2f+i)-(a+2d+g))}{(8*x\_cellsize)} \quad (3.9)$$

The rate of change in the y direction for cell e is calculated with the following algorithm:

$$\left(\frac{dz}{dy}\right) = \frac{((g+2h+i)-(a+2b+c))}{(8*y\_cellsize)} \quad (3.10)$$

The slope map is generated by using the spatial tool available in the ArcMap, for that the input is the resampled and re-projected Carto-DEM of 30m resolution.

4.3.3 Combination of classified raster and slope map

Clear water and shadows seems comparative in optical–infrared remote sensing information and reason disarray for image characterization studies. There are two normal reasons for shadows, they are topographic features and clouds. Direct solar radiation is reflected to satellite sensor and it will be recorded from the hilly terrains and clouds. Then the output image generated from this radiation contains shadows, to remove this is a challenging task for the examiner. The image utilized for this study is caught in cloudless clear atmosphere. Then the shadows showing up in the image are just because of steep and high terrain topography. Generally visual interpretation and manual altering have been broadly proposed for the redress of topographic shadowing impacts. Hence, they are identified and demarcated in a combination of the combined raster image classified from NDWI, MNDWI and NDPI and the slope map.

The slope map is generated from the cartoDEM. The slope map has been classified into diverse expansive classes by utilizing the slicing method. This characterized slope map has been consolidated with the raster image demonstrating water bodies for the reorganization and alteration of the region under shadows included in the class 'water'. Generally, water can be stored in gentle slope (< 10) or flat areas and shadows are connected with ‘very steep (12–200) to precipitous (>300) area in the study region.

Table 4-2 : Slope Classes

S.No.	Class	Slope(^{0})
1	Gentle	<1
2	Moderate	1-3
3	Stiff	3-6
4	Steep	6-12
5	Very steep	12-20
6	Extra Steep	20-30
7	Precipitous	>30

Finally, water features present in the form of reservoirs, small tanks built on small tributaries and some land covered by a thin water film due to springs have been detected. This methodology is used for the extraction of water features at low and coarser resolution. The water features extracted from this can be used for mapping, the scale of map is dependent on the resolution of the satellite datasets. To extract the water features on the high resolution datasets can be done by using mask overlay of classified raster image generated from the low resolution data sets. Through the water can be extracted very easily, but the level of details are missing in the preparation of the large scale maps from the high resolution datasets, that can be achieved by abstracting the classification mechanism.

4.4 Preparation of water mask

The above water mask has prepared by combining the different binary operations. First consider condition SWI is greater than 0.14 (SWI > 0.14) for the separation of snow/ice. Next from MNDWI is greater than zero (MNDWI > 0) from this maximum water features are separated with minimum shadows. Next by the by combining NDVI greater than zero (NDVI > 0) and NDPI less than zero (NDPI < 0), this condition can separate the water features covered by vegetation. By combining all these condition maximum water bodies and shadows are observed and finally subtraction of shadows can be done by slopes greater than 60 has considered for our datasets. Finally the water mask has prepared from the input Landsat 8 dataset.

4.5 Accuracy Assessment

Accuracy assessment as carried out by using the visual interpretation for the generated random points using an option in ERDAS software. There are three types of random point's generation

1. Random points
   This type of random points are normal random points which are generated by the system itself, in this type the input is only, total number of points to be generated.

2. Stratified random points
   This type of random points are generated based on the minimum number points are to be used for the accuracy assessment, and those points are to obey stratification. It is the process of dividing the number of points into homogeneous subgroups and assigned to each class before the assessment and also at-least one point is assigned to each class.

3. Equalized random points
   In this type, random points are generated based on the total number points are given in the input, those points are equally divided and assigned into each class.

From the generated random points check the class values, and fill-up all the new class values by the visual interpret independently for every generated point. Finally generate the accuracy report, this report contains number of points taken for each class, user's accuracy, producer's accuracy, over all accuracy and finally the kappa coefficient for each class.

4.6 Extracting water feature from higher resolution images

From the above methodology the water is extracted on low and coarser resolution images and this is used for the preparation in the small scales. From the low and coarser resolution images only produce the small scale maps, because there is a less detail information. Where in the small scale maps requires the less level of details. To prepare the large scale maps there is a requirement of high level of details, this information can acquired from the high resolution satellite images. In this study, LISS – IV is high resolution satellite image of 5.8m spatial resolution of Resourcesat – 2.

4.6.1 Mask Overlay

To extract the water feature from this satellite image can be done by overlaying the low resolution classified satellite raster data on the high resolution satellite raster image. Due to overlaying of water mask layer on high resolution satellite data, the only water feature has been extracted. The extracted water layer has less in level of details, this information is not sufficient for the preparation of large scale maps. To add the level of details to extracted water layer from the high resolution image can be achieved by the classification of water features.

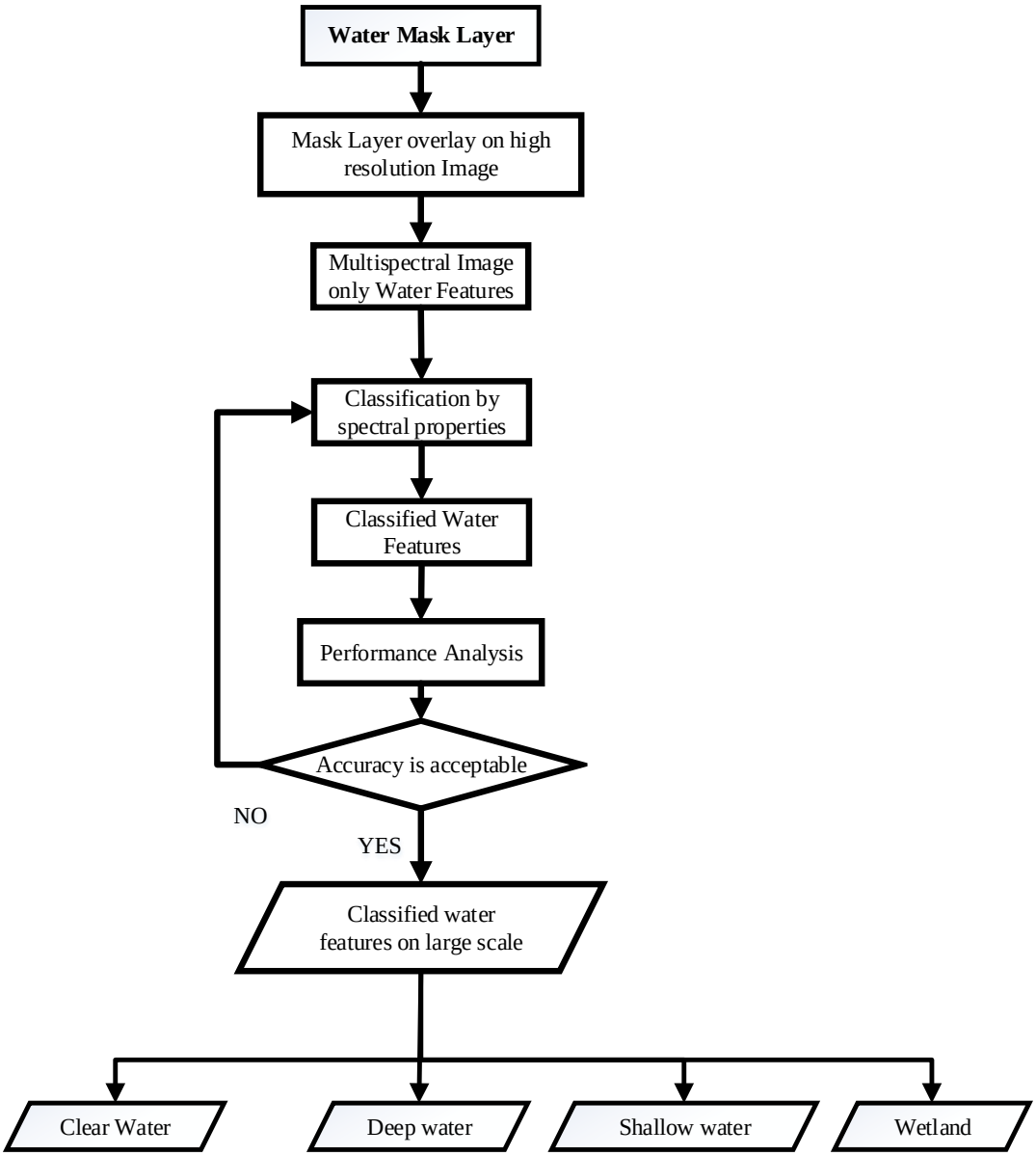

Figure 4-4 : Extracting and classifying the water features on high resolution images

4.6.2 Classification of Water features

To classify water features from the extracted medium and high resolution raster data, for the classification water classes need to be defined. Here, the water features are classified into four classes they are clear water, deep water, shallow water and wetland. These classes can be easily separated by the spectral signatures. The spectral signatures are defined like that for classifying the water features into different water classes as mentioned.

4.6.2.1 Shallow Water

Let us consider the shallow water is a water feature having depth less-than 30cm, and also the ground portion of the water surface is clearly visible, for this range the some portion in the visible can reflect the small amount reflectance from the ground surface. To classify shallow

water features consider the spectral reflectance value of each band must lie in a certain range of values. These values are vary with the sensor used, but the spectral signature of a feature doesn't change. The shallow water feature can have different ranges of values based on the sensor used for collecting the data. If the pixel value of each dataset are present in the specific range as described in the Table 4-4 then it classifies as clear water feature.

Table 4-3 : Range of pixel values for shallow water

Sensor	Blue		Green		Red		NIR		SWIR 1/MIR		SWIR 2	
	MIN	MAX	MIN	MAX	MIN	MAX	MIN	MAX	MIN	MAX	MIN	MAX
Landsat 8 OLI	0.134093	0.138672	0.116383	0.125399	0.097206	0.107439	0.045115	0.049659	0.011914	0.014883	0.006762	0.008944
LISS – III	NA	NA	0.009837	0.011101	0.007714	0.009076	0.006344	0.006488	0.004226	0.004539	NA	NA
LISS – IV	NA	NA	0.008718	0.009154	0.006465	0.007388	0.005381	0.00593	NA	NA	NA	NA

4.6.2.2 Clear Water

Let us consider the clear water is a water feature having depth 30cm to 200cm, and also the ground portion of the water surface is clearly visible. To classify these water features consider the spectral reflectance value of each band must lie in a certain range of values. These values are vary with the sensor used, but the spectral signature of a feature doesn't change. The clear water feature can have different ranges of values based on the sensor used for collecting the data. If the pixel value of each dataset are present in the specific range as described in the Table 4-5 then it classifies as clear water feature.

Table 4-4 : Range of pixel values for Clear water

Sensor	Blue		Green		Red		NIR		SWIR 1/MIR		SWIR 2	
	MIN	MAX	MIN	MAX	MIN	MAX	MIN	MAX	MIN	MAX	MIN	MAX
Landsat 8 OLI	0.13996	0.154342	0.127152	0.14733	0.109907	0.134343	0.050625	0.062825	0.012057	0.012951	0.006655	0.007799
LISS – III	NA	NA	0.010118	0.012647	0.008168	0.011345	0.0062	0.009804	0.004226	0.006573	NA	NA
LISS – IV	NA	NA	0.009543	0.009857	0.005746	0.007794	0.003543	0.006155	NA	NA	NA	NA

1.1.3.1 Deep Water

Let us consider the deep water is a water feature having depth more than 200cm, and the ground portion of the water surface is not visible. To classify deep water features consider the spectral reflectance value of each band must lie in a certain range of values. These values are vary with the sensor used, but the spectral signature of a feature doesn't change. The deep water feature can have different ranges of values based on the sensor used. If the pixel value of each dataset are present in the specific range as described in the Table 4-6 then it classifies as deep water features.

Table 4-5 : Range of pixel values for Deep water

Sensor	Blue		Green		Red		NIR		SWIR 1/MIR		SWIR 2	
	MIN	MAX	MIN	MAX	MIN	MAX	MIN	MAX	MIN	MAX	MIN	MAX
Landsat 8 OLI	0.130014	0.144861	0.108512	0.121392	0.082287	0.106795	0.038281	0.057458	0.012594	0.026725	0.006798	0.01957
LISS – III	NA	NA	0.010118	0.010961	0.008319	0.008773	0.0062	0.006776	0.004226	0.004382	NA	NA
LISS – IV	NA	NA	0.007735	0.010246	0.004682	0.007235	0.003644	0.00415	NA	NA	NA	NA

4.6.2.3 Wetland

Let us consider the wetland is also a type of water feature in this research, the wetlands are also different kinds but in this research considering that, where the semi-submerged and submerged vegetation region is classified as a wetland. In the water mask preparation the threshold is decided that only water features with semi-submerged and submerged vegetation is to be separated not the agriculture and other vegetation features. To classify this type of wetland from the extracted features, it spectral values must lie in the range as described in the

Table 4-7 and some other parameter NDVI, NDWI and MNDWI used in the research are also in the range as shown in the Table 4-8.

Table 4-6 : Range of pixel values for wetland

Sensor	Blue		Green		Red		NIR		SWIR 1/MIR		SWIR 2	
	MIN	MAX	MIN	MAX	MIN	MAX	MIN	MAX	MIN	MAX	MIN	MAX
Landsat 8 OLI	0.119889	0.128798	0.089121	0.101965	0.067225	0.082752	0.129799	0.212051	0.041394	0.100569	0.021001	0.067082
LISS – III	NA	NA	0.009134	0.011101	0.007109	0.009227	0.006055	0.016436	0.003913	0.013459	NA	NA

Table 4-7 : Range of parameter values for wetland

Sensor	NDVI		NDWI		MNDWI	
	MIN	MAX	MIN	MAX	MIN	MAX
Landsat 8 OLI	0.291731	0.495395	-0.37982	-0.16301	0.001127	0.378291
LISS – III	-0.19153	0.377044	-0.26619	0.282359	-0.16538	0.453222

4.6.3 Extraction of River and Canal Networks

Extraction of river and canal networks can be done using the edge detection algorithm, for this extraction the input is high resolution SWIR or MIR band.

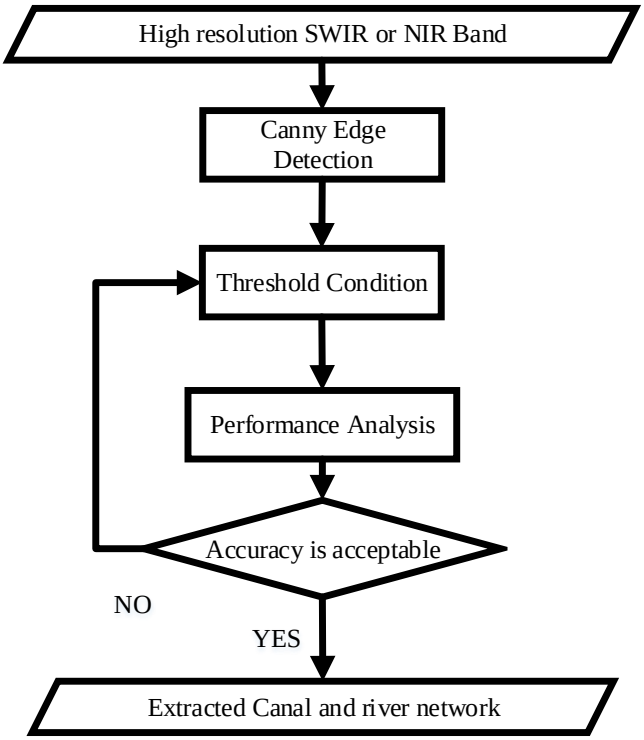

Figure 4-5 : Extraction of river and canal network

4.6.3.1 Canny Edge Detector

The canny edge detection is an optimal edge detection. The process of canny edge detection involves a series of steps to perform the edge detection. This edge detector first smoothes the image to eliminate and noise. It then finds the image gradient to highlight regions with high spatial derivatives. The algorithm then tracks along these regions and suppresses any pixel that is not at the maximum (nonmaximum suppression). The gradient array is now further reduced by hysteresis. Hysteresis is used to track along the remaining pixels that have not

been suppressed. Hysteresis uses two thresholds and if the magnitude is below the first threshold, it is set to zero (made a nonedge). If the magnitude is above the high threshold, it is made an edge. And if the magnitude is between the two thresholds, then it is set to zero unless there is a path from this pixel to a pixel with a gradient above two thresholds ("Canny Edge Detection — OpenCV-Python Tutorials 1 documentation," 2015, "Canny Edge Detection Tutorial," 2015).

In first step, minimizes noise and smoothing an input image before detecting edges, a Gaussian smoothing can be performed by standard convolution using the standard mask, this mask is very small compared to the image applied, so slid over the image, manipulating a square of pixels at a time. The larger the width of the Gaussian mask, the lower is the detector's sensitivity to noise. The localization error in the detected edges also increases slightly as the Gaussian width is increased.

In second step, edge strength or magnitude can be derived using gradient of the image. Sobel operator is used for measuring spatial gradient on an image. This operator uses a pair of 3x3 convolution masks, for estimating the gradient in the x- or column direction and y- or rows direction respectively as shown in figure

-1	0	+1
-2	0	+2
-1	0	+1

Gx

+1	+2	+1
0	0	0
-1	-2	-1

Gy

Figure 4-6 : Sobel operators

The edge strength or magnitude of the gradient is then approximated using the formula represented in the equation (3-11)

$$|G| = |Gx| + |Gy| \qquad (3\text{-}11)$$

In third step, process involves in finding the direction of edge through the formula represented in the equation (3-12)

$$\text{Theta or } \Theta = \text{invtan } (Gy / Gx) \qquad (3\text{-}12)$$

The edge direction is trivial once the gradient in the x and y directions are known. Whenever the gradient in the x direction is equal to zero, assign the edge direction equal to 90^0 or 0^0. Similarly, the gradient in the y direction is equal to zero, assign the edge direction equal to 0^0. Otherwise the edge direction is equal to the 90^0.

In fourth step, relate the edge direction to a direction that can be traced in an image. There are only four possible directions when considering the surrounding pixels in an image. Those direction are shown in the table

Table 4-8 : Sobel edge trace directions

Angle (^{0} degree)	Direction	Value (^{0} degree)
0	Horizontal	0 to 22.5 &157.5 to 180
45	Positive Diagonal	22.5 to 67.5
90	Vertical	67.5 to 112.5
135	Negative Diagonal	112.5 to 157.5

In fifth step, non-maximum suppression is used to trace along the edge in the edge direction and suppress any pixel value (sets it equal to 0) that is not considered to be an edge.

Finally hysteresis has applied for eliminating the streaking. Streaking is the breaking up of an edge contour caused by the operator output fluctuating above and below the threshold. If a single threshold, T1 is applied to an image, and an edge has an average strength equal to T1, then due to noise, there will be instances where the edge dips below the threshold. Equally it will also extend above the threshold making an edge look like a dashed line. To avoid this, hysteresis uses 2 thresholds, a high and a low. Any pixel in the image that has a value greater than T1 is presumed to be an edge pixel, and is marked as such immediately. Then, any pixels that are connected to this edge pixel and that have a value greater than T2 are also selected as edge pixels. If you think of following an edge, you need a gradient of T2 to start but you don't stop till you hit a gradient below T1.

The canny edge detection is applied to the NIR band of high resolution image to find out the edges of the water. Because of the canny edge detection the strong and weak edges are connected. The water edges are separated based on the spectral signatures.

4.6.3.2 Accuracy Assessment

Accuracy assessment developed in (Wiedemann et al., 1998) for evaluation of the extracted road data. For the similar way it is applied for the evaluation of automatic extraction of canal or river network carried out by comparing the automatically extracted canal or river edges with manually plotted river or canal axes used as reference data. Both data sets are given in vector representation. The evaluation is processed in two steps one is matching of the extracted canal or river edges primitives to the reference network and calculation of quality measures.

The purpose of the matching is twofold: Firstly, it yields those parts of the extracted data which are supposed to be canal or river edges, i.e., which correspond to the reference canal or river data. Secondly, it shows which parts of the reference data are explained by the extracted data, i.e., which correspond to the extracted canal or river data.

The quality measure which is considering here in three parameters as described in the (Wiedemann et al., 1998), are completeness, correctness and quality.

4.6.3.2.1 Completeness

The completeness is the percentage of the reference data which is explained by the extracted data, i.e., the percentage of the reference network which lie within the buffer around the extracted data. The optimum value for the completeness is 1. Its value ranges from 0 to 1. The formula representation is

$$Completeness = \frac{length\ of\ matched\ reference}{length\ of\ reference} \qquad (3\text{-}13)$$

4.6.3.2.2 Correctness

The correctness represents the percentage of correctly extracted road data, i.e., the percentage of the extracted data which lie within the buffer around the reference network. The optimum value for the correctness is 1. Its value ranges from 0 to 1. The formula representation is

$$Correctness = \frac{length\ of\ matched\ extraction}{length\ of\ extraction} \qquad (3\text{-}14)$$

4.6.3.2.3 Quality

The quality is a more general measure of the final result combining completeness and correctness into a single measure. The optimum value for the quality is 1. Its value ranges from 0 to 1. The formula representation is

$$Correctness = \frac{length\ of\ matched\ extraction}{length\ of\ extraction + length\ of\ unmatched\ reference} \qquad (3\text{-}15)$$

5. Results and discussions

This chapter explains the details of the results obtained after application of methodology, the obtained results are discussed critically results are analysed.

5.1 Data Pre – processing

Data pre–processing is an essential step for the data preparation, for further information extraction from satellite images. The conversion of digital number (DN) to the top of atmospheric (TOA) reflectance, to convert use the relation as mention in section 4.2.1. After the data conversion to TOA, the independent datasets has to mosaic to cover the entire study area. The mosaic data of Landsat 8 OLI before and after pre-processing shown in figure 5-1.

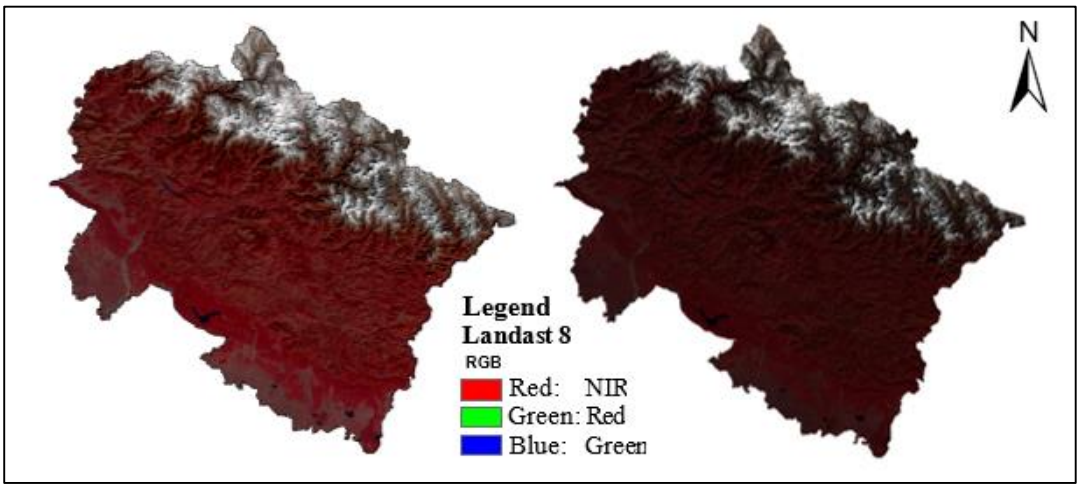

a.DN b.TOA

Figure 5-1 : FCC of mosaicked Landsat 8 OLI Band 2-7.

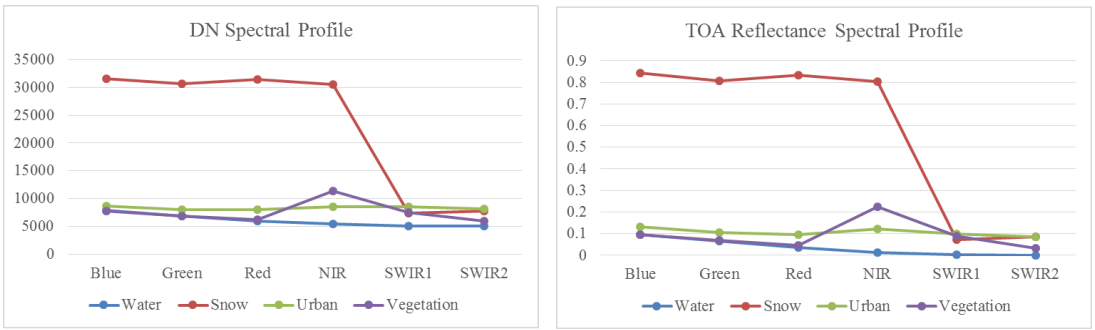

Figure 5-2 : Features spectral profile

In the figure 5-2, the spectral signatures for a DN and the calculated TOA are almost similar for the most commonly observed features like water, snow, urban and vegetation. Water shows decreasing in the reflectance when the wavelength increases, vegetation shows high reflectance in the NIR ban, snow very high reflectance value when compared to the other features in blue, green, red and NIR bands.

5.2 Conversion of DEM to Slope

The carto – DEM data, which is freely available at NRSC – Bhuvan ("Bhuvan | NRSC Open EO Data Archive | NOEDA | Ortho | DEM | Elevation | AWiFS | LISSIII | HySI | TCHP | OHC | Free GIS Data | Download," 2015) with a 30m spatial resolution. The data which is downloaded is not suitable for the further processing. It is essential to rescale and re-project the DEM to the level similar to the input Landsat 8 OLI of selected bands. The rescaled and re-projected DEM data values ranges from 0 to 7100. The DEM values are observed for different locations are Dehradun is 630, Laksar is 212, Rishikesh is 950, Kashipur is 226, Haldwani is 398, Badrinath has 3204, and Kedarnath is 3601 are shown in figure 5-3. The dark pixels in figure 5-3 represents the lowest elevation, and grey values show intermediate height elevations.

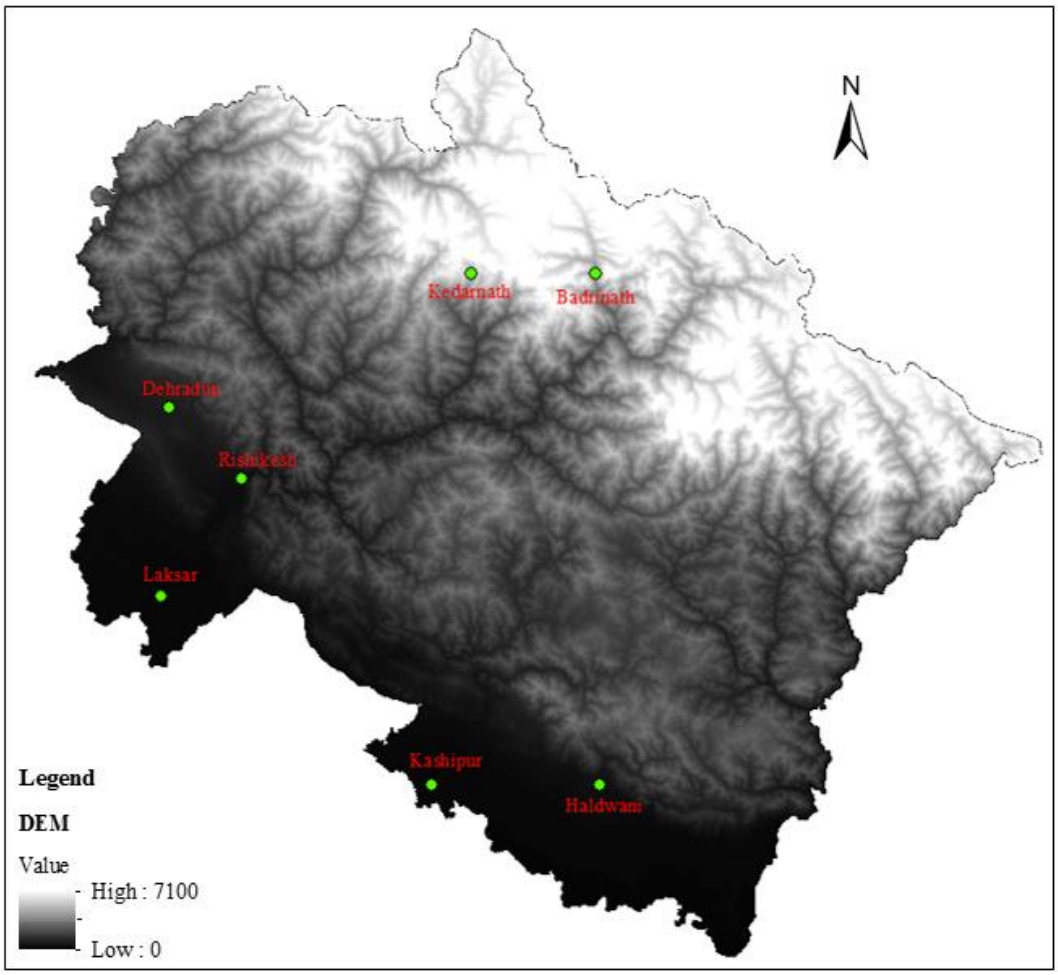

Figure 5-3 : Carto-DEM of 30m spatial resolution.

The DEM contains the elevation value in each pixel, this value is used for finding the elevation value at each point in the entire area, and because the elevation content is not directly used for this research, but it help in finding slope information. Slope gives the information about steepness, which is generally caused for the shadows. The rate of change of gradient in x and y direction gives the slope at that point based on the surrounding pixels. The DEM to slope

conversion can be done as mentioned in the section 2.2.6.2. The converted slope has values ranges from 0 to 87.5518, and it is represented in the image as shown in the figure 5-4, in terms of black and white shades respectively.

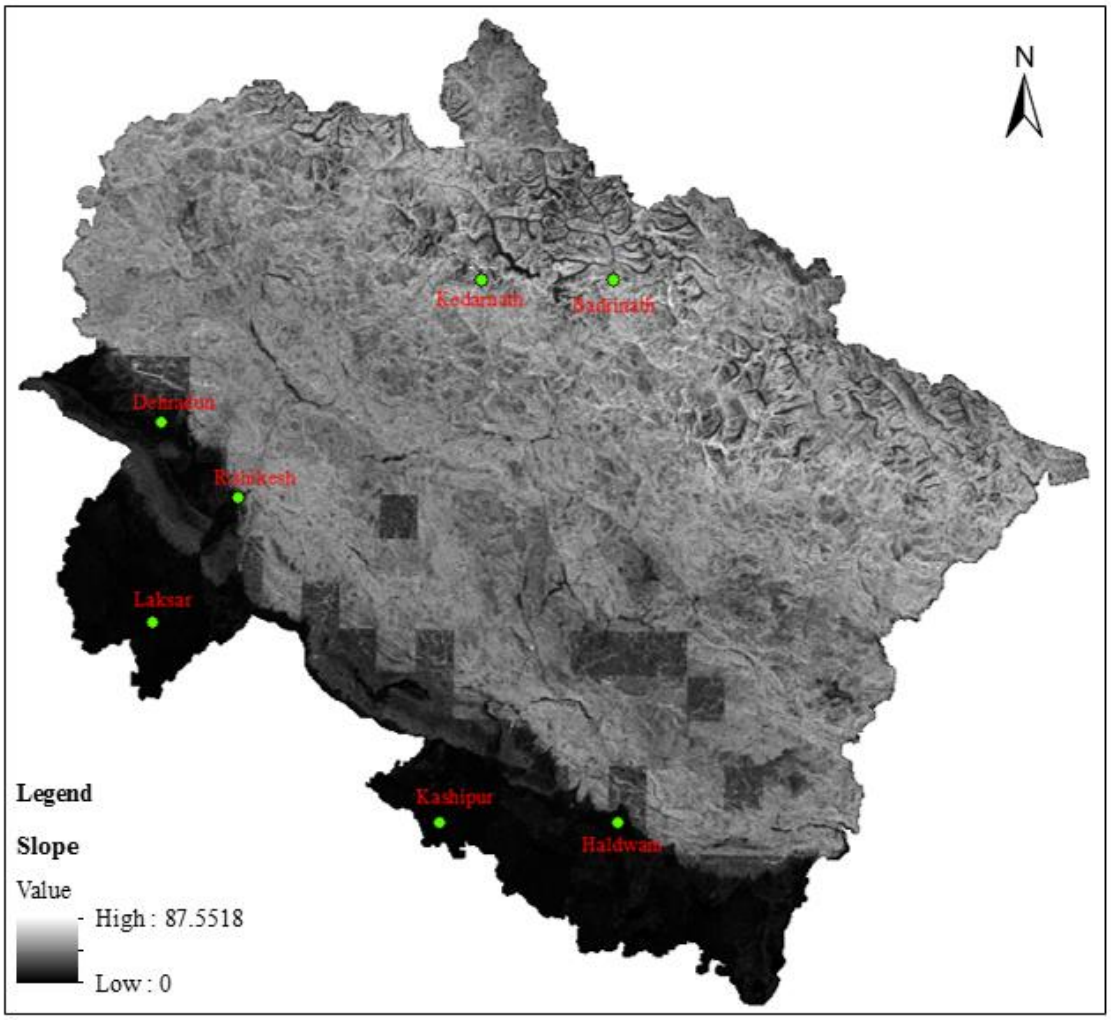

Figure 5-4 : Slope Map which is converted from the carto – DEM.

The slope gives the information about the steepness at that point. The slope map is shown in the above figure 5-4, this map is used for the removal of shadows (because shadows and water features has the same spectral signatures) which is caused due to the steep slopes in the entire study area.

5.3 Indices Generation and Thresholoding

Indices are chosen based on their usefulness and relevance in the extracting the water features. Indices generation and thresholding deals with generating the multiple indices because, the water features can't be separated by the single index, and also the area which is considered in this research is having a vary terrain, with different features like built-up area, snow, vegetation cover, and wetlands. So, going for the multiple indices.

5.3.1 SWI

First of all, the area used in this research has Himalayas and in it some part are covered with the ice/snow. This can be separated from the image by using the SWI.

The SWI is calculated using the relation has shown

$$Surface\ Wetness\ Index\ (SWI) = \big((\rho_{Blue} * 0.1511) + (\rho_{Green} * 0.1973) + (\rho_{Red} * 0.3283) + (\rho_{NIR\ Red} * 0.3407) + (\rho_{SWIR1} * -0.7117) + (\rho_{SWIR2} * -0.4559)\big) \quad (5\text{-}1)$$

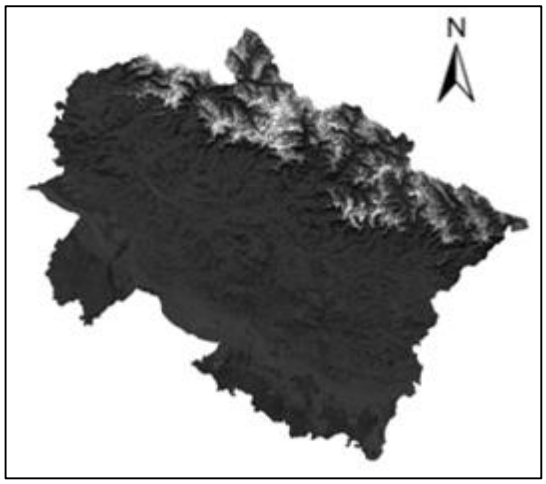

Figure 5-5 : SWI for mosaic TOA of Landsat 8 OLI

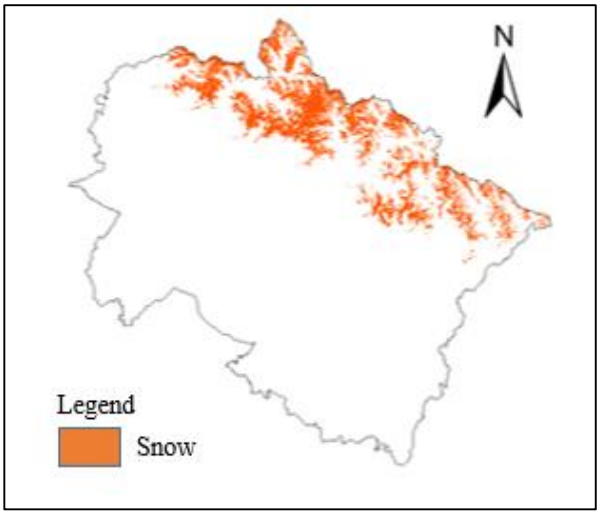

Figure 5-6 : SWI after threshold limit.

The SWI shown in above figure 5-5 is generated using equation 5-1 in this SWI the snow/ ice is easily separated because the snow covered area in the image has high brightness value when compared to the other feature brightness values. The values of SWI ranges from the -0.65 to 1.48, in this range separate very high reflectance values that represented as a snow/ice in the image. By using the density slicing threshold can be found. The founded threshold value is used for the separation snow or ice from the image. For the SWI, general random points are used for the accuracy assessment here 256 random points are used for the accuracy assessment, the overall accuracy achieved is 98%.

Selection of subsets:

The study area is containing several water features like wetland, clear water, shallow water and deep water, so consider two subset for observing the results clearly that should be available of these classes. In this research considered two subsets. Subset 1 is cooresponds to the Bangnaga wetland situated in south portion of Haridwar district, and also some part of river Ganga, contains shallow water, deep water and clear water, Subset 2 is considered like that is distinct from the subset 1, so that this subset 2 is around the Kashipur, contains vegetation cover over the water features has observed in Bhagpur dam, and river kosi. Because of the reasons, these two subsets are considered for the interpretation. The subset 1 and subset 2 as shown in figure 1-7 (a) and (b) are represented in the standard false colour composite of Landsat 8 OLI bands.

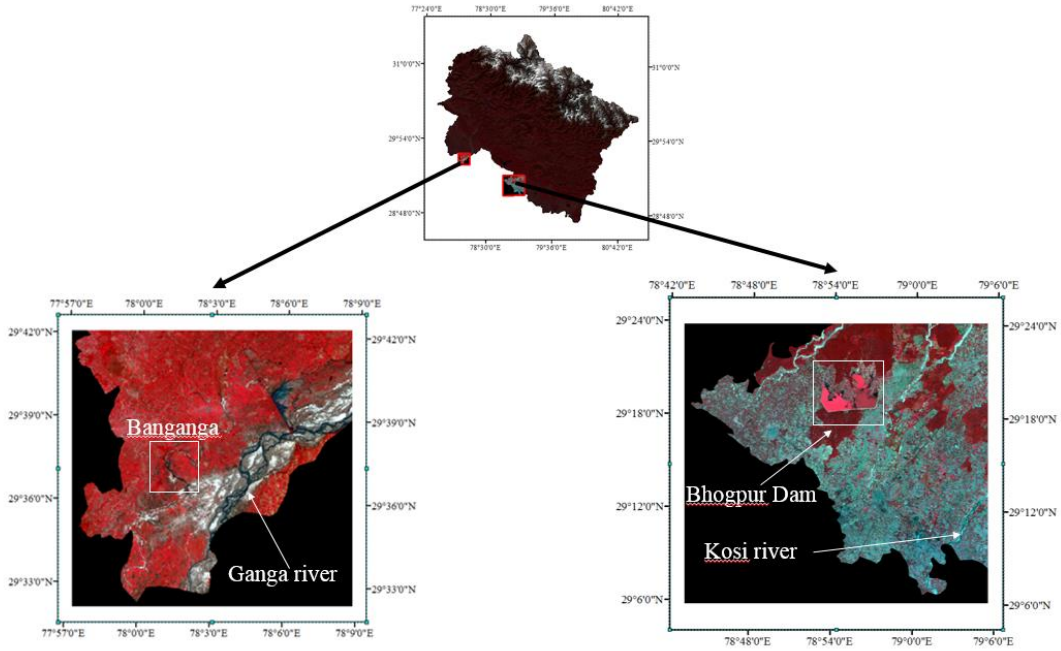

Figure 5-7 : Subsets highlated in the entire study area.

5.3.2 NDWI

The NDWI value generally lies between -1 to +1 because in the equation (5-2) the numerator is always greater than denominator. The figure 1-8 (a) and (d) shows the subset1 and subset2 of Landsat 8 respectively. The normal water features are clearly highlighted as highest brightness value in newly generated NDWI as shown in the figure 1-8 (b). The generated NDWI for the image has values ranges from -0.77 to a value +0.80, this range is lies between the limits of the NDWI. The binary image based on the threshold decided by density slicing method, is shown in figure 1-8 (c). Similarly in figure 1-8 (e) normal water features are highlighted, but in this subset some of the water features are covered with the vegetation are not highlighted and then binary image has prepared based on the threshold decided by density slicing method, is shown in figure 1-8 (f).

$$Normalized\ Difference\ Water\ Index\ (NDWI) = \frac{\rho_{Green} - \rho_{NIR}}{\rho_{Green} + \rho_{NIR}} \quad (5\text{-}2)$$

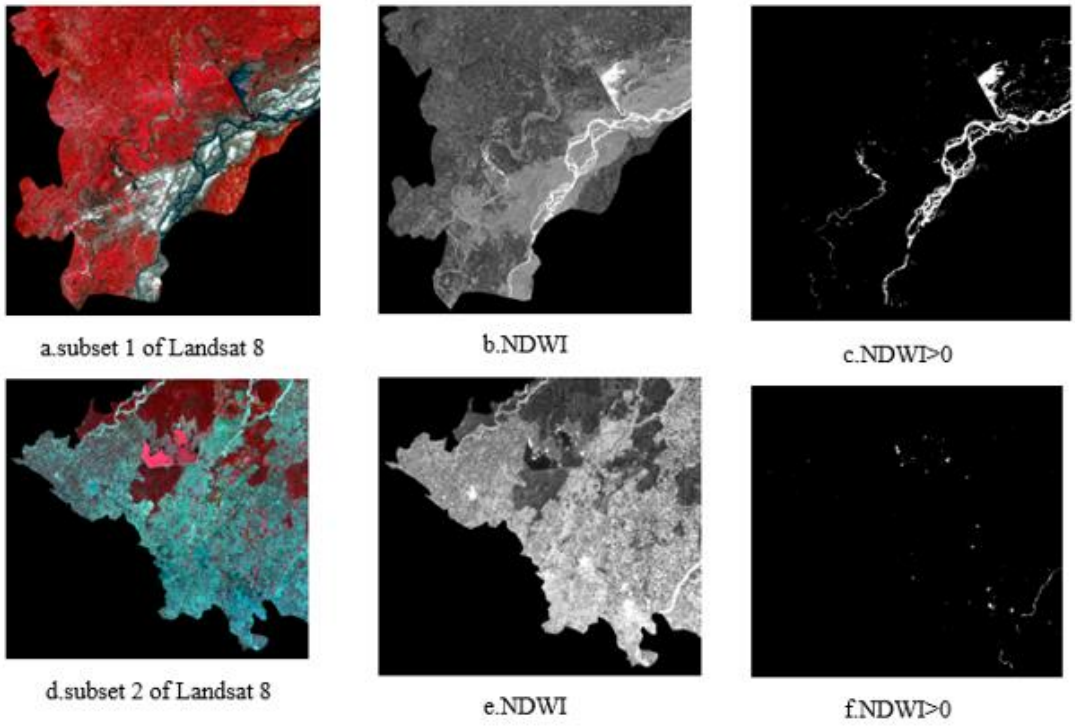

Figure 5-8 : Extraction of water features from NDWI

In figure 1-8 (b) and (e), normal water features are highlighted as increase in the brightness values, because reflectance value of green band is high compared to reflectance of NIR band. But in figure 1-8 (e) has some of water features are covered with the vegetation cover those features are not highlighted because vegetation cover has high reflectance in the NIR band. In figure 1-8 (c) and (f), water features are separated, but not all water features, the NIR band has high reflectance value from ground surface of shallow water and also vegetation covered water features, due to these reasons some of the water features are not separated in the used threshold respectively.

5.3.3 MNDWI

Similarly, as NDWI, MNDWI value also lies between -1 to +1 because in the equation (5-3) the numerator is always greater than denominator. The figure 1-9 (a) and (d) shows the subset1 and subset2 of Landsat 8 as respectively. The normal water features are clearly highlighted as highest brightness value in newly generated MNDWI as shown in the figure 1-9 (b). The generated MNDWI for the image has values ranges from -0.67 to a value +0.97, this range is lies between the limits of the MNDWI. The binary image based on the threshold decided by density slicing method, is shown in figure 1-9 (c). Similarly in figure 1-9 (e) normal water features are highlighted, but in this subset some of the water features are covered with the vegetation are not highlighted and then binary image has prepared based on the threshold decided by density slicing method, is shown in figure 1-9 (f).

$$Modified\ Normalized\ Difference\ Water\ Index\ (MNDWI) = \frac{\rho_{Green} - \rho_{MIR}}{\rho_{Green} + \rho_{MIR}} \quad (5\text{-}3)$$

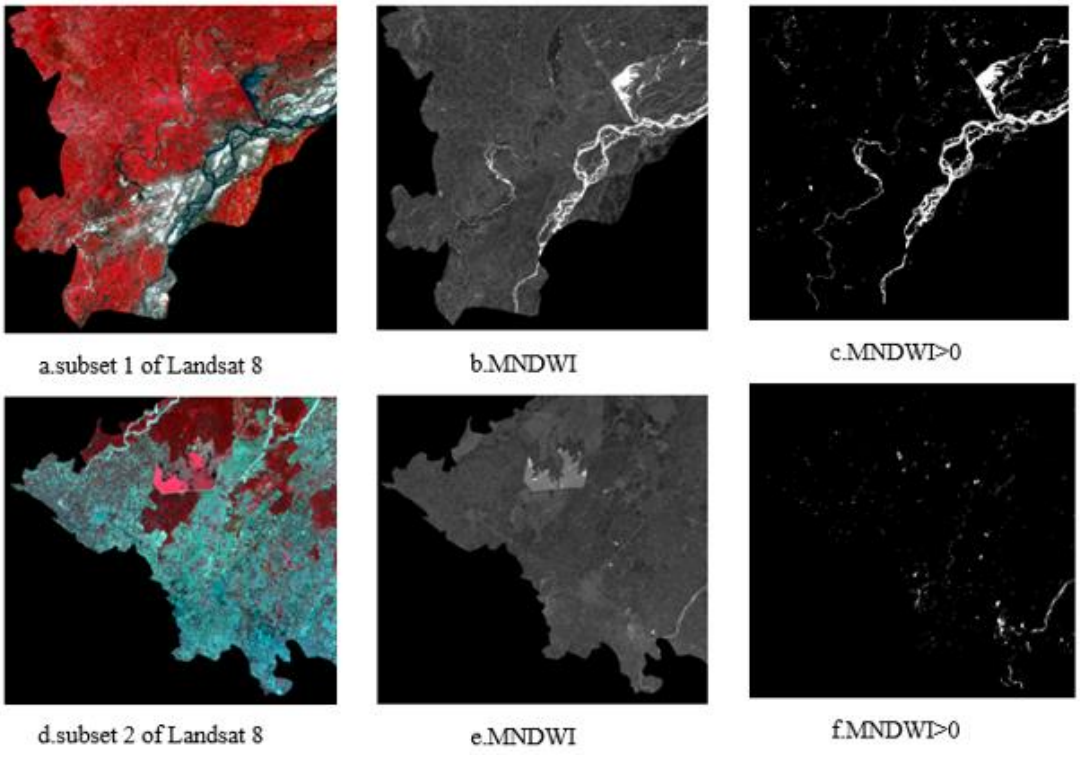

Figure 5-9 : Extraction of water features from MNDWI

In figure 1-9 (b) and (e), normal water features are highlighted as increase in the brightness values, because reflectance value of green band is high compared to reflectance of MIR or SWIR1 band. But in figure 1-9 (e) has some of water features are covered with the vegetation cover those features are not highlighted because vegetation cover has high reflectance in the MIR band. In figure 1-9 (e) and (f), maximum water features are separated, except vegetation covered water features, due to MIR band has high reflectance for the vegetation.

5.3.4 NDVI

Similarly, as NDWI, NDVI value also lies between -1 to +1 because in the equation (5-4) the numerator is always greater than denominator. The figure 1-10 (a) and (d) shows the subset1 and subset2 of Landsat 8 as respectively. The normal water features are clearly highlighted as very low brightness value in newly generated NDVI as shown in the figure 1-10 (b). The generated NDVI for the image has values ranges from -0.60 to a value +0.84, this range is lies between the limits of the NDVI. The binary image based on the threshold decided by density slicing method, is shown in figure 1-10 (c). Similarly in figure 1-10 (e) normal water features are highlighted, but in this subset some of the water features are covered with the vegetation are not highlighted and then binary image has prepared based on the threshold decided by density slicing method, is shown in figure 1-10 (f).

$$Normalized\ Difference\ Vegetation\ Index\ (NDVI) = \frac{\rho_{NIR}-\rho_{red}}{\rho_{NIR}+\rho_{red}} \quad (5\text{-}4)$$

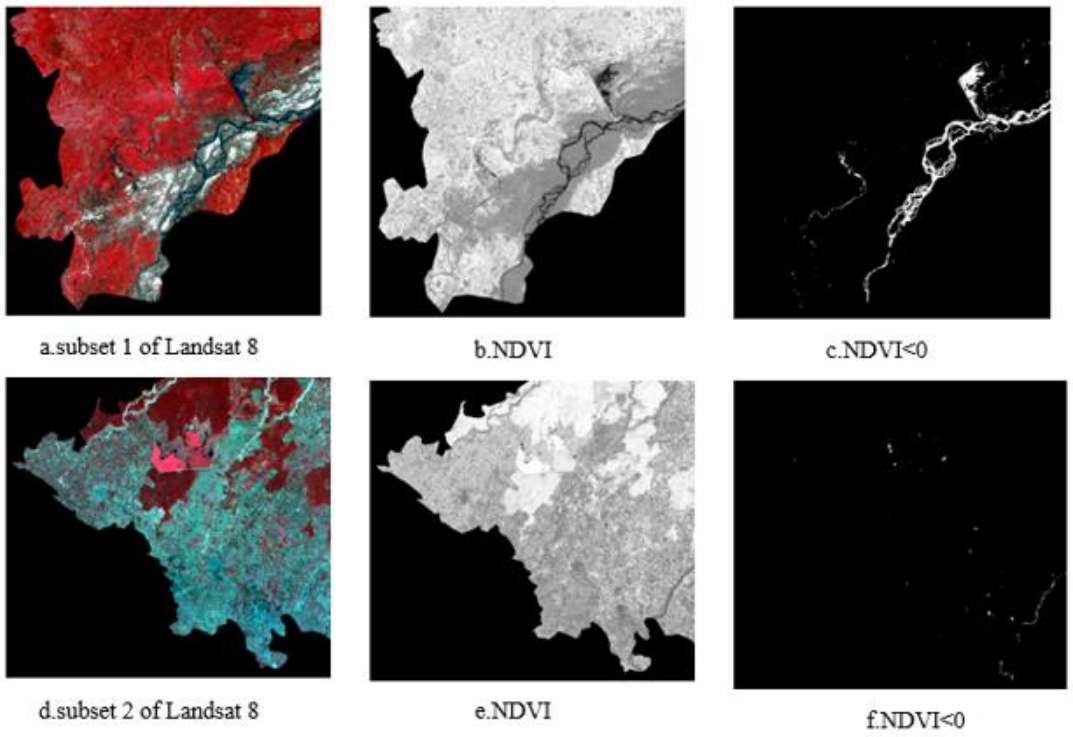

Figure 5-10 : Extraction of water features from NDVI

In figure 1-10 (b) and (e), normal water features are highlighted as decrease in the brightness values, because reflectance value of NIR band is low compared to reflectance of red band. But in figure 1-10 (e) has some of water features are covered with the vegetation cover those features are not highlighted because vegetation cover has high reflectance in the NIR band. In figure 1-10 (c) and (f), water features are separated, but not all water features, the NIR band has high reflectance value from ground surface of shallow water and also vegetation covered water features, due to these reasons some of the water features are not separated in the used threshold respectively.

5.3.5 NDPI

Similarly, as NDWI, NDPI value also lies between -1 to +1 because in the equation (5-5) the numerator is always greater than denominator. The figure 1-11 (a) and (d) shows the subset1 and subset2 of Landsat 8 as respectively. The normal water features are clearly highlighted as very low brightness value in newly generated NDPI as shown in the figure 1-11 (b). The generated NDPI for the image has values ranges from -0.98 to a value +0.67, this range is lies between the limits of the NDPI. The binary image based on the threshold decided by density slicing method, is shown in figure 1-11 (c). Similarly in figure 1-11 (e) normal water features are highlighted, but in this subset some of the water features are covered with the vegetation are not highlighted and then binary image has prepared based on the threshold decided by density slicing method, is shown in figure 1-11 (f).

$$Normalized\ Difference\ Pond\ Index\ (NDPI) = \frac{\rho_{MIR}-\rho_{Green}}{\rho_{MIR}+\rho_{Green}} \quad (5\text{-}5)$$

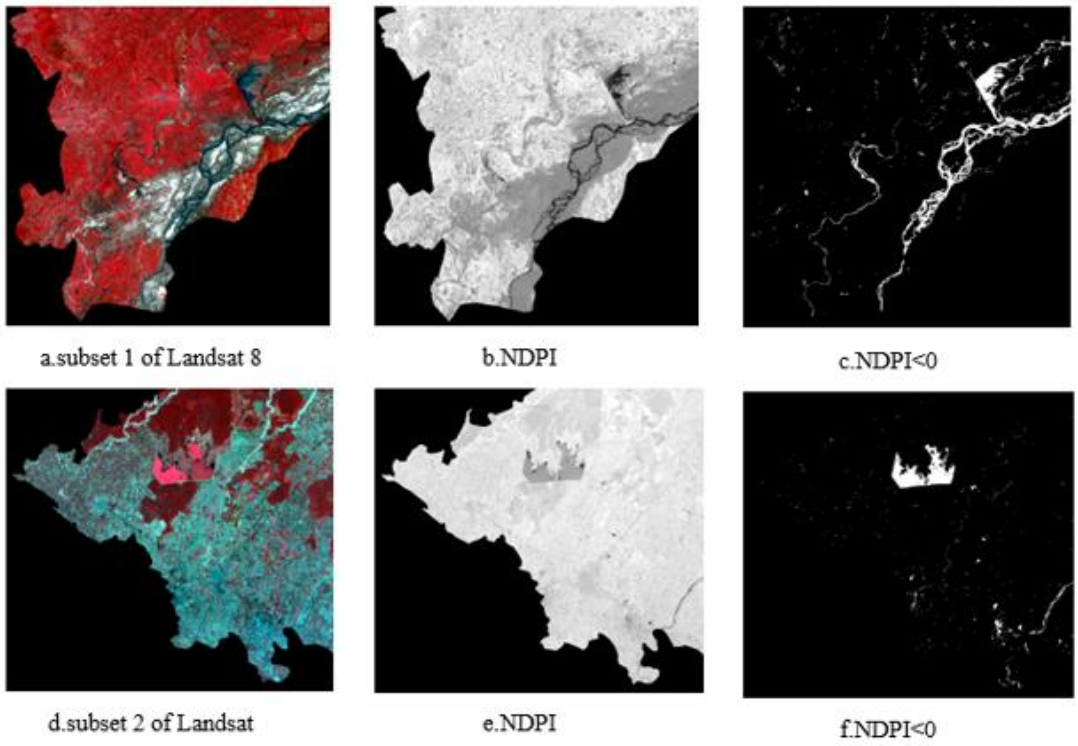

Figure 5-11 : Extraction of water features from NDPI

In figure 1-11 (b) and (e), normal water features are highlighted as decrease in the brightness values, because reflectance value of MIR or SWIR1 band is low compared to reflectance of green band. But in figure 1-11 (e) has some of water features are covered with the vegetation cover those features are also highlighted because vegetation cover has high reflectance in the MIR band. In figure 1-11 (c) and (f), maximum water features are separated, by using this threshold from this index.

5.4 Preparation of water mask

The preparation of water mask involves in combining of the above indices in a rule based as mention in the section 4.4. First the SWI is use for the separate of the snow/ice form the entire datasets. After the calculation of MNDWI is used for the separation of water features with the minimum number of shadows. The shadows are eliminated by using the slope derived from DEM. The combination of NDVI and NDPI is used for the separation of the vegetation covered water features. By combining all the steps maximum water features are extracted as a binary image. This binary image is called the water mask in this research study.

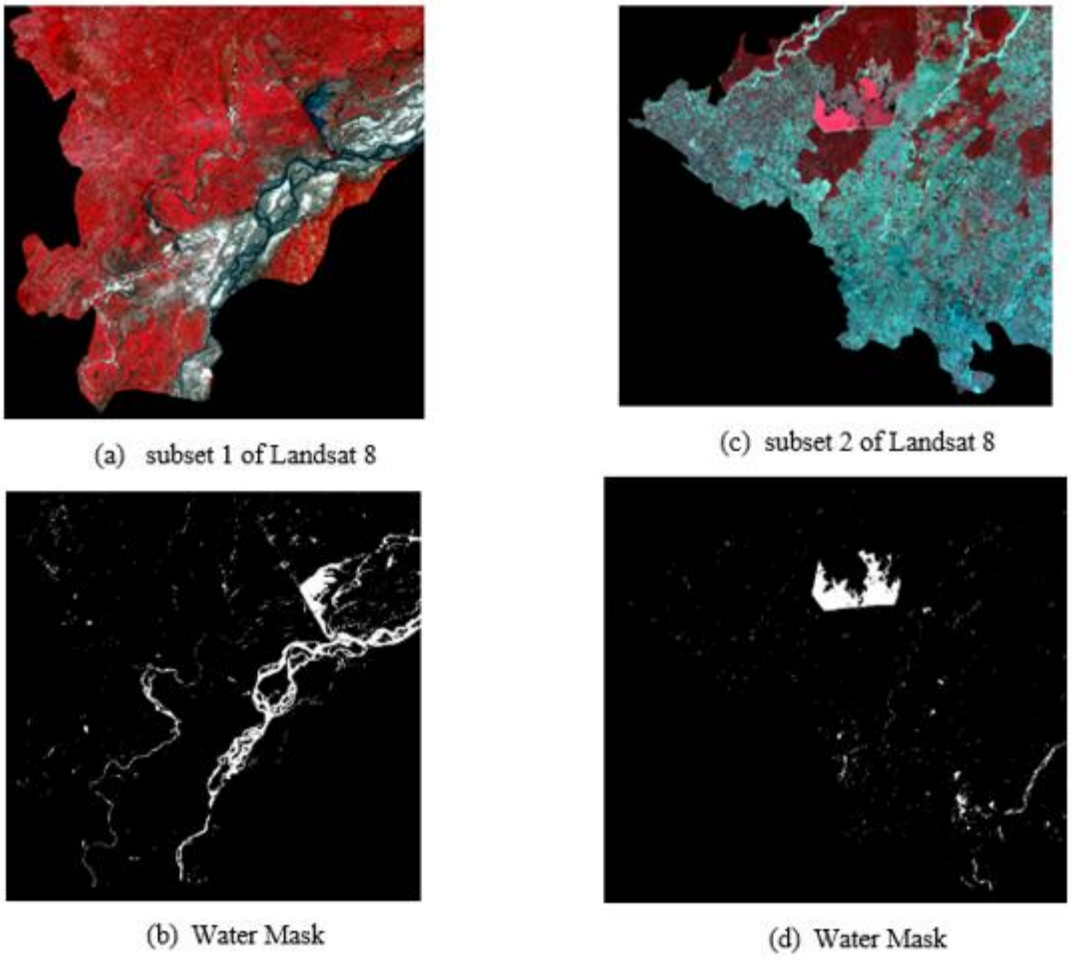

Figure 5-12 : Extraction of water Mask

In figure 1-12 (b) and (d) are the generated water mask by performing different binary operation. These figures contains the maximum water features. These features contains the vegetation covered water features, normal water feature, and some portion of wetlands. The water mask which also contains the wetlands, the wetlands that are near to the water bodies and those are submerged in the water are also considered in this water mask layer these all are in the binary form. This prepared water mask layer has an overall accuracy of 92.50% achieved through the visual interpretation performed on the generated stratified random points over the entire study area.

5.5 Mask Extraction and Classification

5.5.1 Extraction and Classification results for Landsat 8 OLI

The prepared binary mask has to overlay on the Landsat 8 OLI data and extract the reference values respected to each band. These extracted values are to be stored in the new image contains the same number of bands as input. The extracted image is shown in the figure 5-13 (b) and (e). This image contains the different water features like clear water, deep water, shallow water and wetland were are spectrally distinct in the FCC. The water features are classified as discussed in the section 4.6.2 and it is shown in the figure 5-13 (c), (f), and the enlarged image are shown in the figure 5-14, and figure 5-15.

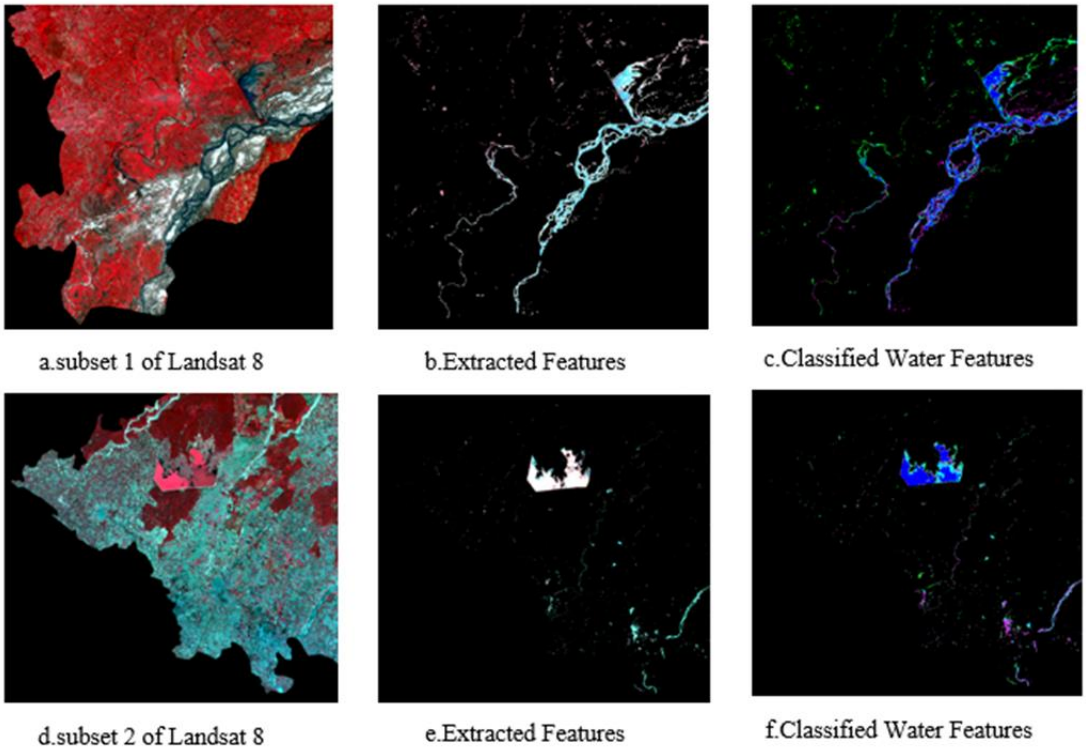

Figure 5-13 : Water feature extraction and Classification of Landsat 8

Figure 1-13 (b) and (e) are extracted water features with respect to each band. The standard false colour composite represented can be observed in the figure shown. As discussed in the methodology the extracted water feature image is used for the classification.

As described previously the water features are to be classified into four different classes which are clear water, shallow water, deep water and wetland. The detailed visibility of classified image is shown in figure 5-14 and 5-15 for the two considered subsets.

The classified image has deep water portion which are clearly observed in the river Ganga and some small portion in the Ban-ganga wetland of subset 1, and in the subset 2 the entire vegetation covered area is deep water. The clear water features that has been observed along the edges of the deep water and end of Ban-ganga wetland and in the subset 2, Kosi river beside the Kashipur contains some portion of clear water. The shallow water has observer in

the end of the Ban-ganga and side portion of the river Ganga in subset 1 and from the subset 2 the maximum canal and rivers portion are filled with the shallow water. The remaining portion is called a wetland which is mixed with vegetation and the water features.

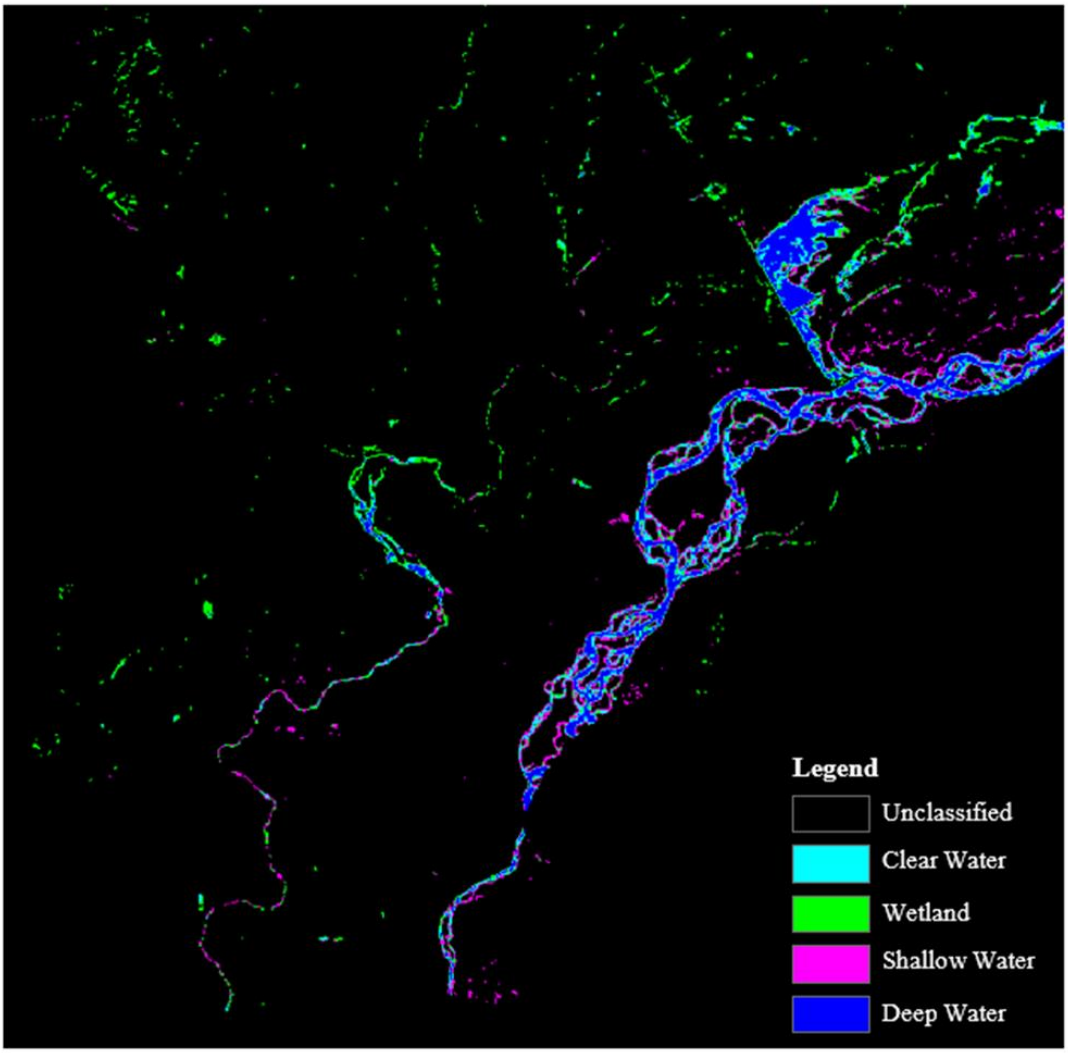

Figure 5-14 : Classified Water Features for subset 1 of Landsat 8

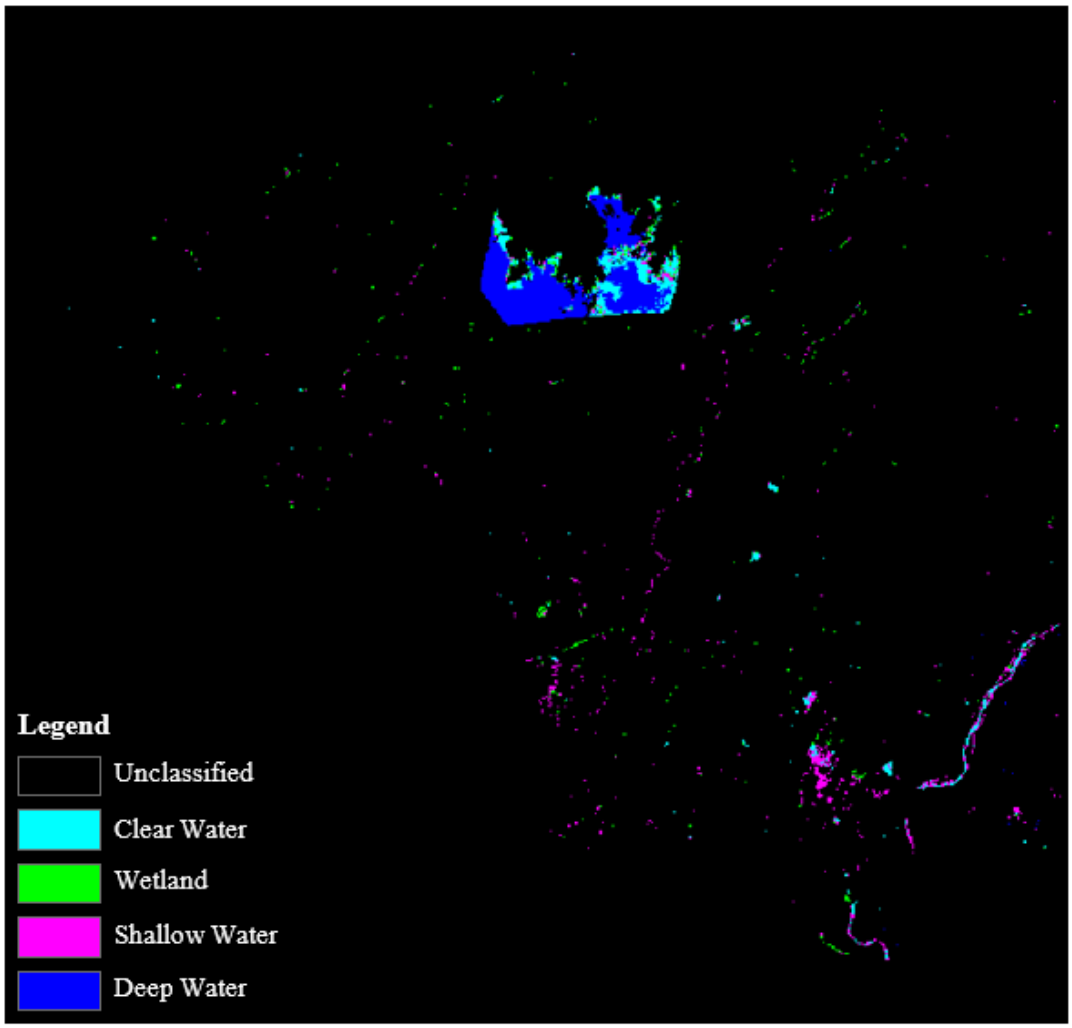

Figure 5-15 : Classified Water Features for subset 2 of Landsat 8

Accuracy Assessment:

In the classifications the water features into four different classes has mentioned in section 4.5. The accuracy is calculated for the defined classes by generating stratified random points, overall classification accuracy is 91.67% and each class accuracy and coefficient as shown in table 5-1.

Table 5-1 : Classification accuracy of Landsat 8 OLI

Class Name	Reference Total	Classified Total	Number Correct	Producers Accuracy	Users Accuracy	Kappa coefficient
Unclassified	24	24	24	----	----	1.0000
Clear Water	23	24	21	91.30	87.50	0.8454
Wetland	26	24	22	84.62	91.67	0.8936
Shallow Water	25	24	22	88.00	91.67	0.8947
Deep Water	22	24	21	95.45	87.50	0.8439
Toatal	120	120	110	----	----	-----

Comparison with Field Spectra:

The field spectra which is continuous in range from the 350nm to 2500nm. This collected field spectra is resampled based on wavelength of the Landsat 8 OLI datasets. The normalized field spectral is also having a greater values compared to the pixel values because, in image atmospheric noise added in this research for datasets only TOA reflectance is calculated. So calculated the correlation factor between resampled spectra with the random points collected based on the classification of each class.

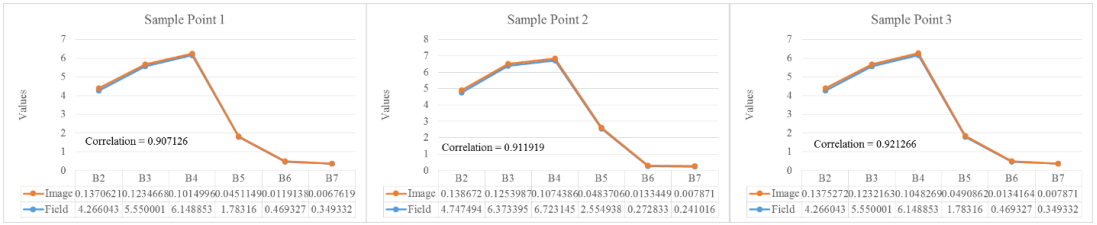

a. Shallow water correlation

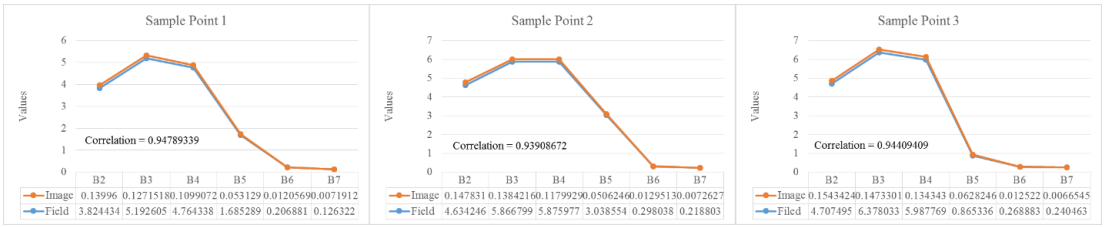

b. Clear water correlation

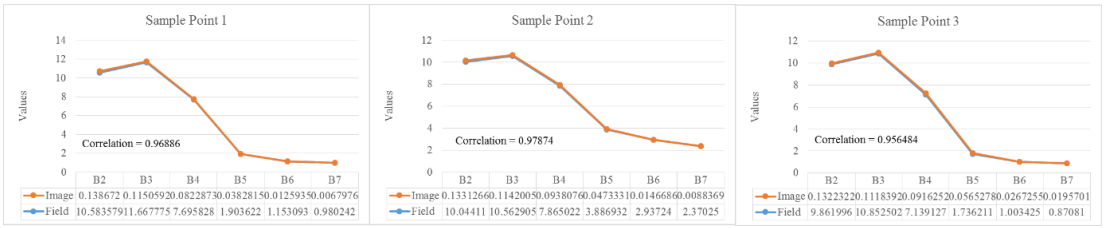

c. Deep water correlation

Figure 5-16 : Correlation comparison between field and Landsat 8 OLI

In the above figure 5-16 a, b, and c, the field spectra is compared with the random sample points collected from the extracted water features based on the classified image. Here three sample points has taken to compare each class. The spectral signature shallow water raises from the blue band to red band and steep fall has observed from red to NIR and decreases in SWIR1 and SWIR2 bands. For the shallow water spectral signature is raises from blue to green and it have small stabilize from green to red and it decreases from red to SWIR2 bands. Similarly the spectral signature has small difference between blue and green band and steep decrease ha observed from the green to red to NIR and small decrement from the NIR to SWIR2. The obtained correlation factor for each class is shown in the figure 5-16. The classification schema which has taken in the present research is having good correlation factor with the field spectra

5.5.2 Extraction and Classification results for LISS – III

The prepared binary mask has to overlay on the LISS – III data and extract the reference values respected to each band. These extracted values are to be stored in the new image contains the same number of bands as input. The extracted image is as shown in the figure 5-16 (b) and (e). This image contains the different water features like clear water, deep water, shallow water and wetland are spectrally observed in the FCC. The water features are classified as per discussed in the previous chapter and it is shown in the figure 5-16 (c), (f), and the enlarged image are shown in the figure 5-17.

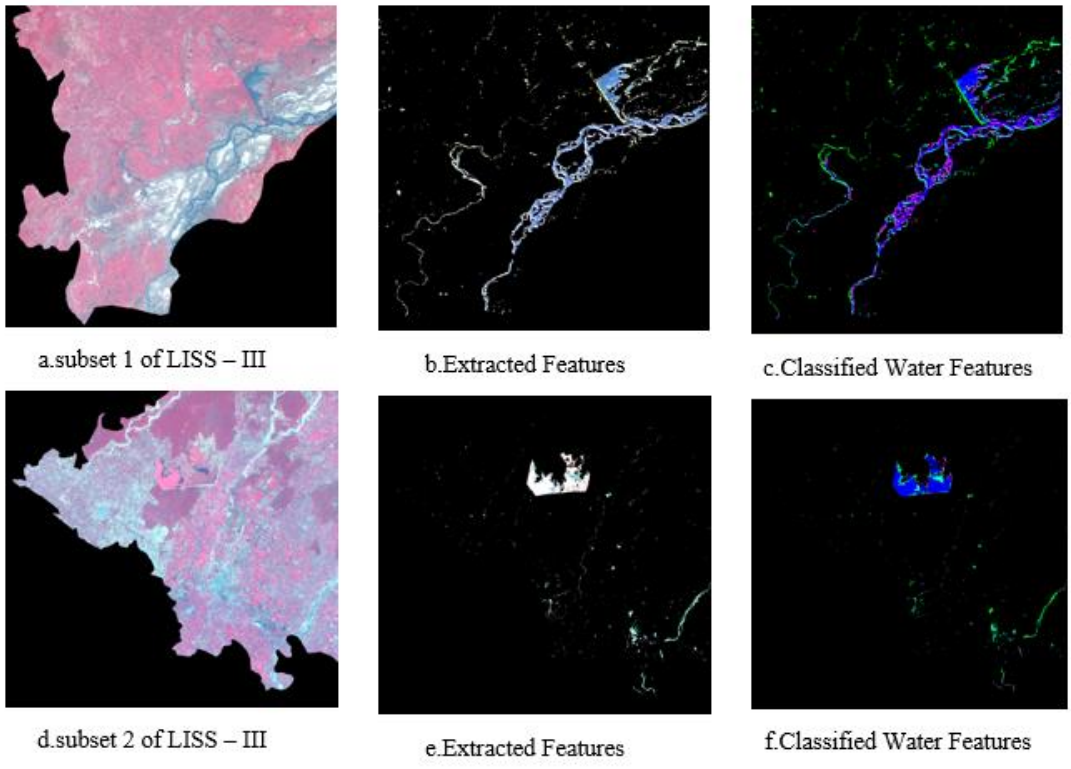

Figure 5-17 : Water feature extraction and Classification of LISS – III

Extracted water features from LISS – III image with respect the mask prepared are shown in figure 5-16 (b) and (e) in the standard false colour composite. This image is used for further classification of water features as described in the section 4.6.2.

Based on the rules defined on the spectral values as described in the section 4.6.2, the water features are further classified in to clear water, deep water, shallow water and wetland.The classified image is shown in the figure 5-16 for the considered subset 1. The classified image has deep water portion are clearly observed in the river Ganga and some small portion in the Ban-ganga wetland of subset 1, and in the subset 2 the entire vegetation covered area is a deep water. The clear water features that has been observed in the edges of the deep water and end of Ban-ganga wetland and in the subset 2 Kosi river in the image is classified as clear water and remaining water features around it are classified as wetland. The shallow water is clearly

highlighted in the wide portion in the wetland and also it is surrounded by the vegetation and in the subset 2 the shallow water is less detected when compared to the other classes.

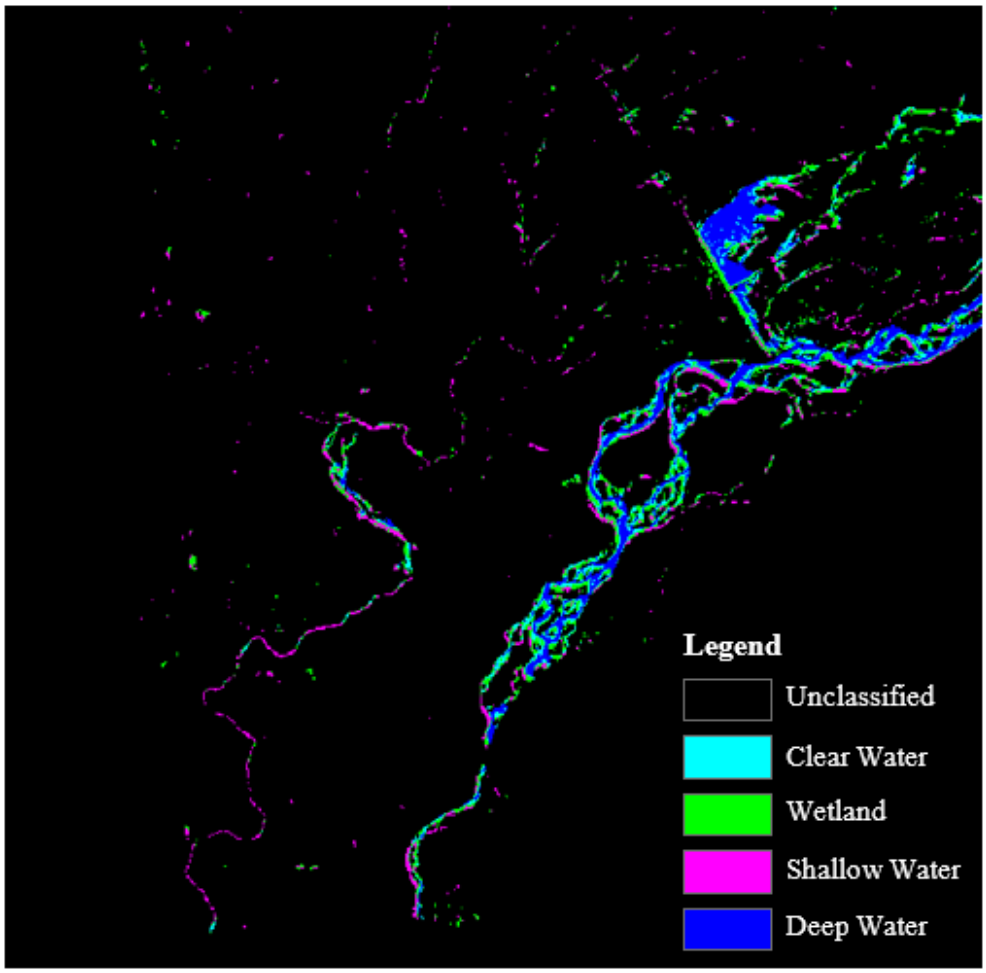

Figure 5-18 : Classified Water Features for LISS – III

Accuracy Assessment:

In the classifications the water features into four different classes has mentioned in section 4.5. The accuracy is calculated for the defined classes by generating stratified random points, overall classification accuracy is 84.17% and each class accuracy and coefficient as shown in table 5-2.

Table 5-2 : Classification accuracy of LISS – III

Class Name	Reference Total	Classified Total	Number Correct	Producers Accuracy	Users Accuracy	Kappa coefficient
Unclassified	24	24	24	----	----	1.0000
Clear Water	25	24	21	84	87.50	0.8421
Wetland	26	24	19	73	79.17	0.7340
Shallow Water	25	24	18	72	75.00	0.6842
Deep Water	20	24	19	95	79.17	0.7500
Toatal	120	120	101	----	----	

Comparison with Field Spectra:

The field spectra which is continuous in range from the 350nm to 2500nm. This collected field spectra is resampled based on wavelength of the LISS – III datasets. The normalized field spectral is also having a greater values compared to the pixel values because, in image atmospheric noise added in this research for datasets only TOA reflectance is calculated. So calculated the correlation factor between resampled spectra with the random points collected based on the classification of each class.

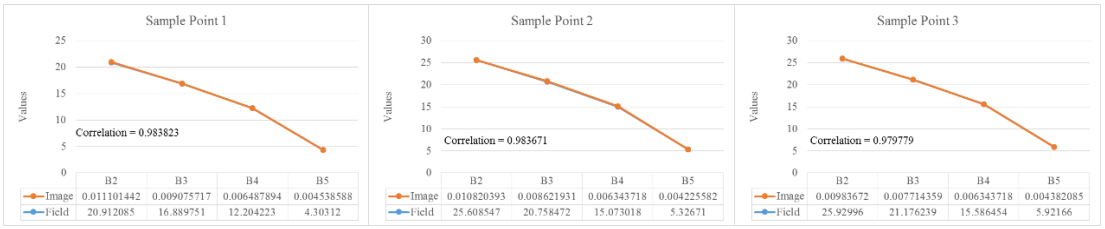

a. Shallow water correlation

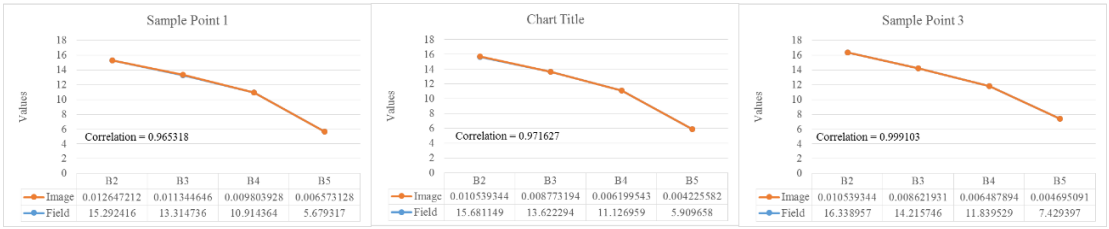

b. Clear water correlation

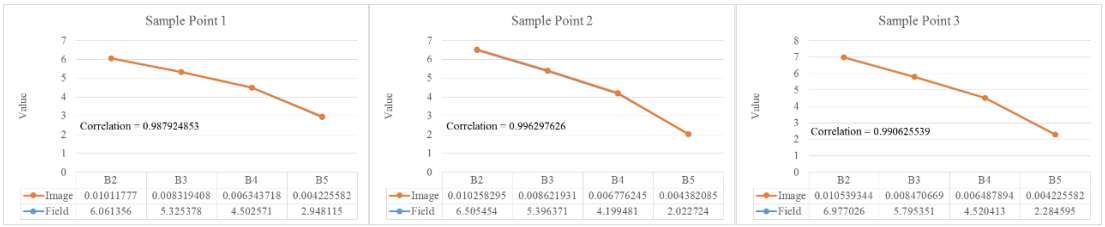

c. Deep water correlation

Figure 5-19 : Correlation comparison between field and LISS – III.

In the figure 5-19 a, b, and c, the all graphs are having good correlation but observation are made based on the range of values for the shallow water the range of green band is very high is as observed as above 20, for the clear water the value of green band lies in the 14 to 16 and finally the deep water for the green band has not exceeded the value 8. Similarly, the value of red band and NIR band variations for shallow, clear and deep water has decreases respectively. Finally, the steep decrement has observed from the NIR to MIR bands and the steepness differences has a decrement value from the shallow, clear and deep water resspecively.

5.5.3 Extraction and Classification results for LISS – IV

The prepared binary mask has to overlay on the LISS – IV data and extract the reference values respected to each band. These extracted values are to be stored in the new image contains the same number of bands as input. The extracted image is as shown in the figure 5-18 (b). This image contains the different water features like clear water, deep water, and shallow water are clearly observed in the FCC. The water features are classified as per discussed in the section 4.6.2 and it is shown in the figure 5-18 (c), and the enlarged image are shown in the figure 5-19.

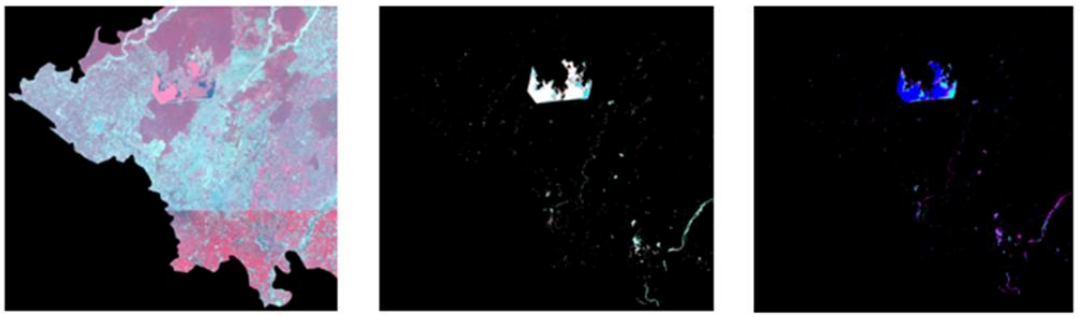

a.subset 2 of LISS – IV b.Extracted Features c.Classified Water Features

Figure 5-20 : Water feature extraction and Classification of LISS – IV

Discussion:

Figure 5-18 (b) shows the extracted water features with respect to each band. The standard false colour composite represented can be observed in the figure shown. As discussed in the methodology the extracted water feature image is used for the classification.

As described in the previous chapter the water features has to classify into four different classes which are clear water, shallow water, deep water and wetland. But the absence of MIR or SWIR1 band in the LISS –IV, the wetland classification is not possible, so the classification of water feature in to three classes that are clear water, deep water and shallow water. The classified image is as shown in the figure 5-19. In this the vegetation covered area are considered entirely in the deep water, the river and canals are classified as water features because of high resolution and finally only some portion in the image has observed clear water. The maximum water feature which is classified as deep water.

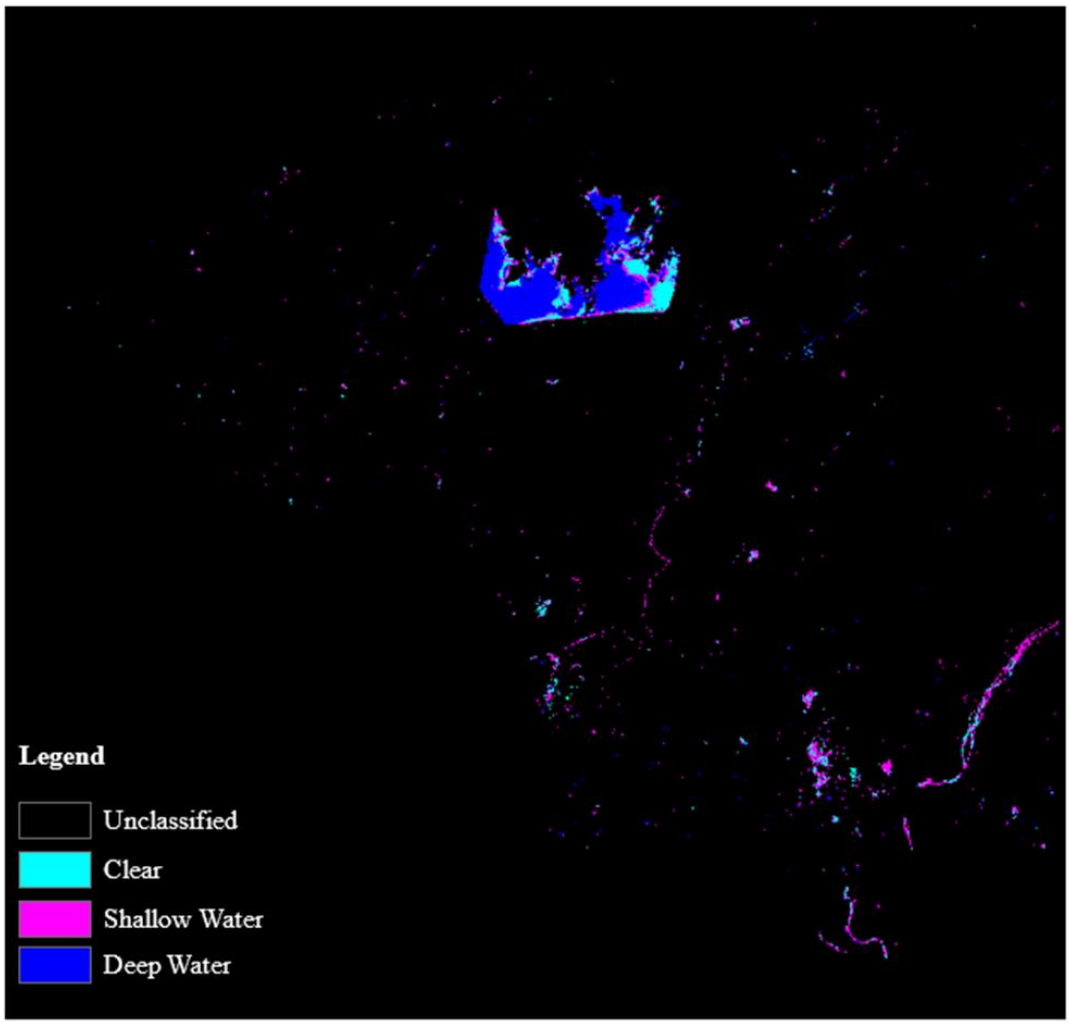

Figure 5-21 : Classified Water Features for LISS - IV

Accuracy Assessment:

In the classifications the water features into four different classes has mentioned in section 4.5. The accuracy is calculated for the defined classes by generating stratified random points, overall classification accuracy is 87.50% and each class accuracy and coefficient as shown in table 5-2.

Table 5-3 : Classification accuracy of LISS – IV

Class Name	Reference Total	Classified Total	Number Correct	Producers Accuracy	Users Accuracy	Kappa coefficient
Unclassified	27	30	27	----	----	1.0000
Deep Water	36	30	29	80.56	96.67	0.9524
Shallow Water	34	30	26	76.47	86.67	0.8140
Clear Water	23	30	23	100.00	76.67	0.7113
Toatal	120	120	105	----	----	----

Comparison with Field Spectra:

The field spectra which is continuous in range from the 350nm to 2500nm. This collected field spectra is resampled based on wavelength of the LISS – IV datasets. The normalized field spectral is also having a greater values compared to the pixel values because, in image atmospheric noise added in this research for datasets only TOA reflectance is calculated. So calculate the correlation factor between resampled spectra with the random points collected based on the classification of each class.

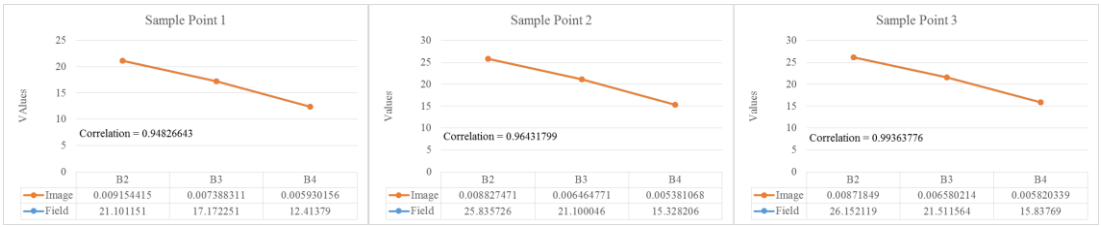

a. Shallow water correlation

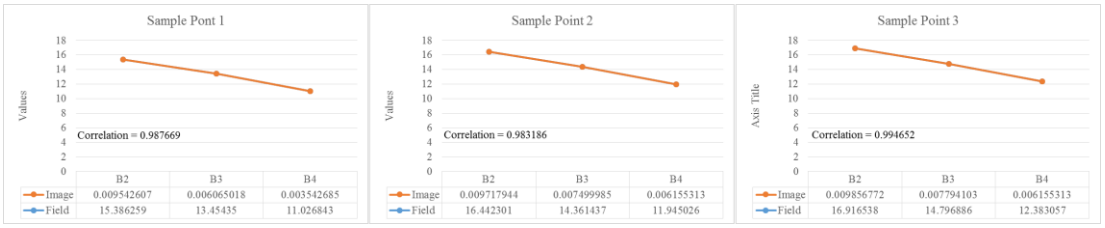

b. Clear water correlation

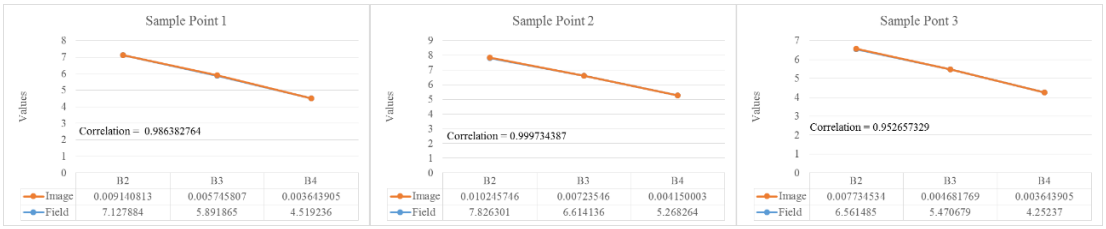

c. Deep water correlation

Figure 5-22 : Correlation comparison between field and LISS – IV.

LISS – III and LISS – IV variation are observed similarly from green to NIR bands that has shown in the figure 5-22 a, b, and c. The images are look same in the figure 5-22 but on clear observing the range of values is differed in each class,. Shallow water has maximum values when compare to the clear water and deep water classes, the deep water has values very low when compare to the remaining classes. Clear water range is observed in between these two classes.

5.6 Comparisons of Landast 8, LISS – III & LISS – IV

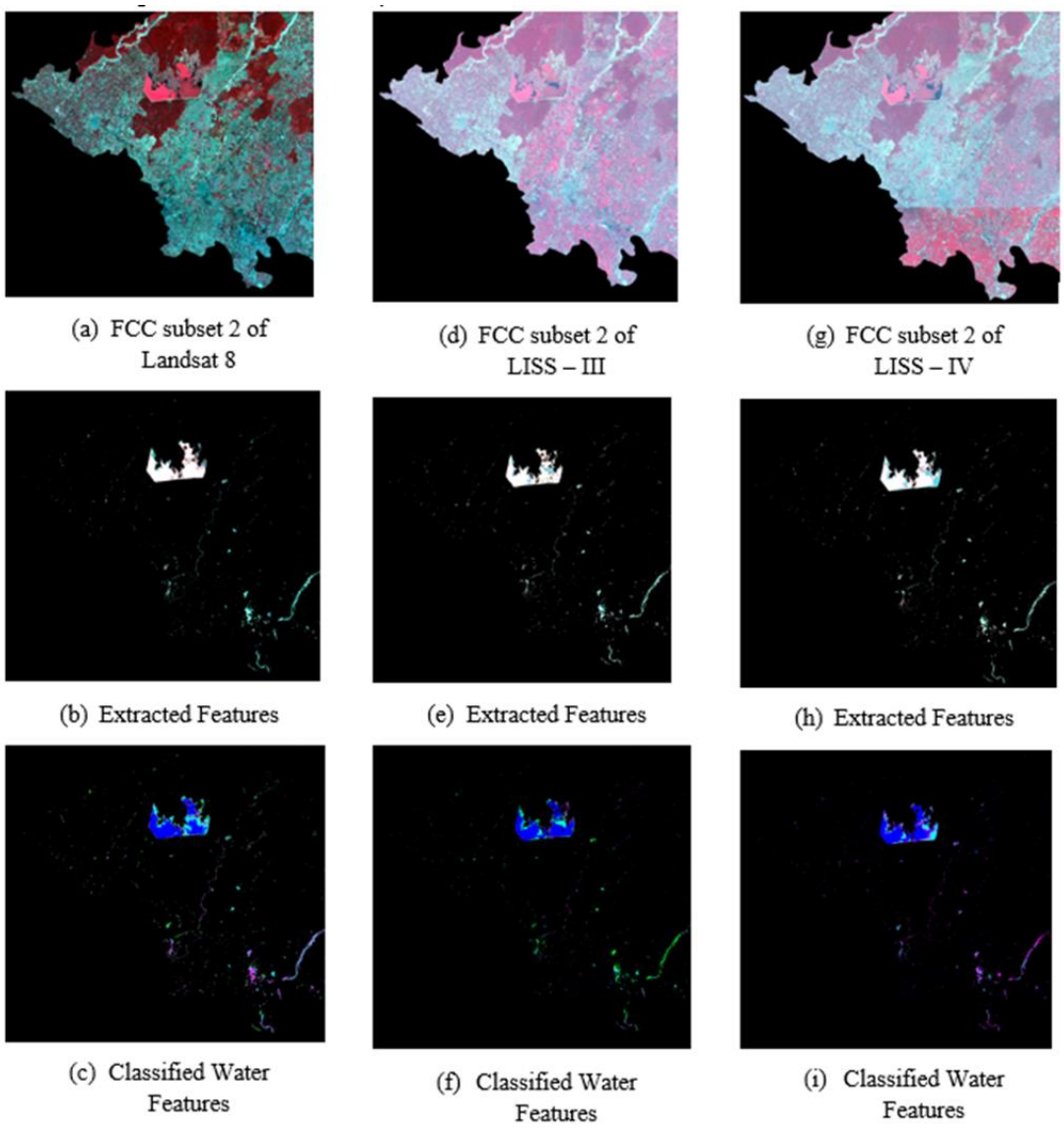

Figure 5-23 : Comparision of Landsat 8, LISS – III & LISS – IV

Discussion:

In the comparison of Landsat 8, LISS – III & LISS – IV, Landsat 8 has better accuracy because the presence of greater number of bands compared to the LISS –III and LISS – IV. In LISS – III some portion of shallow water is classified has wetland, that is clearly observed in figure 5-23 (c), (f) and (i) through the interpretation also.

5.7 Extraction of water network on high resolution datasets

Extraction of water network can be done on the SWIR band of the high resolution datasets. The SWIR band gives the exact water edges because the maximum radiance are absorbed by water features. So, reflectance image of the SWIIR band has low values for the water features when compared to other features in the image. By using this positive feature the edges are separated. In this research study LISS – IV datasets are used for the extraction of water network. The dataset used does not have the SWIR band, so in the place of SWIR, NIR band of the LISS – IV dataset is shown in the figure () is used for this extraction, NIR band also absorbs maximum water content not that compared to SWIR.

Figure 5-24 : NIR Band subset of LISS – IV.

5.7.1 Canny Edge detection

In this research, for the extraction of edges canny edge detection is used. Canny edge detection process involves, first it remove noise and smoothens the image using the Gaussian. Then finding the gradient of the edges in the both x and y direction and also find the direction of the edges. Once the edges are detected the non-maximum suppression has applied and finally hysteresis has applied for eliminating streaking. The final output which is extracted through this edge extraction technique is shown in the figure (5-22).

Figure 5-25 : Canny edge detection output.

The image shown in the figure 5-22 is the output of the canny edge detection, which contains the strong edges and weak edges. The strong edges describes the water boundaries and also some of weak edges which are connected are the also considered has boundaries of water features. So separate the strong and weak edges by using the threshold value is greater than 0.16. The separated strong edge from the edge extraction is shown in the figure (5-23).

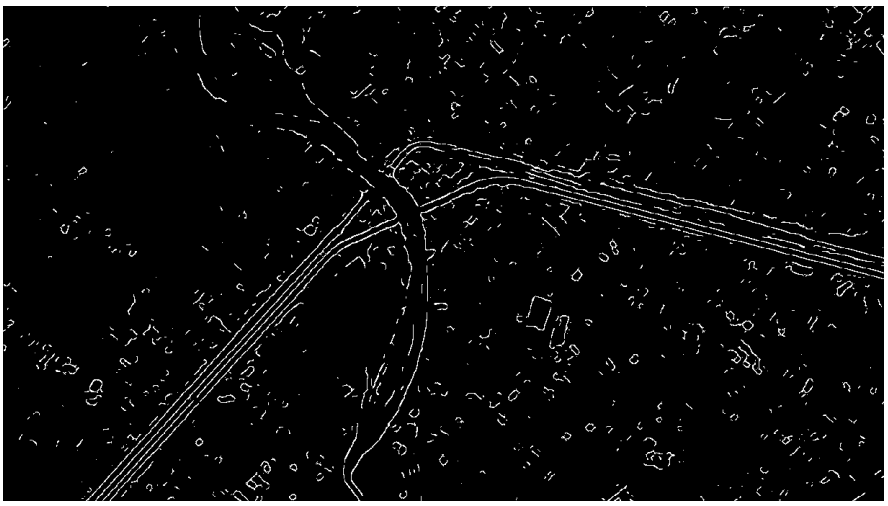

Figure 5-26 : Separation strong edges in edge extraction.

In figure (5-23), the maximum water boundaries are separated by using the threshold. This image shows the not only the water boundaries but also it contains the some of the vegetation boundaries, because in the NIR band the vegetation range has also match with the water features, so that's why the vegetation boundaries are also separated in the used threshold values.

5.7.2 Connecting the river and canal networks

Finally suppression of the vegetation boundaries has observed and it is shown in the figure (5-24). This figure also contains the minimum vegetation boundaries.

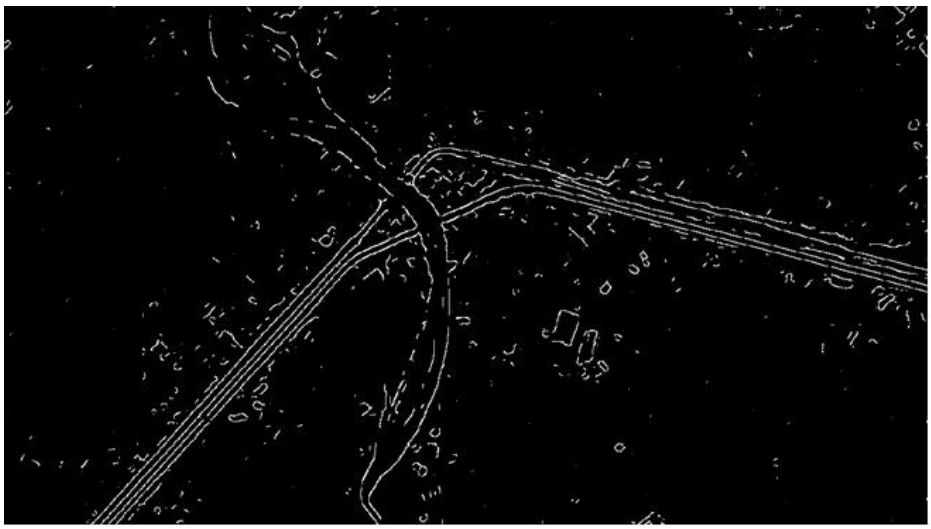

Figure 5-27 : Extracted river and canal network

The extracted river and canal network has observed in the figure (5-24). In this figure, not only canal and river network has highlighted but also some other features which has gradient value is similar to the water features are also highlighted.

Accuracy Assessment

The accuracy assessment is carried out for the extracted river or canal network as described in the section 4.6.3. The accuracy of all edge features that is extracted carried for the edge length as highlighted in the figure 5-28.

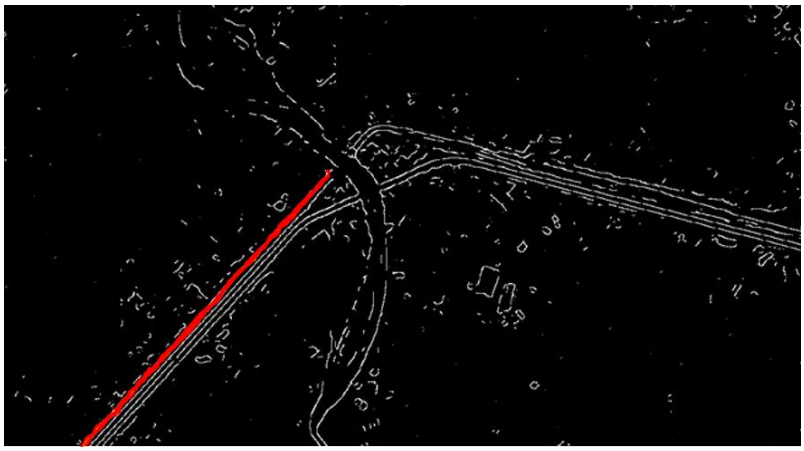

Figure 5-28 : Highlighted edge for accuracy assessment.

For the accuracy assessment the size of the buffer is consider as 10m, values of different parameters used for the accuracy assessment is shown in table 5-3 and 5-4.

Table 5-4 : Based on Reference Buffer

Parameter	Value (m)
Length of Match Extraction	3068.364225
Length of Extraction	3472.358821
Length of Unmatched Extraction	403.9945955

Table 5-5 : Based on Extracted Buffer

Parameter	Value (m)
Length of Matched Reference	3312.648845
Length of Reference	3640.547599
Lingth of Unmatched Reference	327.898754

Based on the values represented in the table 5-3 and 5-4 is the accuracy assessment are carried out by calculating completeness, correctness and quality is shown in the table 5-5.

Table 5-6 : Edge extraction accuracy factors

Parameter	Value
Correctness	0.883654
Completeness	0.909931
Quality	0.80741

The best way of analysing the results is lies in the visual interpretation. The values which are calculated are satisfactory. The reason

5.8 Tool for automated extraction of water features

A tool is developed using python and its libraries for the entire methodology as discussed in chapter 4. The inputs for this tool are TOA corrected of Landsat 8 OLI or LISS – III or LISS – IV and also rescaled and reprojected cartoDEM of 30m resolution of same type as MSS images. Give the path for the outputs where the results are to be stored and finally give the sensor details. After all the inputs are given then the process as to be begin by clicking the 'Generate Indexs' icon on the GUI, this will generate indices and it takes predefined thresholds for the generated indices and finally it will create binary indices after the threshold then it enables the 'Water Mask Generation' icon. On pressing the new enabled icon it will takes the binary indices as input from the output folder and it will create binary water mask. After the creation it will enables the 'Mask Overlay' option, on pressing it will creates a new multispectral image with only water features of the selected sensor and also it enables 'Classify Water Features' on clicking the new button the final classified output will save in the output folder. Finally edge extraction can be done by inputting the NIR or SWIR bands as inputs it will perform the canny edge extraction with the and automatically it will separates remaining edges and finally the output will save in the output folder.

The tool is developed using the pycham IDE for the python programming, using the interpreter python 2.7.9, for this version the almost all libraries were added. The most important libraries are GDAL, for processing the raster data with the projection information, scipy and numpy are used for the scientific and numerical processing and implementing the logic of the methodology. The entire programs are not based on the independent array it is a mask array processing for calculating in the less time. Finally rsgislib, is used for the canny edge detection using the python code. PyQt is used for making the graphic user interface as shown in figure 5-29.

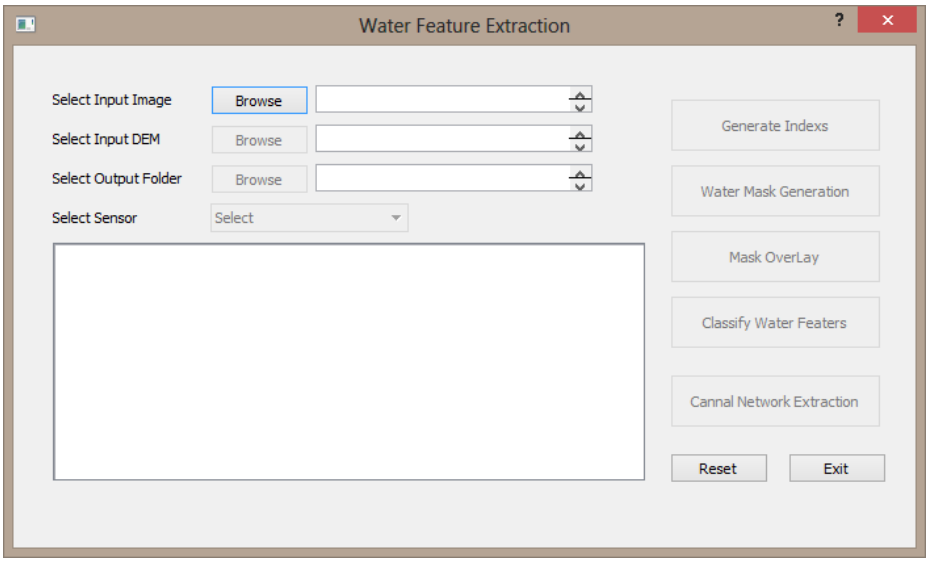

Figure 5-29 : Tool for feature extraction and classification

6. Conclusions and Recommendations

This chapter is the summary of the objectives achieved in this thesis work with recommendations for future work. The work carried out in the research study is to extract the water features at multiple scales and classify these water features on the medium and high resolution datasets.

6.1 Conclusion

The presented research has attempted to extract and classify the different water features at multiple scales, and also separately extract the river and canal network. The research topic considered different datasets from medium resolution (Landsat 8 OLI, and LISS – III) to high resolution (LISS – IV) to extract and classify respected features at variable scales. The study has given detailed overview of different satellite derived parameters like NDWI, MNDWI, NDVI, NDPI and SWI. Finding the optimized threshold for these parameters to extract of water features on Landsat 8 OLI. By using this threshold water features are extracted with an accuracy 92.50% has achieved.

Then it also gives detailed explanation on classification of water features over medium to high resolution images based on the spectral signatures. The signatures are based on the individual value of each band of the image has considered for classifying the shallow water, clear water, and deep water. Along these values and also taken account NDWI, MNDWI and NDVI values for classifying the wetland. With these the water features are classified on Landsat 8 OLI, LISS – III and LISS – IV with an accuracy of 91.67%, 84.17%, and 87.50% respectively. Finally by applying the canny edge detection on NIR of LISS – IV river and canal network was extracted separately.

This study has proposed the customized tool for the extraction and classification of water features at variable scales and it has been achieved successfully in the python by using different python libraries. This tool is totally automated for the entire process as discussed in section 5.8.

6.1.1 Answers to research questions

1. **How to decide the threshold factor for satellite derived parameters for delineation of water features?**

The threshold factor was decided after the normalization of data. This can be done by converting DN to TOA reflectance. Conversion of the original datasets to a TOA, each sensor has its own formula. After the conversion, the data is suitable for further processing, this processing is involved in the calculation of different satellite derived parameters. For each parameter, which include SWI, NDWI, MNDWI, NDPI, and NDVI density slicing was applied independently, for a particular value to which the maximum water feature content has to be extracted. In this research the SWI is used only for the separation of the snow, using density slicing method.

2. **Which rules and parameters are appropriate for classifying the extracted image?**

The spectral rules are used for the classification of the image. The spectral signatures was collected for the defined classes clear water, shallow water, deep water and wetland. Those

signatures are resampled to a values based on wavelengths of the dataset used. The different spectral signatures from the extracted input data are used and match with the present spectra and classify those features in to different classes as predefined classes.

3. How can accuracy be assessed for the extracted and classified features?

Accuracy assessment as carried out by using the visual interpretation for the generated random points. There are three types of random point's generation

1. Random points

   This type of random points are normal random points which are generated by the system itself, in this type the input is only, total number of points to be generated.
2. Stratified random points

   This type of random points are generated based on the minimum number points are to be used for the accuracy assessment, and those points are to obey stratification. It is the process of dividing the number of points into homogeneous subgroups and assigned to each class before the assessment and also at-least one point is assigned to each class.
3. Equalized random points

   In this type, random points are generated based on the total number points are given in the input, those points are equally divided and assigned into each class.

From the generated random points check the class values, and fill-up all the new class values by the visual interpret independently for every generated point. Finally generate the accuracy report, this report contains number of points taken for each class, user's accuracy, producer's accuracy, over all accuracy and finally the kappa coefficient for each class.

Accuracy assessment for the edge detection was carried out in two steps, one was matching of the extracted canal or river edge with the reference edge which is manually digitized and the second step was calculation of quality measures which includes completeness, correctness and quality as described in the section 4.6.3.2, based on assumption buffer range of 10m for both reference and extracted edges.

6.2 Recommendations

1. In the extraction of water feature on the high resolution image can be improved by combining with the output of the canal and river network image and extrapolating the gaps between the edges and extracted water features.
2. Classification accuracy can be improved by adding additional rules and also classes can increase in the high resolution image by considering several spectral bands.
3. The tool which is developed can be extended to include extraction and classification from microware and hyperspectral data.

References

Adhikari, B. S., & Babu, M. M. (2008). Floral diversity of Baanganga Wetland, Uttarakhand, India. *Check List*, *4*(3), 279–290.

Ang, Z., Ang, Z., Xiaolin, T., & Yan-kui, S. (2011). Morphologic weak edge detection by multi-structure and multi-scale in anterior chamber OCT images. In *Image and Signal Processing (CISP), 2011 4th International Congress on* (Vol. 2, pp. 963–966). IEEE. Retrieved from http://ieeexplore.ieee.org/xpls/abs_all.jsp?arnumber=6100286

ArcGIS, B. (2010). On map scale and raster resolution | ArcGIS Blog. Retrieved January 8, 2015, from http://blogs.esri.com/esri/arcgis/2010/12/12/on-map-scale-and-raster-resolution/

ArcGIS Help 10.1 - Slope function. (2015). Retrieved June 9, 2015, from http://resources.arcgis.com/en/help/main/10.1/009t/009t00000056000000.htm

Baig, M. H. A., Zhang, L., Shuai, T., & Tong, Q. (2014). Derivation of a tasselled cap transformation based on Landsat 8 at-satellite reflectance. *Remote Sensing Letters*, *5*(5), 423–431. http://doi.org/10.1080/2150704X.2014.915434

Barsi, J. A., Markham, B. L., & Pedelty, J. A. (2011). <title>The operational land imager: spectral response and spectral uniformity</title> In J. J. Butler, X. Xiong, & X. Gu (Eds.), (p. 81530G–81530G–11). http://doi.org/10.1117/12.895438

Barsi, J., Lee, K., Kvaran, G., Markham, B., & Pedelty, J. (2014). The Spectral Response of the Landsat-8 Operational Land Imager. *Remote Sensing*, *6*(10), 10232–10251. http://doi.org/10.3390/rs61010232

Basu, M. (2002). Gaussian-based edge-detection methods-a survey. *IEEE Transactions on Systems, Man, and Cybernetics, Part C*, *32*(3), 252–260.

Bhagat Vijay, S. (2008). Delineation of groundwater utility status areas using GIS technique. Retrieved from http://www.researchgate.net/publication/231302839_Delineation_of_groundwater_utility_status_areas_using_GIS_technique/file/79e41506703152771b.pdf

Bhagat, V. S., & Sonawane, K. R. (2011). Use of Landsat ETM+ data for delineation of water bodies in hilly zones. *Journal of Hydroinformatics*, *13*(4), 661. http://doi.org/10.2166/hydro.2010.018

Bhuvan | NRSC Open EO Data Archive | NOEDA | Ortho | DEM | Elevation | AWiFS | LISSIII | HySI | TCHP | OHC | Free GIS Data | Download. (2015). Retrieved June 7, 2015, from http://bhuvan.nrsc.gov.in/data/download/index.php

Bindraban, P., Van Keulen, H., & Warner, J. (2006). Guest Editorial. *International Journal of Water Resources Development*, *22*(1), 1–2. http://doi.org/10.1080/07900620500405064

Canny Edge Detection — OpenCV-Python Tutorials 1 documentation. (2015). Retrieved June 12, 2015, from http://opencv-python-tutroals.readthedocs.org/en/latest/py_tutorials/py_imgproc/py_canny/py_canny.html

Canny Edge Detection Tutorial. (2015). Retrieved June 12, 2015, from http://dasl.mem.drexel.edu/alumni/bGreen/www.pages.drexel.edu/_weg22/can_tut.html

Canny, J. (1986). A Computational Approach to Edge Detection. *IEEE Trans. Pattern Anal. Mach. Intell.*, *8*(6), 679–698. http://doi.org/10.1109/TPAMI.1986.4767851

Cowardin, Carter, Golet, & LaRoe. (2013). Classification of Wetlands and Deepwater Habitats of the United States. Retrieved from http://www.fgdc.gov/standards/projects/FGDC-standards-projects/wetlands/nvcs-2013

Crist, E. P., & Cicone, R. C. (1984). A physically-based transformation of Thematic Mapper data—The TM Tasseled Cap. *Geoscience and Remote Sensing, IEEE Transactions on*, (3), 256–263.

DATA, M. S. (1984). PJASA E85_10082. Retrieved from http://ntrs.nasa.gov/archive/nasa/casi.ntrs.nasa.gov/NTRS-PDF/19850013437_1985013437.pdf

De Roeck, E. R., Verhoest, N. E. C., Miya, M. H., Lievens, H., Batelaan, O., Thomas, A., & Brendonck, L. (2008a). Remote Sensing and Wetland Ecology: a South African Case Study. *Sensors*, *8*(5), 3542–3556. http://doi.org/10.3390/s8053542

De Roeck, E. R., Verhoest, N. E. C., Miya, M. H., Lievens, H., Batelaan, O., Thomas, A., & Brendonck, L. (2008b). Remote Sensing and Wetland Ecology: a South African Case Study. *Sensors*, *8*(5), 3542–3556. http://doi.org/10.3390/s8053542

D. R. Montello. (n.d.). Scale in Geography. In *International Encyclopaedia of the Social & Behavioural Sciences* (pp. 13501–13504). Elsevier Science Ltd. Retrieved from http://www.geog.ucsb.edu/~montello/pubs/scale2.pdf

Elachi, C. (New York : Wiley, c1987). *Introduction to the physics and techniques of remote sensing*. New York: Wiley. Retrieved from http://www.loc.gov/catdir/toc/onix05/86032411.html

Electromagnetic Radiation. (2015). Retrieved January 1, 2015, from http://chemwiki.ucdavis.edu/Physical_Chemistry/Spectroscopy/Fundamentals/Electromagnetic_Radiation

EPA, U. (2011). Report on the Environment. Retrieved from http://www.epa.gov/roe/

EPA, U. (2015). US Environmental Protection Agency [Collections and Lists]. Retrieved January 13, 2015, from http://www.epa.gov/

Feyisa, G. L., Meilby, H., Fensholt, R., & Proud, S. R. (2014). Automated Water Extraction Index: A new technique for surface water mapping using Landsat imagery. *Remote Sensing of Environment*, *140*, 23–35. http://doi.org/10.1016/j.rse.2013.08.029

FSF: SVC HR-1024 Field Spectroradiometer. (2015). Retrieved June 9, 2015, from http://fsf.nerc.ac.uk/instruments/svc_hr-1024.shtml

Gao, W., Zhang, X., Yang, L., & Liu, H. (2010). An improved Sobel edge detection. In *Computer Science and Information Technology (ICCSIT), 2010 3rd IEEE International Conference on* (Vol. 5, pp. 67–71). IEEE. Retrieved from http://ieeexplore.ieee.org/xpls/abs_all.jsp?arnumber=5563693

Gilmore, M. S., Wilson, E. H., Barrett, N., Civco, D. L., Prisloe, S., Hurd, J. D., & Chadwick, C. (2008). Integrating multi-temporal spectral and structural information to map wetland vegetation in a lower Connecticut River tidal marsh. *Remote Sensing of Environment*, *112*(11), 4048–4060. http://doi.org/10.1016/j.rse.2008.05.020

Goverment of India. (2007). THE CONSTITUTION OF INDIA. Retrieved from http://lawmin.nic.in/coi/coiason29july08.pdf

Haibo, Y., Zongmin, W., Hongling, Z., & Yu, G. (2011). Water Body Extraction Methods Study Based on RS and GIS. *Procedia Environmental Sciences*, *10*, 2619–2624. http://doi.org/10.1016/j.proenv.2011.09.407

How much water is there on Earth, from the USGS Water Science School. (1983). Retrieved June 14, 2015, from http://water.usgs.gov/edu/earthhowmuch.html

IMD, P. (2010). WebCite query result. Retrieved January 14, 2015, from http://www.webcitation.org/6GmnoaB0m

Institute of Electrical and Electronics Engineers, Autumn meeting. Polish Information Processing Society (PIPS), Computational liguistics - applications (CLA), IMCSIT, International Conference on Principles of Information Technology and Applications (PITA), International Multiconference on Computer Science and Information Technology, … Workshop on Computational Optimization (WCO). (2009). *International Multiconference on Computer Science and Information Technology, 2009: IMCSIT '09 ; Mragowo, Poland, 12 - 14 Oct. 2009 ; co-located with the XXV Autumn meeting of the Polish Information Processing Society (PIPS) ; [including 11 workshops/conferences]*. Piscataway, NJ: IEEE. Retrieved from http://ieeexplore.ieee.org/servlet/opac?punumber=5341930

Introduction to Remote Sensing. (2015). Retrieved June 13, 2015, from http://www.seos-project.eu/modules/remotesensing/remotesensing-c01-p05.html

Islam, M. A., Thenkabail, P. S., Kulawardhana, R. W., Alankara, R., Gunasinghe, S., Edussriya, C., & Gunawardana, A. (2008a). Semi-automated methods for mapping wetlands using Landsat ETM+ and SRTM data. *International Journal of Remote Sensing*, *29*(24), 7077–7106. http://doi.org/10.1080/01431160802235878

Islam, M. A., Thenkabail, P. S., Kulawardhana, R. W., Alankara, R., Gunasinghe, S., Edussriya, C., & Gunawardana, A. (2008b). Semi-automated methods for mapping wetlands using Landsat ETM+ and SRTM data. *International Journal of Remote Sensing*, *29*(24), 7077–7106. http://doi.org/10.1080/01431160802235878

Jiang, H., Feng, M., Zhu, Y., Lu, N., Huang, J., & Xiao, T. (2014). An Automated Method for Extracting Rivers and Lakes from Landsat Imagery. *Remote Sensing*, *6*(6), 5067–5089. http://doi.org/10.3390/rs6065067

Ji, L., Zhang, L., & Wylie, B. (2009). Analysis of dynamic thresholds for the normalized difference water index. *Photogrammetric Engineering & Remote Sensing*, *75*(11), 1307–1317.

J.K, M., & Ghosh, A. (2013). Edge Detection by Modified OTSU Method (pp. 233–240). Academy & Industry Research Collaboration Center (AIRCC). http://doi.org/10.5121/csit.2013.3626

Jongman, R. H. G., & Padovani, C. R. (2006). Interaction between Stakeholders and Research for Integrated River Basin Management. *International Journal of Water Resources Development*, *22*(1), 49–60. http://doi.org/10.1080/07900620500405270

Kaur, E. M. (2011). A New Approach to Edge Detection using rule based Fuzzy Logic. *Journal of Global Research in Computer Science*, *2*(9), 15–19.

Kaur, K., & Malhotra, S. (2013). A Survey on Edge Detection Using Different Techniques. *International Journal of Application or Innovation in Engineering and Management (IJAIEM)*, *vol2*, (4), 496–500.

Kaur, N. (2012). A REVIEW OF EDGE DETECTION TECHNIQUES FOR IMAGE SEGMENTATION. Retrieved from http://www.ijcsit-apm.com/Uploads/Media/Journal/20140612164448_GV_ICRTEDC_77.pdf

Kauth, R. J., & Thomas, G. S. (1976). The tasselled cap–a graphic description of the spectral-temporal development of agricultural crops as seen by Landsat. In *LARS Symposia* (p. 159). Retrieved from http://docs.lib.purdue.edu/cgi/viewcontent.cgi?article=1160&context=lars_symp

Kumar, S., Shirke, K. D., & Pawar, N. J. (2008). GIS-based colour composites and overlays to delineate heavy metal contamination zones in the shallow alluvial aquifers, Ankaleshwar industrial estate, south Gujarat, India. *Environmental Geology*, *54*(1), 117–129. http://doi.org/10.1007/s00254-007-0799-2

Kumar, T., & Sahoo, G. (2010). A novel method of edge detection using cellular automata. *International Journal of Computer Applications*, *9*(4), 38–44.

Lacaux, J. P., Tourre, Y. M., Vignolles, C., Ndione, J. A., & Lafaye, M. (2007). Classification of ponds from high-spatial resolution remote sensing: Application to Rift Valley Fever epidemics in Senegal. *Remote Sensing of Environment*, *106*(1), 66–74. http://doi.org/10.1016/j.rse.2006.07.012

Landsat Team. (2012). LANDSAT DATA CONTINUITY MISSION (LDCM) MISSION DATA DATA FORMAT CONTROL BOOK (DFCB).

Leica Zeno 5 - GPS Handheld - Leica Geosystems - India. (2015). Retrieved June 9, 2015, from http://www.leica-geosystems.in/en/Leica-Zeno-5_99189.htm

Lillesand, T. M., & Kiefer, R. W. (New York : Wiley & Sons, c1994). *Remote sensing and image interpretation*. New York: Wiley & Sons.

Luo, J., Sheng, Y., Shen, Z., & Li, J. (2010). High-precise water extraction based on spectral-spatial coupled remote sensing information. In *Geoscience and Remote Sensing Symposium (IGARSS), 2010 IEEE International* (pp. 2840–2843). IEEE. Retrieved from http://ieeexplore.ieee.org/xpls/abs_all.jsp?arnumber=5648978

Marr, D., & Hildreth, E. (1980). Theory of edge detection. *Proceedings of the Royal Society of London B: Biological Sciences*, *207*(1167), 187–217.

McFeeters, SK. (1996). The use of the normalized difference water index (NDWI) in the delineation of open water features. *INTERNATIONAL JOURNAL OF REMOTE SENSING*, *17*(7), 1425–1432. http://doi.org/10.1080/01431169608948714

Mioca, D., Nickersonb, B., MacGillivrayc, E., Mortonc, A., Antond, F., Frasera, D., … Lianga, G. (2008). Early warning and mapping for flood disasters.

Nadernejad, E., Sharifzadeh, S., & Hassanpour, H. (2008). Edge detection techniques: Evaluations and comparison. *Applied Mathematical Sciences*, *2*(31), 1507–1520.

NagaRaju, C., NagaMani, S., rakesh Prasad, G., & Sunitha, S. (2011). Morphological edge detection algorithm based on multi-structure elements of different directions. *International Journal of Information and Communication Technology Research*, *1*(1). Retrieved from

http://citeseerx.ist.psu.edu/viewdoc/download?doi=10.1.1.208.2589&rep=rep1&type=pdf

Nawaz, N., Srinivasulu, S., & Rao, P. K. (2013). Automatic Extraction of Water Bodies Using Whole-R Method, *7*(12). Retrieved from http://www.waset.org/publications/9996774

Nguyen Dinh Duong. (2012, August). WATER BODY EXTRACTION FROM MULTI SPECTRAL IMAGE BY SPECTRAL PATTERN ANALYSIS.pdf. International Archives of the Photogrammetry, Remote Sensing and Spatial Information Sciences.

NRSC, I. (2013). Technical Methodology for Countrywide DEM and Ortho Product Generation for India Using Cartosat-1 Stereo Data. Retrieved from http://bhuvan.nrsc.gov.in/data/download/tools/document/SISDP-DEM-GENERATION-BHUVAN.pdf

Oskoei, M. A., & Hu, H. (2010). A survey on edge detection methods. *University of Essex, UK*. Retrieved from http://dces.essex.ac.uk/staff/hhu/Papers/CES-506.pdf

Otsu, N. (1975). A threshold selection method from gray-level histograms. *Automatica*, *11*(285-296), 23–27.

Pal, I. (2015). Land Use and Land Cover Change Analysis in Uttarakhand Himalaya and Its Impact on Environmental Risks. In *Mountain Hazards and Disaster Risk Reduction* (pp. 125–137). Springer. Retrieved from http://link.springer.com/chapter/10.1007/978-4-431-55242-0_7

Patel, N. R., Mohammed, A. J., & Rakhesh, D. (2006). Modeling of Wheat Yields Using Multi-temporal Terra/MODIS Satellite Data. *Geocarto International*, *21*(1), 43–50. http://doi.org/10.1080/10106040608542373

Pavlov, S. S., Roerink, G. J., Hellegers, P. J. G. J., & Popovych, V. F. (2006). Irrigation Performance Assessment in Crimea, Ukraine. *International Journal of Water Resources Development*, *22*(1), 61–78. http://doi.org/10.1080/07900620500405593

Pawar, N. J., Pawar, J. B., Kumar, S., & Supekar, A. (2008). Geochemical Eccentricity of Ground Water Allied to Weathering of Basalts from the Deccan Volcanic Province, India: Insinuation on CO2 Consumption. *Aquatic Geochemistry*, *14*(1), 41–71. http://doi.org/10.1007/s10498-007-9025-9

Prakashvel, J., & Scholar, M. S. (2003). GIS and Visualisation Capabilities for Interlinking of Indian Rivers. Retrieved from http://www.gisdevelopment.net/technology/gis/pdf/ma03203.pdf

Pratt, W. K. (2001). *Digital image processing PIKS inside*. New York; Chichester: John Wiley & Sons. Retrieved from http://www3.interscience.wiley.com/cgi-bin/booktoc?ID=91014054

Priyadarshini, S., & Sahoo, G. (2010). A New Edge Detection Method based on Additions and Divisions. *International Journal of Computer Applications*, *9*(10), 10–13.

Ramsar Convention. (2013). The Ramsar Convention Manual: a guide to the Convention on Wetlands (Ramsar, Iran, 1971). Retrieved from http://www.ramsar.org/sites/default/files/documents/library/manual6-2013-e.pdf

Rashmi, Kumar, M., & Saxena, R. (2013). Algorithm and Technique on Various Edge Detection : A Survey. *Signal & Image Processing : An International Journal*, *4*(3), 65–75. http://doi.org/10.5121/sipij.2013.4306

Resourcesat-2 Project Team, ISRO. (2011). RESOURCESAT-2 Data Users' Handbook. Retrieved from http://www.nrsc.gov.in/pdf/resourcesat2.pdf

Rosenfeld, A., & Kak, A. C. (1982). *Digital picture processing* (2nd ed). New York: Academic Press.

Rouse, J. W., Jr., Haas, R. H., Schell, J. A., & Deering, D. W. (1974). Monitoring Vegetation Systems in the Great Plains with Erts. *NASA Special Publication*, *351*, 309.

Sabins, F. F. (2007). *Remote Sensing: Principles and Interpretation* (3 edition). Long Grove, Ill.: Waveland Pr Inc.

Schowengerdt, R. A. (2007). *Remote sensing models and methods for image processing*. Burlington, MA: Academic Press. Retrieved from http://search.ebscohost.com/login.aspx?direct=true&scope=site&db=nlebk&db=nlabk&AN=196149

Shen, J., & Castan, S. (1993). Towards the unification of band-limited derivative operators for edge detection. *Signal Process.*, *31*(2), 103–119. http://doi.org/10.1016/0165-1684(93)90060-N

SINGH, G. S. A. K. A. (2014). REVIEW ON IMAGE ENHANCEMENT USING CANNY EDGE DETECTION METHOD: LITERATURE SURVEY. *GLOBAL JOURNAL OF MULTIDISCIPLINARY STUDIES*, *3*(12). Retrieved from http://www.gjms.co.in/index.php/gjms/article/view/638/569

Small, C. (2004). The Landsat ETM+ spectral mixing space. *Remote Sensing of Environment*, *93*(1-2), 1–17. http://doi.org/10.1016/j.rse.2004.06.007

S. Muralikrishnan, Shashivardhan Reddy, B.Narender, & Abhijit Pillai. (2011). *Evaluation of Indian National DEM from Cartosat-1 Data Summary Report (Ver.1)*. Retrieved from http://bhuvan.nrsc.gov.in/data/download/tools/document/CartoDEMReadme_v1_u1_23082011.pdf

Subramaniam, S., & Saxena, M. (2011). Automated Algorithm for Extraction of Wetlands from IRS Resourcesat Liss III Data. *ISPRS-International Archives of the Photogrammetry, Remote Sensing and Spatial Information Sciences*, *3820*, 193–198.

Subramaniam, S., Suresh Babu, A. V., & Roy, P. S. (2011). Automated Water Spread Mapping Using ResourceSat-1 AWiFS Data for Water Bodies Information System. *IEEE Journal of Selected Topics in Applied Earth Observations and Remote Sensing*, *4*(1), 205–215. http://doi.org/10.1109/JSTARS.2010.2085032

The Mathematics of Satellite Images. (2015). Retrieved June 13, 2015, from http://www-users.math.umn.edu/~rogness/Satellites/MathSatellites_LegoLeague.html

Tian, J., Yu, W., & Xie, S. (2008). An ant colony optimization algorithm for image edge detection. In *Evolutionary Computation, 2008. CEC 2008.(IEEE World Congress on Computational Intelligence). IEEE Congress on* (pp. 751–756). IEEE. Retrieved from http://ieeexplore.ieee.org/xpls/abs_all.jsp?arnumber=4630880

Tobler, W. (1987). Measuring spatial resolution. *Proceedings, Land Resources Information Systems Conference*, 12–16.

Tobler, W. (1988). Resolution, Resampling, and All That. *Building Data Bases for Global Science*, 129–137.

Troell, J., Bruch, C., Cassar, A., & Schang, S. (2005). Transboundary environmental impact assessment as a tool for promoting public participation in international watercourse management., 53–80.

US EPA, O. (2015). Wetlands. Retrieved June 14, 2015, from http://water.epa.gov/type/wetlands/

U.S. Geological Survey. (2013). *Landsat 8* (USGS Numbered Series No. 2013-3060). Reston, VA. Retrieved from http://pubs.er.usgs.gov/publication/fs20133060

Using the USGS Landsat 8 Product. (2015). Retrieved June 13, 2015, from http://landsat.usgs.gov/Landsat8_Using_Product.php

Van Dam, J. C., Singh, R., Bessembinder, J. J. E., Leffelaar, P. A., Bastiaanssen, W. G. M., Jhorar, R. K., … Droogers, P. (2006). Assessing Options to Increase Water Productivity in Irrigated River Basins Using Remote Sensing and Modelling Tools. *International Journal of Water Resources Development*, *22*(1), 115–133. http://doi.org/10.1080/07900620500405734

Vikram, K., Upashyaya, N., Roshan, K., & Govardhan, A. (2010). Image Edge Detection. *Special Issues of International Journal of Computer Science and Informatics (IJCSI)*, *2*. Retrieved from http://www.interscience.in/IJCSI_Vol2Iss1/IJCSI_Paper_38.pdf

Wang, H., Pan, L., & Zheng, H. (2008). Multi-texture-Model for Water Extraction Based on Remote Sensing Image (pp. 710–714). IEEE. http://doi.org/10.1109/CISP.2008.19

Warner, J. F., Bindraban, P. S., & Van Keulen, H. (2006). Introduction: Water for Food and Ecosystems: How to Cut which Pie? *International Journal of Water Resources Development*, *22*(1), 3–13. http://doi.org/10.1080/07900620500405080

Wiedemann, C., Heipke, C., Mayer, H., & Jamet, O. (1998). Empirical evaluation of automatically extracted road axes. *Empirical Evaluation Techniques in Computer Vision*, 172–187.

Xu, H. (2006). Modification of normalised difference water index (NDWI) to enhance open water features in remotely sensed imagery. *International Journal of Remote Sensing*, *27*(14), 3025–3033. http://doi.org/10.1080/01431160600589179

Yarbrough, L. D., Easson, G., & Kuszmaul, J. S. (2005). QuickBird 2 tasseled cap transform coefficients: a comparison of derivation methods. In *Pecora* (Vol. 16, pp. 23–27). Retrieved from http://www.researchgate.net/profile/Greg_Easson/publication/228825263_QuickBird_2_Tasseled_Cap_Transform_coefficients_A_comparison_of_derivation_methods/links/54466d190cf2d62c304dbd15.pdf

Yu, F., & Jiaxing-Xueyuan (Eds.). (2009). *Proceedings / the 2009 International Symposium on Information Processing (ISIP 2009): 21 - 23 August 2009, Huangshan, China*. Oulu: Academy Publ.

Zhang, J., He, K., Zheng, X., & Zhou, J. (2010). An Ant Colony Optimization Algorithm for Image Edge Detection (pp. 215–219). IEEE. http://doi.org/10.1109/AICI.2010.167

Zhang, S., Zhang, S., & Zhang, J. (2000a). A study on wetland classification model of remote sensing in the Sangjiang Plain. *Chinese Geographical Science*, *10*(1), 68–73.

Zhang, S., Zhang, S., & Zhang, J. (2000b). A study on wetland classification model of remote sensing in the Sangjiang Plain. *Chinese Geographical Science*, *10*(1), 68–73.

Zhang, Z., Prinet, V., & Ma, S. (2003). Water body extraction from multi-source satellite images. In *INTERNATIONAL GEOSCIENCE AND REMOTE SENSING SYMPOSIUM* (Vol. 6, pp. VI–3970). Retrieved from http://www.researchgate.net/publication/224748500_Water_body_extraction_from_multi-source_satellite_images/file/e0b4951e44461f0fe9.pdf

Zhou, P., Ye, W., Xia, Y., & Wang, Q. (2011). An Improved Canny Algorithm for Edge Detection. *Journal of Computational Information Systems*, *7*(5), 1516–1523.

Zhu, S. (2011). Edge detection based on multi-structure elements morphology and image fusion. In *Computing, Control and Industrial Engineering (CCIE), 2011 IEEE 2nd International Conference on* (Vol. 2, pp. 406–409). IEEE. Retrieved from http://ieeexplore.ieee.org/xpls/abs_all.jsp?arnumber=6008150

Ziou, D., Tabbone, S., & others. (1998). Edge detection techniques-an overview. *Pattern Recognition and Image Analysis C/C of Raspoznavaniye Obrazov I Analiz Izobrazhenii*, *8*, 537–559.